FINAL REPORT

LABORATORY STUDIES OF THE DIFFUSE REFLECTANCE SPECTRA OF FROSTS AND MINERALS OCCURRING ON ASTRONOMICAL OBJECTS

by

Frederic M. Glaser
Pan American University
Edinburg, Texas 78539

prepared for:

NATIONAL AERONAUTICS AND SPACE ADMINISTRATION

Headquarters: Washington, D. C. 20546

June, 1978

(NASA-CR-157298) LABORATORY STUDIES OF THE DIFFUSE REFLECTANCE SPECTRA OF FROSTS AND MINERALS OCCURRING ON ASTRONOMICAL OBJECTS Final Report (Pan American Univ., Edinburg, Tex.) 83 p HC A05/MF A01 CSCL 03A G3/89

N78-28019

Unclas
23406

Contract NASA Grant NSG-7278

ABSTRACT

A vacuum monochromator has been integrated into the system and optics chosen to increase data collection in the infrared spectral region. Using a InSb detector, good reflectance data has been obtained to 5.5μm from a variety of samples. The samples include magnesium oxide, barium sulfate, water frost and Bloedite.

The reflectance of barium sulfate and magnesium oxide was measured using barium sulfate as the standard. Magnesium oxide was found to be a poorer reflector than the barium sulfate throughout the visible and near infrared region. The reflectance of barium sulfate was determined as a function of the angle of incidence. This material was shown to be a Lambert reflector in the visible region and over an angular range of 60°. This is in agreement with several previous studies.

Several samples of water frost were prepared and the reflectance measured from 0.3μm to 5.5μm. The fine grained frosts were better reflectors than the coarse grained frosts, usually by 20% or more, over the entire spectral range. Measurements of the angular dependence of the reflectance were taken using a fine grained frost. Only a rather limited angular range was covered, but these results indicate that water frost does not deviate strongly from a Lambert type reflector.

The minerals Bloedite and sulfur were also investigated further. The Bloedite powder could not be completely dehydrated even after heating to 200°C for three days. The water bands in the near infrared continued to be the only major features observed from 0.3μm to 2.5μm. A broad ultraviolet band centered near 0.25μm was observed to be independent of temperature from 295K to 80K. The ultraviolet band in the sulfur spectrum was shown to have the expected temperature dependence, but not as strongly as other investigators have reported. The shift of the band edge to shorter wavelengths is essentially completed on cooling to 160K.

Improvements in Instrumentation and Techniques.

One of the advantages of the present system is that a wide spectral region can be investigated without changing or disturbing the sample. The system was designed to operate from 0.11μm to beyond 20μm continuously by changing sources, detectors, etc. To extend the measurements to beyond 2.0μm, a vacuum monochromator with gold optics was placed into operation. The instrument is a MacPherson 0.3m scanning monochromator pumped with a 4 inch diffusion pump and mechanical vacuum pump. The freon refrigeration unit cools a baffle to prevent oil migration into the monochromator. The pressure is monitored by a thermocouple gauge and a cold cathode ionization gauge. There is a 4 inch gate valve to isolate the pumping stack from the chamber. In this way the grating can be changed and the system re-evacuated in about thirty minutes. Three gratings blazed for 4, 8, and 12μm are used with this instrument. The infrared source is a directly heated ceramic rod purchased from the Perkin-Elmer Corporation. This source is designed to operate in air and uses natural air convection to cool the supports and leads. A brass housing for the source and a two mirror light collecting system was constructed. This housing is evacuated by the forepump for the monochromator and is provided with water cooling. There is a cesium iodide window to isolate the source assembly from the entrance slit and main chamber of the monochromator. An attempt to operate this source in vacuum at full power failed; the ceramic rod broke and the mirrors, the inside of the

housing and the CsI window were covered with an evaporated film. After cleaning the entire assembly a new ceramic source was put into the system. This source is run in a dry nitrogen atmosphere rather than a low vacuum. The source housing is evacuated, backfilled with nitrogen, re-evacuated, and then filled with dry nitrogen. A stream of nitrogen is maintained at a positive pressure of about 15 psig. This arrangement allows the source to operate at full power and so far no further problems have developed.

An indium antimonide detector was also purchased so that data could be taken to 5.0μm without having to deal with liquid helium to cool the bolometer. The sensitivity of this detector is not great but it performs reasonably satisfactorily. The relative intensity of the radiation from the ceramic source is shown in Figure 1. The 4μm blazed grating and 200 micron slits were used with the 0.3μm vacuum monochromator. The InSb detector was used to measure the infrared radiation. The first portion of this data was taken using a 1.9μm long pass filter and the second portion using a 3.4μm long pass filter. The intensity result from 2μm to 4μm is typical of a blazed grating shortward of its blaze wavelength. The actual intensity in this region is about 50% greater than the longer wavelength portion because of the greater amount of energy available at the shorter wavelengths. The intensity function from 3.5μm to 5.5μm is bounded by the filter at 3.4μm and the long wavelength limit of the detector at 5.5μm. In general, this combination is quite satisfactory from 3.5μm to 5.5μm

but another shorter blazed grating is needed to improve the radiation throughput from 2.0μm to 3.5μm.

The reflectance of the barium sulfate standard and water frost has been measured to 5.5μm using this arrangement. The results tend to be noisy because of the small signal generated by the detector. The data are useful and will be discussed later.

Extension of the measurements into the ultraviolet below 0.2μm has been extremely difficult. Most materials are opaque in the extreme ultraviolet and thus are also very poor reflectors of this radiation. A technical problem with the source of short wavelength radiation has also developed. A pulsed DC discharge through a low pressure inert gas is a classic method of producing continuum radiation in the vacuum ultraviolet. A 10 kV at 150 mA power supply is used to charge a small condenser bank which is then discharged through the gas filled capillary lamp. The repetition rate is generally taken as the maximum of the trigger supply 2000 pps. When the gas pressure, flow rate, power supply operating conditions and pulse rate are adjusted, the argon continuum extending from above 0.11μm to 0.16μm can be obtained with sufficient intensity to be useful. The discharge occurs through a six inch capillary with an air cooled anode and a water cooled cathode at ground potential. The monochromator is grounded and forms part of the high voltage current return path. However, the monochromator and any other apparatus connected to it, such as the experiment chamber and pumps, etc., act as

an audio frequency antenna. It is possible to draw a large high frequency spark from the grounded apparatus. The apparatus "broadcasts" a large amount of audio frequency power into the laboratory. The digital equipment used for data acquisition does not operate in such an environment. The analog equipment does not seem to be adversely affected by the large amounts of radiated power. Several ideas were tried to alleviate this problem but none seem at all effective.

The ultraviolet source lamp can be driven by a steady DC discharge as well as pulsed. The steady, cold cathode type discharge produces predominately atomic or molecular line spectra. There is a hydrogen continuum extending from about 0.16μm to 0.35μm. An example of this continuum is shown in Figure 2; this spectrum was taken with an effective band pass of 7 A using the 1/2 m Seya-Naimoka monochromator with the 2500 A blazed grating. The quartz envelope of the photomultiplier tube prevented detection of radiation whose wavelength is shorter than about 0.17μm. The multiline spectra of hydrogen and argon are shown in Figures 3 and 4. The same combination of monochromator and source was used to generate and disperse the radiation as the continuum. A different photomultiplier tube, one which is sensitive to radiation in range from 0.11μm to 0.18μm, was used and the hydrogen pressure in the lamp was much lower than when the continuum radiation was of interest. The wavelength band pass was 7 A again, which is the theoretical value when the 100 micron slits are used. The appearance of an underlying continuum in each of these spectra is false; the lines are very wide in appearance and overlap because of the astigmatism present in the

monochromator. The Seya-Naimoka design is well known to suffer a large degree of astigmatism which can be corrected by the use of curved slits and special grating shapes. These corrections are not incorporated into the present instrument.

The line intensities in Figures 3 and 4 are essentially zero for wavelengths shorter than 0.12μm. This is simply because the grating efficiency is very low at these short wavelengths. The monochromator is usually equipped with the 1000 A blazed grating when operating with radiation shorter than about 0.15μm.

The reflectance of magnesium oxide was measured relative to the barium sulfate standard and the results for the wavelength region from about 0.13μm to 0.3μm are displayed in Figure 6. An attempt was made to measure the reflectance of water frost and the mineral Bloedite at these short wavelengths. No satisfactory data could be collected due to the extremely low intensities encountered at wavelengths below about 0.2μm. A sample of high purity magnesium fluoride powder was obtained and will be tested to determine whether it can serve as a suitable standard reflector. There also is the possibility of using a matte gold surface as the reflectivity standard in the vacuum ultraviolet.

Barium Sulfate Reflectance Standard.

Eastman White Reflectance Standard has been used as a comparison standard for all the reflectance measurements taken during this investigation. This material has been used as a diffuse reflectance standard for a number of years, but questions pertaining to its suitability as a standard remain. Several exhaustive studies of the absolute reflectivity and stability

have been made over the past ten years with somewhat differing conclusions. Apparently water can be adsorbed on the surface of the material and thus give rise to spurious bands at the usual water positions in the infrared. Further, the absolute reflectance at short wavelengths, below 3000A, is not well characterized. This could be a stability problem in which the ultraviolet radiation causes photodecomposition of the barium sulfate or other changes such as those observed to occur in magnesium oxide reflectance standards. No indication of such changes in the standard have been noted here, but the standard is usually changed when a new sample is prepared. When working with a succession of water frosts, the standard is not changed as often; however, no variations in the results have been attributable to changes in the standard in these experiments.

For reference, the sample holder and the standard holder were packed with the barium sulfate reflectance material and the reflectance of the sample measured. Figure 5 shows the reflectance of the barium sulfate in the sample position as measured against the standard. The reflectance should be identically 1.02 throughout the entire spectral region where measurements were made. In this case, data was obtained from about 5.5μm to 0.2μm. The sample and standard reflector do not lie in the same plane, but the sample is approximately 5mm behind the standard. Consequently the geometry of the source, sample, and light collecting mirror is slightly different from the geometry of the source, standard, and mirror. The geometry

of the optical system yields a phase angle* of 33° for the standard reflector and 31° for the sample. Both the standard and the sample are illuminated normally so that the angle of emergence is equal to the phase angle. Assuming that the material obeys Lambert's law, then the ratio of the measured intensities is equal to the ratio of the cosines of these angles. This yields 1.02 as the expected reflectance. The reflectance is seen to be about 0.87 throughout most of the region. The absolute reflectance of barium sulfate is near 1.00 over this range but it is of no consequence since the sample and standard are the same material. The explanation of this 0.15 difference probably is that the image formed by the light collecting mirror is in a different position for the sample and standard. The 5 mm change in the object position causes a 30 mm shift in the image position. The size of the image and the amount of astigmatism change corresponding to the object position shift. The mirror is rotated to bring the beam back onto the detector but it cannot be refocused. Apparently about 15% of the light is not being detected when the sample is measured as compared to when the standard is measured.

The result obtained in the infrared shows that the reflectance is more nearly 1.0 or slightly greater in the span from 2.5μm to 5.5μm. The results in this region are less

---

*The phase angle is defined here to be the angle between the chief incident ray and the chief emergent ray to the center of the collecting mirror.

reliable due to the poorer signal-to-noise ratio and the small signal values measured. Small errors in the intensity values result in large errors in the intensity ratio when both values are small. The greater noise in the data is clearly evident in this infrared portion where the noise contributes to yield a standard deviation of roughly ±0.1. A standard deviation of about ±0.03 is a good description of the results obtained at shorter wavelengths. Since the image positions, sizes and degree of image quality remain the same in the infrared as in the visible, no ready explanation can be put forward as to why the infrared result is in better accord with theory than the visible result. If anything, one would expect a larger deviation from the expected reflectance of 1.02, since the size of the InSb element is smaller than the photocathodes of the photomultiplier tubes. Thus a greater fraction of the radiate energy will not strike the sensitive element. Apparently the same fraction of the available energy reflected by the standard strikes the detector as when the sample is the reflector.

There are two systematic changes in these data in addition to the random noise. There seems to be a small decrease in the reflectance at 1.0μm from 0.87 to 0.82 at 2.5μm. This is probably not a real change and the reflectance should be constant somewhere near 0.87 or so. The reflectance is constant from 1.2μm to 0.3μm. From about 0.3μm to 0.2μm the reflectance increases from 0.86 to somewhat less than 0.95. This is just the region in which previous workers have

encountered varying absolute reflectance values for this material. The results plotted in this Figure are relative reflectances so that if this increase is real, as it appears to be, there must be some other cause. A definite increase in reflectivity of water frost shortward of 0.3μm indicates that the standard is absorbing strongly in this region. If barium sulfate does absorb strongly at wavelengths less than 0.3μm, then deviations from Lambert's law can be expected. These deviations could cause the relative reflectivity to show an increase.

Magnesium Oxide Reflectance Standard.

The material used as a white reflectance standard in the past has been freshly prepared magnesium oxide. This standard is usually made by smoking a substrate with the oxide produced by burning magnesium ribbon in air. The oxide can also be prepared by heating strongly several magnesium compounds, e.g., carbonate and hydroxide. Magnesium oxide was prepared by firing very high purity hydroxide powder at 900°C for three days. After cooling in a desiccator, this material was packed into the sample holder so that a layer approximately 2 mm thick was obtained. A freshly dried barium sulfate standard was also provided.

Figure 6 shows the measured reflectance of this magnesium oxide sample relative to the barium sulfate. It is clear that this material is a poorer reflector than the barium sulfate; the reflectance varies from about 0.75 to 0.55. There is a sharp band near 1.4μm but no clear evidence for absorption at

1.9μm. This indicates that a small amount of hydroxide did not dehydrate to the oxide or atmospheric water could have reacted with the oxide to reform the hydroxide. There also appear to be two broad bands centered near 0.3μm and 0.35μm in the ultraviolet. Transition metals generally have absorptions in this region but the sample analysis showed less than 0.005% heavy metals combined. Thus, these bands may be due to some unknown instrumental error that went unnoticed during the experiment. There is also a general decreasing trend of the reflectivity with increasing wavelength. The reflectivity is near 0.75 at 0.4μm and steadily decreases to near 0.55 at 2.0μm. The absolute reflectance of freshly prepared magnesium oxide is 0.98 or better throughout the visible region. The absolute reflectance of magnesium oxide is not much different from the barium sulfate in the visible region. There does not seem to be a ready explanation for the result that the observed barium sulfate reflectivity is around 0.87 while the magnesium oxide is 0.75 to 0.55. It is possible that the re-hydrated oxide could be the reason for the observed decline in reflectivity as the wavelength increases. These results using ostensibly pure magnesium oxide are somewhat puzzling and further work is needed using MgO freshly prepared by burning magnesium ribbon. Using MgO made in this way should clarify this behavior by indicating that either the previous sample was the cause or some instrumental error has been overlooked.

An attempt was made to determine the reflectivity of the

magnesium oxide relative to that of barium sulfate in the far ultraviolet. The results are shown in Figure 6 where a strong band is seen near 0.16μm. This band may be due to either the MgO or the $BaSO_4$. Barium sulfate has been reported to be a useful reflectance standard to 0.16μm but, as discussed above, its absolute reflectivity is still in question shortward of 0.3μm. It is encouraging to note that although the noise level is high, about ±0.1, these results agree with another portion in the 0.2μm to 0.3μm region. The sample and the standard were unchanged during this entire experiment. The portion of the spectrum from 0.1μm to 0.3μm was obtained using the 1/2 m Seya-Namioka monochromator and the hydrogen discharge discussed in a previous section. The portion from 0.2μm to 0.7μm was obtained using a deterium lamp and tungsten filament lamp with the 1/4 m Ebert monochromator. The spectra from 0.2μm to 0.3μm show the reflectivity of MgO to be about 0.75 decreasing to around 0.65 at the longer wavelength. The portion of the spectrum from 0.1μm to 0.2μm appears to fit into the general trend. It is surprising that the reflectivity is 0.9 or greater for radiation approaching 0.1μm. Bear in mind that these are relative measurements and the absolute reflectance is very small. In all cases the signal was quite small and noisy; the standard deviation in this data appears to be near ±0.1.

Barium Sulfate as a Lambert Scatterer.

The reflectance standard barium sulfate has been shown to obey Lambert's law. This law states that the observed

intensity is proportional to the cosine of the incident angle and to the cosine of the angle of emergence. Written in this form:

$$I_{sam} = I_o \cos i \cos e.$$

As explained previously, the geometry of the sample and standard are not exactly the same, so we write this relation for the standard as

$$I_{std} = I_o \cos i' \cos e' .$$

The standard is always presented to the incident beam so that $i' = 90°$. Further, the position of the light collecting mirrors is such that the phase angle is given*

$$\phi = e+i = 31°$$

$$\phi' = e' + i' \approx 33°.$$

The sample plane can be rotated and provides a 60° or more variation in incident angle with values ranging from about -20° to +40°. The sample can be rotated in a complete revolution, but, due to the thickness of the sample holder, an edge will receive the incident radiation instead of the sample plane. This effectively restricts the angular range to 60°.

The reflectance of the barium sulfate in the sample holder was measured in the visible region as a function of the angle of incidence. These reflectivity measurements are presented in Figure 7. This Figure shows that the curves are parallel to one another and are displaced on the intensity

---

*We take the angle of incidence as negative when the incident and emergent rays lie on the same side of the normal.

scale by varying amounts depending on the angle of incidence. The reflectivity at 0.5μm and at each angle was taken directly from the numerical data listing. The points are also shown in this Figure. To determine whether Lambert's law is obeyed in this instance, the data are fit with the full line graph of the equation:

$$R = I_{sam}/I_{std} = \cos i \cos e/\cos e' .$$

There are no free parameters in this expression which can be adjusted to fit the points. Examination of this result shows that allowing for a standard deviation of ±0.02 the data points are fit very well except at the 40° angle of incidence. It is possible that edge effects are contributing to this point because the sample holder is circular. The upper and lower portion of the lip of the sample holder may be illuminated slightly. Since the holder is gold plated and rough, additional radiation may be scattered onto the light collecting mirror from this surface. This additional radiation may be why the point is about 0.05 greater than the expected Lambert curve.

In general, the description of the barium sulfate standard as a Lambert type diffuse reflector is valid in the visible region and angular range investigated. Based on previous worker's results, barium sulfate would appear to be a Lambert reflector for wavelengths greater than 0.3μm on out to 5μm or more. The behavior of this material at shorter wavelengths does not seem as certain. Additional measurements need to be taken at the short wavelengths in an effort to determine whether this material can serve as a working standard.

Water Frost.

The spectroscopic properties of water in various forms have been studied for a long time. This investigation has presented some data which in general agreed with previous workers. Several samples of water frost have again been investigated; the principal objectives of these experiments were to determine the dependence of the frost reflectance on crystal morphology, illumination angle, and temperature. Figures 8 and 9 show photomicrographs of two frost samples. Figure 8 shows a very coarse frost; the crystallites were block-like with the larger individuals estimated to be 0.5 mm across. Circular rings can be seen in these photographs; they are remnants of machining tool marks. This sample was more like a sheet of ice which had developed a cracked and crazed surface but remained fairly transparent. The other frost shown in Figure 9 was a fine grained sample consisting of a mass of fine crystals with a few long needle-like crystals on the sharp corners of the sample holder. The white areas in both sets of photographs are due to specular reflection from properly oriented crystallites. The plane of the sample is parallel to the film plane and the illumination is at an incidence angle of 45° to the sample. An estimate of the size of the individual crystals can be obtained by noting that the graticule has 50 microns as the smallest division.

The reflectance of the coarse frost shown in Figure 8 is presented in Figure 10 and is labeled sample A. The reflectance of the fine grained frost shown in Figure 9 is presented in Figure 11 and is sample B. The reflectance

spectra of several more frost samples are shown in Figures 12 to 15. Although no photographic documentation is presented due to a shutter mechanism failure in the camera, these were all fine grained frost samples except perhaps sample C shown in Figure 14. This sample may not have been a fine grained frost sample. A fine grained, optically thick frost sample can be produced with an appropriate combination of vapor flow rate, pressure and substrate temperature. Samples with reproducible spectroscopic properties can be achieved with care. A problem with aging of water frost samples was noted and is illustrated by the frost sample shown in Figure 8. Generally a frost sample requires several hours to grow to become optically thick, usually 3 mm or more of frost is formed on the substrate. The vapor pressure in the experiment chamber is adjusted to be in the range 10 to 50 milliTorr by throttling the vacuum pump and adjusting the vapor flow rate. When a suitable frost sample is formed, the vapor flow is discontinued and the remaining water vapor pumped out to reach a pressure in the 10^{-6} Torr range. The vapor pressure of solid water at 160K is in the 10^{-7} Torr range. But the construction of the Cryo-Tip is such that there is a large amount of frost formed along the cold end which is at much higher temperatures. The vapor pressure of this material can be in the high 10^{-4} Torr range. Thus, if the sample chamber is continuously pumped, the frost sublimes away and there is no sample in about eight to ten hours. On the other hand, if the experiment chamber is isolated from the pump, the pressure increases and the vapor transports heat from the

chamber walls which are at room temperature to the remaining solid. This energy is removed by the sample cooling system. Water is a notoriously poor thermal conductor and apparently it can happen that the "hot" vapor molecules can cause surface heating on the frost. This energy at the sample surface can melt the crystallites or otherwise cause major changes in the sample morphology before the heat can be removed by the Cryo-Tip. A run-away process begins; the quantity of vapor increases and the pressure increases with more heat transported to the remaining sample. Soon the refrigeration capacity of the sample cooler is exceeded and the sample melts.

The frost sample shown in Figure 8 was formed late in the day and was originally a fine grained dense frost. It was allowed to stand overnight isolated from the vacuum pump. The next morning the sample temperature had warmed from 160K to about 190K and the chamber pressure was above 1 Torr. The sample's appearance had changed markedly. It looked very coarse, as if the original sample had melted and refrozen and had cracked and crazed on freezing. This behavior has not been observed before because either the frost was not "saved" overnight or not visually observed after long standing. Now samples are not retained for long periods, but a new one is formed for each data collecting run. The chamber pressure is monitored and when it reaches the low 10^{-3} Torr range, the chamber is re-evacuated to the 10^{-6} Torr region. In this way the sample morphology is unchanged while only a small amount of material is removed, since about six inches of cold-end have a frost coating which is warmer than the sample. Some

material which sublimes from the warmer portions of the cold-end recondenses onto the sample substrate. This is not believed to interfere with the measurements because the vapor is removed quickly as the pressure begins to show on the thermocouple pressure gauge. Further, the experiment time is kept as short as possible and the area of the sample substrate is reasonably large, ca 2500 mm^2, so that only a thin additional coating would be expected. No simple method of testing whether this is in fact true suggests itself; however, no systematic trends in the data have been observed which can be attributed to changing sample thickness with time. Differences among the results obtained with various samples have been seen which are due to different thickness, but no variations within a single sample data set caused by changing thickness have been observed.

The reflectance spectra of the various water frost samples are presented in Figures 10 to 15 and show some interesting similarities and differences. Previous work presented water frost experiments which indicated that the reflectance was featureless from 0.21μm to 0.8μm with strong absorption shortward of 0.2μm and the strong near infrared bands near 1.3μm and broad unresolved system at 1.5μm were seen. The visible reflectivity from 0.21μm to 0.8μm was measured to be about 0.80 to 0.85 with no established variations in absorption outside these limits. The data presented were taken using a thick, fine grained frost. Examination of the results shown in Figure 10 shows a considerably different behavior. This is the coarse grained frost which perhaps is

better described as an ice sheet. The reflectivity shows absorption in the ultraviolet and into the blue-green to about 0.5μm where it slowly increases to about 0.55 and becomes constant at this value from 0.7μm to 1.2μm or so. Water is essentially transparent from 0.25μm to 1.0μm and this data is the reflectivity of the gold plated sample holder viewed through the ice sheet. The reflectivity of gold is small, only about 0.35 at wavelengths less than 0.5μm then gradually rising to about 0.95 at 0.7μm. The reflectance spectra in this Figure mirrors this behavior out to wavelengths in the near infrared where the water is no longer transparent. The water band systems at 1.3μm, 1.5μm, and 1.9μm are clearly evident. The gold plating is probably not influencing the observed reflectance beyond about 1.2μm. Because of the strong water absorptions in this region, the radiation is absorbed or scattered before penetrating to the ice-gold interface. In other words, the sample is optically thick in the infrared region; whereas, it is not optically thick in the visible region. Frosts and other materials become optically thick when the number of scattering centers and absorption centers together with their cross sections become large enough to insure that the radiation will be totally removed from the incident beam. Statistically this would require an infinitely thick layer, but this condition is met when the measured reflectance becomes independent of the sample depth. The physical thickness necessary is less the greater the concentration of scattering and absorbing centers. This sample does meet the conditions to be optically thick in

the infrared on the basis of water being a strong absorber in this region.

Figure 11 displays the reflectance of the fine grained frost pictured in Figure 9. The ultraviolet, visible, and near infrared, 0.4μm to 1.2μm, reflectance is nearly constant and about 0.80 throughout. The infrared portion from 1.0μm to 3.0μm is very similar to that presented in Figure 10 except that the overall reflectivity is increased by 15%. Work with powders has shown that the reflectivity of not too strongly absorbing materials increases as the mean particle size decreases. In regions of strong absorbance, the reflectivity is little influenced by particle size. The absorption bands at 1.5μm and 1.9μm appear much deeper and sharper in the spectra of the fine grained frost when compared with the coarse grained frost. The reflectance of the coarse grained sample near 1.5μm is shown on an expanded scale in Figure 13; the reflectivity is 3% or less in this region. Light scattering within the monochromator and the optical system has not been determined, but 1% to 2% would be about what might be expected overall. Thus, the absorption is essentially total from 1.5μm to 1.6μm for the coarse grained frost, but as much as 0.20 is reflected from the fine grained frost. A similar statement can be made about the absorption band at 1.9μm. These results need to be verified and further data gathered and analyzed closely in view of the uncertainties concerning the nature of the coarse grained frost and the amount of scattered light in the optical system.

It has been previously reported that water frost has a temperature dependent absorption band at 1.67μm. This band is clearly seen in the reflectance spectra of both the coarse and fine grained frost. The coarse grained frost was cooled to 100K and the near infrared reflectance measured from 1.2μm to 2.5μm. These results are shown in Figure 12. This spectrum is very similar to that taken when the frost sample was cooled to 160K. The absorption bands appear to be a bit sharper at the lower temperature and a bit more resolved structure near 1.4μm is evident in the spectrum of the cooler sample. The region from about 1.5μm to 1.7μm is shown on an expanded scale in Figure 13. The band at 1.67μm shows clearly in these data and note that the data taken at 100K show a smaller reflectivity at all wavelengths in this region, but due to the uncertainties expressed above, no quantitative statement will be made. It may be fortuitous that the band at 1.67μm is stronger in the spectrum taken with the 100K sample temperature, but the absorption is clearly there at these two low temperatures.

A third water frost sample was made and its reflectance spectrum is given in Figure 14. No photographs were taken, but it was noted that the sample appeared to be a fine grained frost. The spectrum does not agree with this observation. The frost shows a featureless spectrum from about 0.35μm to 1.0μm, but the reflectivity is only about 0.60 throughout. The bands at 1.3μm, 1.5μm, and 1.9μm are shown strongly by this sample and the infrared features of this sample and those shown in Figure 10 for the coarse grained ice are very

similar. This third sample, C, appears to be a coarse grained frost which is optically thick in the visible as well as in the near infrared. It may have been a fine grained frost when first made, but later was subject to local surface melting and recrystallization yielding a much coarser grained material. The visible reflectance was measured as a function of angle of incidence by rotating the sample holder about its vertical axis. The spectra taken at five angles of incidence and emergence are shown in Figure 15. As the angle of incidence is increased to -10 and then -20 degrees, the reflectance decreases accordingly. But when the angle of incidence is increased to +10 and then to +20 degrees, the reflectance remains about constant instead of increasing as the angle increases. The reflectance behavior is inconsistent if water frost is a simple Lambert reflector. The angular dependence of the reflectivity of water frost was investigated further and the results discussed below. These data indicate that fine grained water frost could be described as a Lambert reflector as a good first approximation. The spectra of the frost shown in Figures 14 and 15 are not those of a fine grained, optically thick sample. This sample was probably a coarse grained, optically thick sample which would be consistent with these results.

Two more frost samples were made which were fine grained and closely monitored to detect any changes in crystal habit which might occur. The vapor pressure in the experiment chamber was carefully watched and not allowed to exceed a few microns before being removed. The sample was visually

observed every third data run and no changes were perceived in the structure of either sample. Only portions of the spectrum were investigated and these pieces are presented in Figure 16. The portions of spectrum taken at zero angle of incidence agree closely with the corresponding portions of the spectrum shown in Figure 11. All of these frosts are fine grained samples and their spectra appear to be identical.

The reflectance at seven separate wavelengths is plotted as a function of angle of incidence. This plot is Figure 17. The data at each wavelength is fitted with a Lambert type function where the maximum intensity, R_o, was chosen for best fit. The form of the function was again taken to be

$$R = R_o \cos i \cos e/\cos e' .$$

In the case of these water frosts, R_o is a free parameter chosen for goodness of fit by trial and error. The quality of each data point does not warrant an elaborate fitting procedure; an error of several percent would seem to be a conservative estimate based on past experience.

The fit of these data by a Lambert type function appears to be a good description of these results. Table I gives the wavelength at which the intensity was determined at each angle. The intensity values were taken from the data which is graphed in Figure 16. The value of the parameter R_o, giving the fit shown, is listed along with the wavelength values. Examination of the curves in Figure 17 shows that the fit of the Lambert function appears to be equally good for each wavelength. The wavelengths chosen include the relatively flat reflectance region extending from the ultraviolet into the near infrared

as well as wavelengths near the minimum absorption at 1.5μm. Several wavelengths at relative reflectance maximums in the infrared were also selected. Thus, these results imply that water frost acts as a Lambert reflector throughout this spectral region. Further data are required to confirm this conclusion especially data taken at greater angles of incidence. The points taken at 20 degrees angle of incidence and short wavelength all lie considerably above the Lambert fit curve. This may just be due to error in the data or a departure from Lambert scattering. Further data taken at the larger angles of incidence are in order and will be of value in determining the reflectance behavior of water frost.

Bloedite, California.

A portion of the Bloedite crystal fragments was dried in a vacuum oven at 200°C for three days. The portion dried was taken from the powdered sample investigated previously. This mineral is known to be a hydrated sulfate of sodium and magnesium. Some of the water of hydration is very loosely bound; whereas it appears that some molecules are well integrated into the crystal structure. Previous work indicated that this material could be completely dehydrated by moderate heating under vacuum. The results presented here do not agree with this conclusion; there is strong evidence of water remaining in the sample. On the other hand, an unheated sample which presumedly has considerable water of hydration can lose part of this water when placed in vacuum. The sample has been lost on several occasions due to shrinking as the sample dehydrates.

Spectra of the Bloedite sample at 295K and 160K are presented in Figures 18 and 19, respectively. The spectrum taken at room temperature clearly shows broad bands near 1.4μm, 1.9μm, and 2.5μm which are diagnostic of water. When the sample temperature was reduced to 160K, the absorptions at these wavelengths increase and appear somewhat sharper, but they are still very broad. The absorption near 1.4μm has the appearance of a step followed by a broad flat plateau and a small rise in reflectance near 1.8μm. This band is quite strong in the case of water frost and some fine structure has been observed. The noise level is too great to discern any positive fine changes in reflectance in this band in Bloedite. The same statement can be made for the water bands at 1.9μm and 2.5μm.

The reflectance throughout the visible and near infrared remains nearly constant with a reflectivity of 0.70 to 0.75. There may be an absorption band near 0.5μm, but it appears weak and the noise level is about ±0.04 there which is very nearly the band depth. Previous spectra of this material showed two weak bands at 0.7μm and 0.78μm which were attributed to ferric iron. No clear indication of these bands can be seen in either of these Bloedite spectra.

The bands at 0.7μm and 0.78μm were thought to be due to a form of hematite. The large Bloedite crystal has many inclusions of black material. When a portion of the crystal was ground to a fine powder, this black material was not reduced in size but remained as moderate size (≈0.5mm diameter) flecks. Since the inclusions are not uniformly distributed

through the crystal, it is likely that a given sample could contain only a small amount of this material. In this way these bands would be very weak and escape detection.

There is what appears to be a very broad band in the ultraviolet portion of the Bloedite spectra. The reflectivity begins to decrease around 0.35μm and shows a very shallow minimum about 0.25μm followed by an increasing reflectivity with shorter wavelengths. The reflectivity decreases from about 0.7 to 0.6 at the band minimum. A similar decrease in reflectivity was observed in previous spectra of Bloedite. An attempt was made to determine if this absorption is temperature dependent. Figure 20 shows the ultraviolet reflectivity of Bloedite at five different temperatures: 295K, 200K, 160K, 120K, and 80K. The broad shallow absorption is seen to extend from 0.33μm to 0.23μm, more or less. These five spectra all fall with a reflectance value of ±.02 of one another. The spectra do not show a trend with temperature to within this error. It must be pointed out that this absorption may in fact be due to the barium sulfate standard. These reflectance values are all relative to barium sulfate and are not corrected for changes in the absolute reflectance of the standard.[1] Thus the final conclusion as to whether this is an absorption due to Bloedite must wait until the absolute reflectivity of barium sulfate at short wavelengths is clarified. However, the reflectivity of Bloedite does not appreciably change with temperature within the ultraviolet region investigated and shown in Figure 20. This is a valid conclusion irrespective of the uncertainty in the standard

reflectance because the standard was unchanged during these measurements. It was only the temperature of the Bloedite sample that was varied and no detectable change occurred in the reflectance of the sample.

Sulfur, Louisiana.

A sample of natural elemental sulfur was reduced to a fine powder. Sulfur is a good reflector of infrared and visible radiation down to about 0.5μm. A strong absorption edge begins near 0.5μm and extends into the ultraviolet. The reflectivity of this sulfur sample is shown in Figure 21 covering the range from 0.35μm to 0.65μm. These spectra were taken with the sample at various temperatures as indicated in the Figure.

The reflectance is constant at about 0.80 for wavelengths longer than 0.5μm and is unaffected by the change in temperature. The statistical error is ±0.02 or less in the red end of the spectrum; it is less than ±0.01 toward the blue. Only a small amount of data taken in the ultraviolet is available which is due to the uncertainty in the absolute reflectance of the barium sulfate standard. The results for the shorter wavelengths, 0.4μm to 0.35μm, show that the reflectance is about 0.05 and here too it is not greatly affected by lowering the temperature.

The absorption edge from 0.5μm to 0.4μm is affected by changing the temperature. As the temperature decreases the edge becomes sharper in the sense that the reflectivity remains constant near 0.80 to shorter wavelengths before

decreasing quickly to the 0.05 level. Note that in all cases the reflectivity has reached its minimum value at 0.4μm irrespective of the temperature. Thus, the band position does not change just the slope of the long wavelength edge. On cooling from room temperature (295K) to 160K, the edge at half maximum shifted about 120Å toward shorter wavelengths. On further cooling to 80K the edge shifted an additional 20Å shortward. The data taken at 120K are not reliable in this region due to problems of electrical interference with the data acquisition system. Considering only the results taken at 295K, 160K, and 80K, it appears that the absorption edge is little influenced by temperatures below 160K. The actual band shift may be nearly complete at higher temperatures and a more thorough examination might be an interesting experiment. Also if a suitable standard at the short wavelengths can be found, then the reflectance of sulfur below 0.4μm would prove to be a useful and valuable experiment.

Acknowledgements

The author wishes to thank Dr. L. Lebofsky of the University of Arizona for his aid and fruitful suggestions during this study. I am grateful to Drs. F. P. Fanale, D. L. Matson, and T. V. Johnson of the Jet Propulsion Laboratory for their suggestions and support of this work. The assistance of Anival Ramirez and Paul Killam is gratefully acknowledged.

TABLE I

Intensity Parameter, R_o, for Water Frosts

Wavelength (μm)	Parameter, R_o
2.2	0.54
1.75	0.57
1.6	0.32
1.5	0.19
0.8	0.93
0.55	0.88
0.35	0.95

Figure Captions

Figure 1. Relative intensity of infrared radiation available at exit slit of monocrhomator using the 4μm blazed grating and the InSb detector. Part a includes a 1.9μm long pass filter. Part b includes a 3.4μm long pass filter.

Figure 2. Relative intensity of hydrogen continuum passed by the 0.5m S-N monochromator as detected by the UV-VIS PMT.

Figure 3. Relative intensity of hydrogen line spectrum passed by the 0.5m S-N monochromator detected by the solar blind PMT.

Figure 4. Relative intensity of argon line spectrum passed by the 0.5m S-N monochromator and detected by the solar blind PMT.

Figure 5. Reflectance of barium sulfate in the sample position and using barium sulfate as the standard. The sample and standard are at room temperature.

Figure 6. Reflectance of magnesium oxide in the sample position and using barium sulfate as the standard. The sample and standard are at room temperature.

Figure 7. Part a. Reflectance of barium sulfate as the sample and the standard is as a function of the angle of incidence.
Part b. Fit of the reflectance at 0.5μm to the Lambert function.

Figure 8. Photomicrograph of a coarse grained water frost. The smallest division on the scale is 50 microns.

Figure 9. Photomicrograph of a fine grained water frost.

Figure 10. Reflectance of the coarse grained water frost at 160K. Parts a, b, and c are taken with frost sample A shown in Figure 8.

Figure 11. Reflectance of fine grained frosts at 160K. Parts a, b, and c are frost sample B shown in Figure 9. Part e is frost Sample F.

Figure 12. Reflectance of fine grained frost sample A at 100K.

Figure 13. Examination of the 1.4μm water frost band at 160K and 100K. The fine grained frost, sample A, is shown.

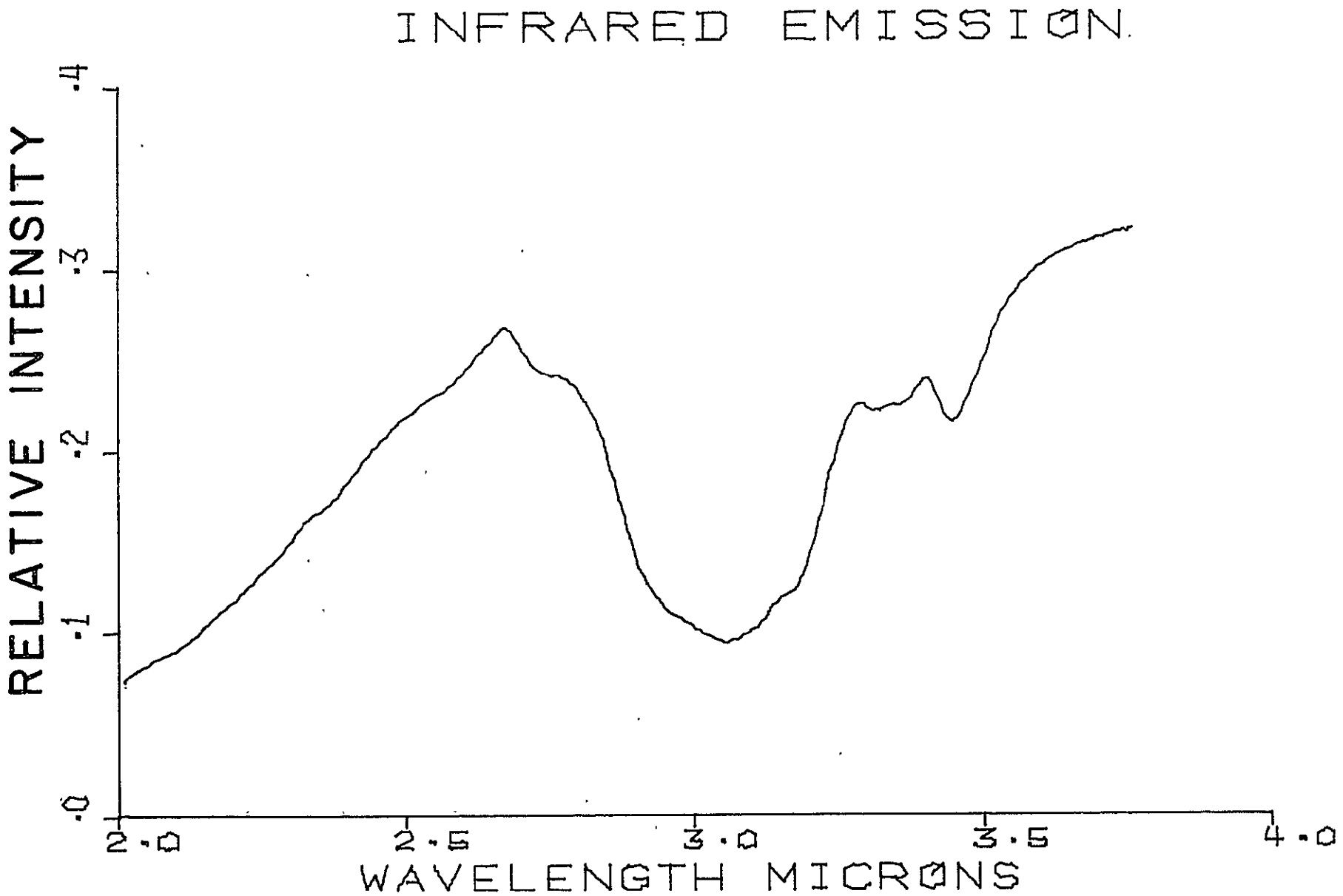
INFRARED EMISSION
RELATIVE INTENSITY
.0
.1
.2
.3
.4
2.0
2.5
3.0
3.5
4.0
WAVELENGTH MICRONS

FIG Ia

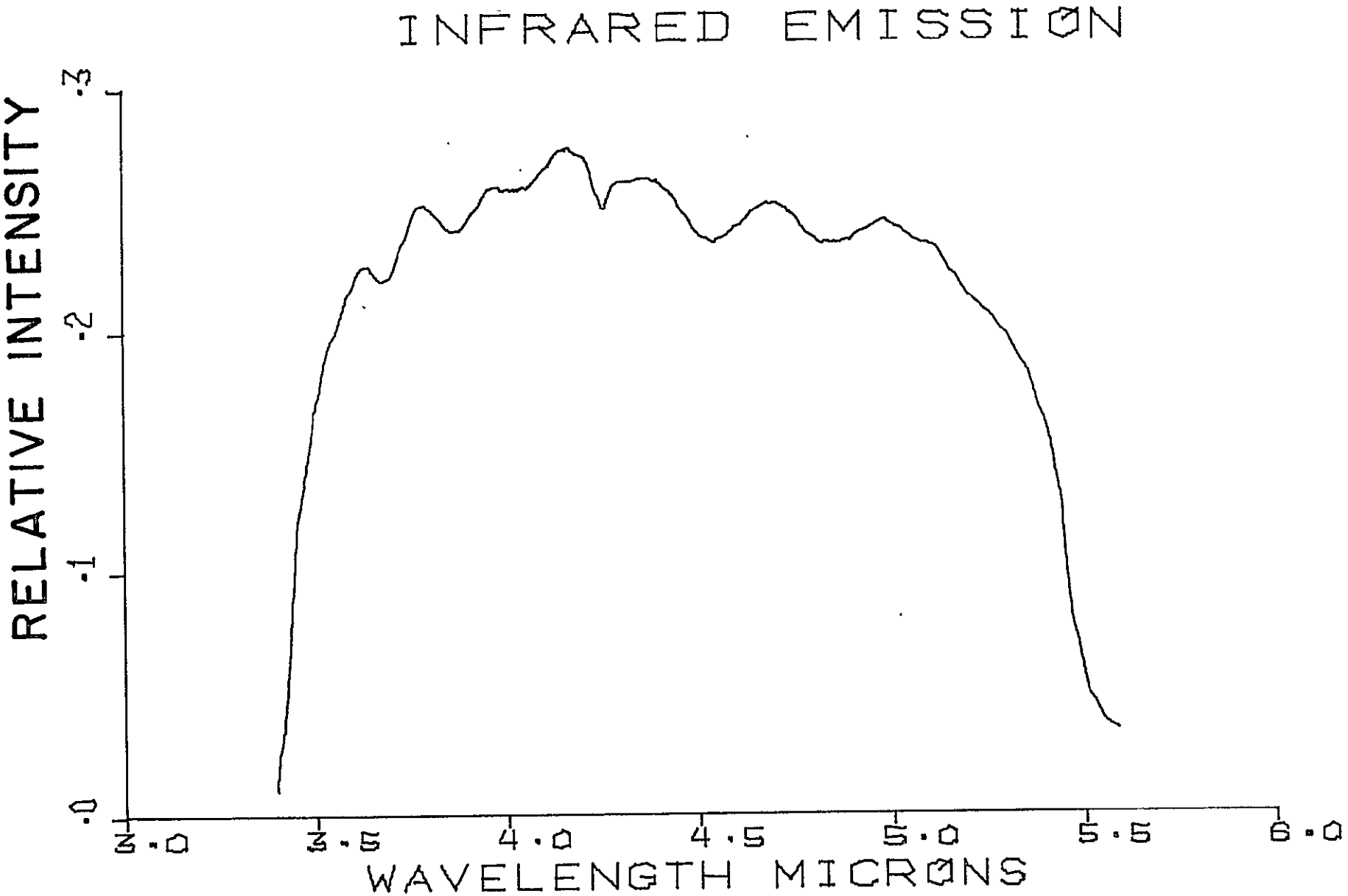
INFRARED EMISSION
RELATIVE INTENSITY
.0
.1
.2
.3
3.0
3.5
4.0
4.5
5.0
5.5
6.0
WAVELENGTH MICRONS

FIG 1b

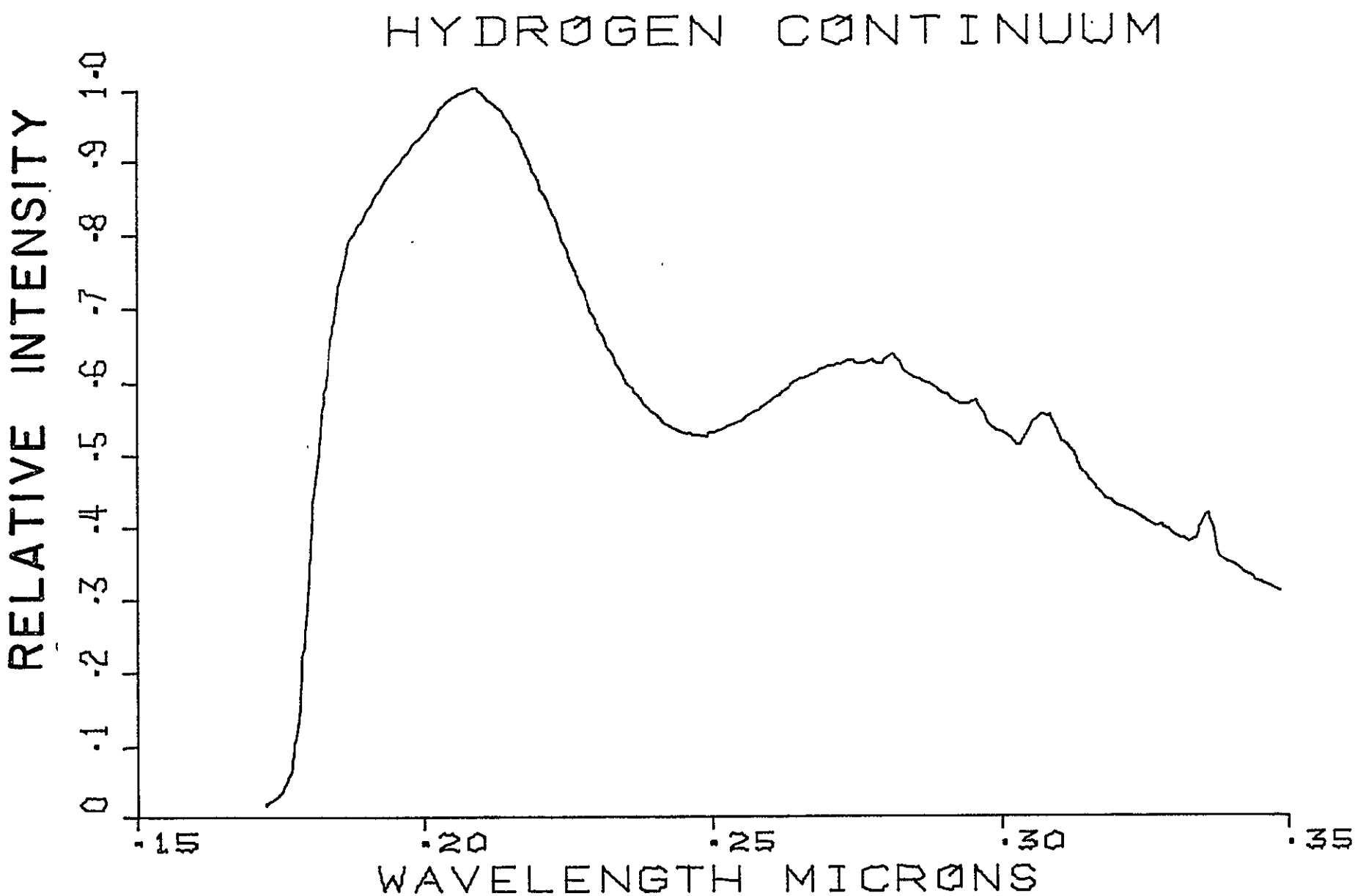
HYDROGEN CONTINUUM
RELATIVE INTENSITY
0
.1
.2
.3
.4
.5
.6
.7
.8
.9
1.0
.15
.20
.25
.30
.35
WAVELENGTH MICRONS

FIG 2

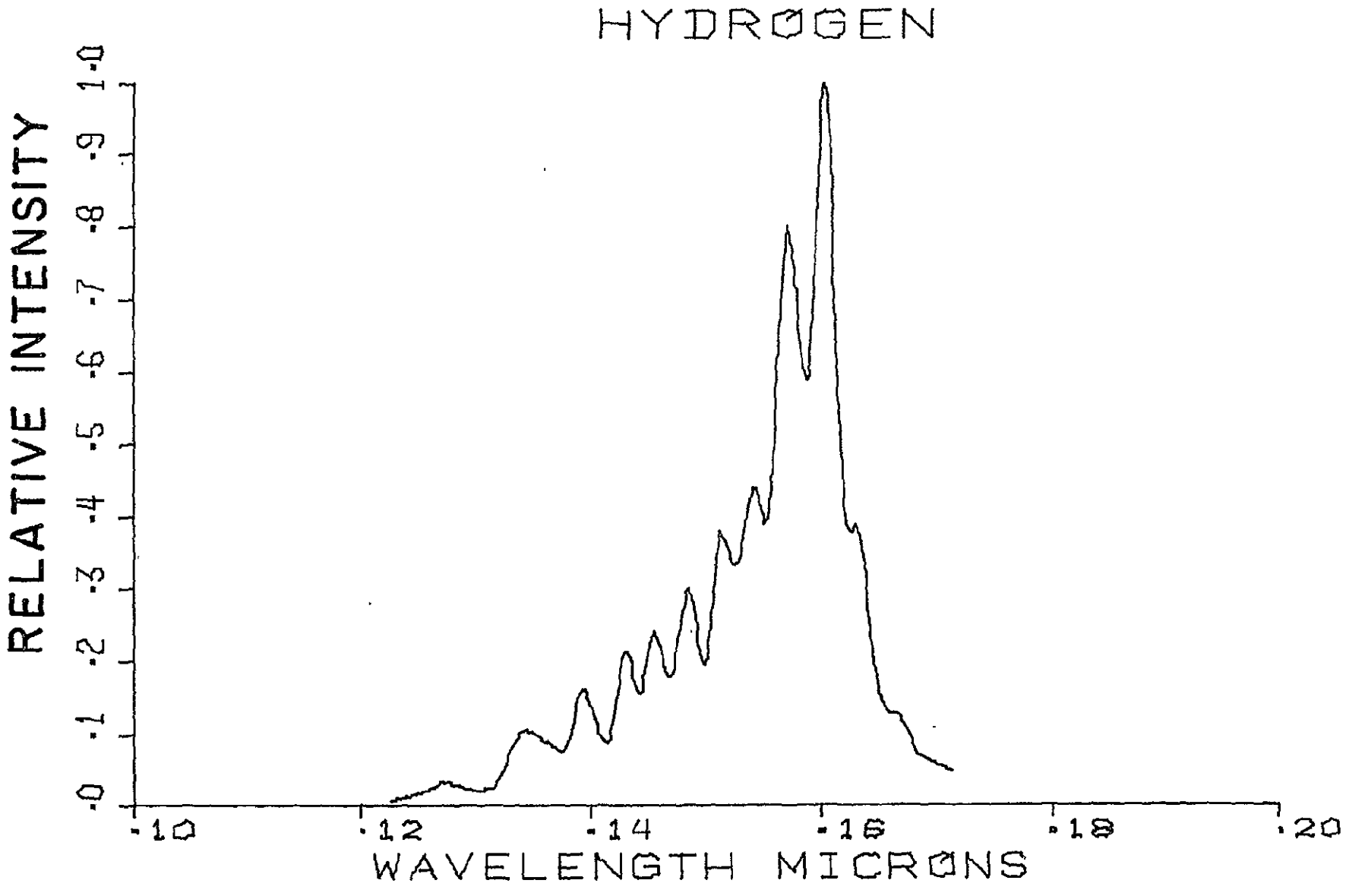
HYDROGEN
RELATIVE INTENSITY
.0
.1
.2
.3
.4
.5
.6
.7
.8
.9
1.0
.10
.12
.14
.16
.18
.20
WAVELENGTH MICRONS

FIG 3

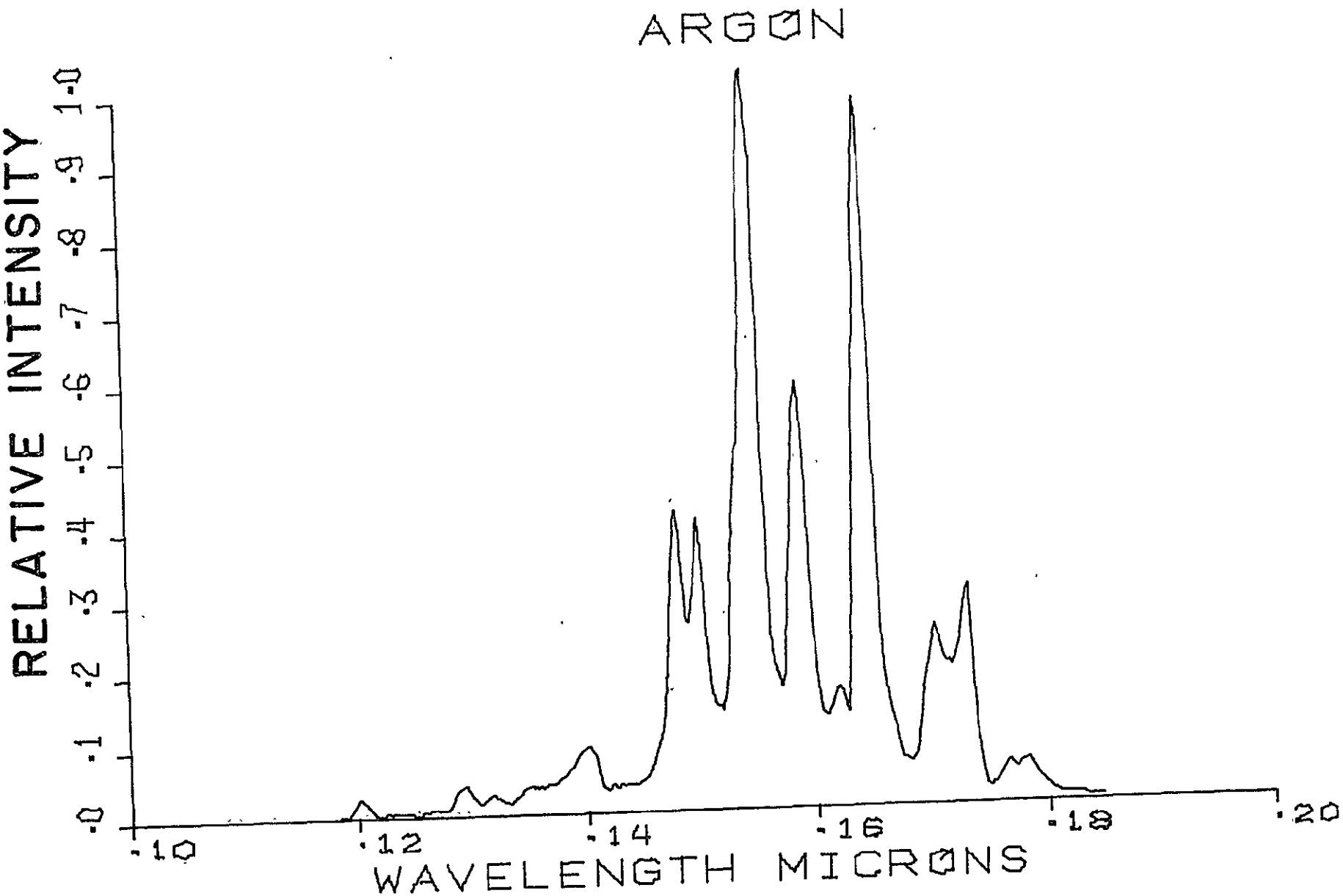
ARGON
RELATIVE INTENSITY
0
.1
.2
.3
.4
.5
.6
.7
.8
.9
1.0
.10
.12
.14
.16
.18
.20
WAVELENGTH MICRONS

FIG 4

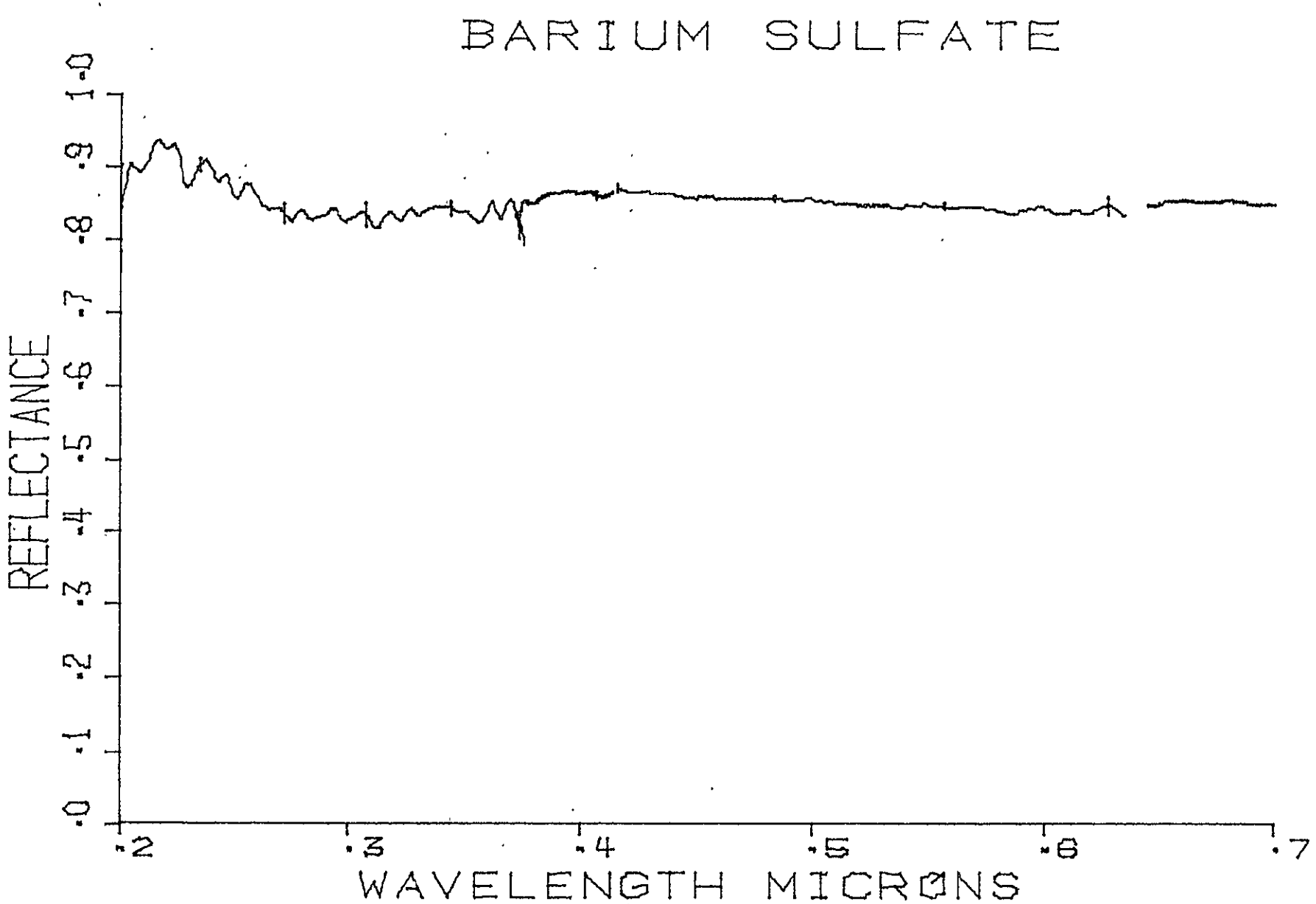
BARIUM SULFATE
REFLECTANCE
.0
.1
.2
.3
.4
.5
.6
.7
.8
.9
1.0
.2
.3
.4
.5
.6
.7
WAVELENGTH MICRONS

FIG 5a

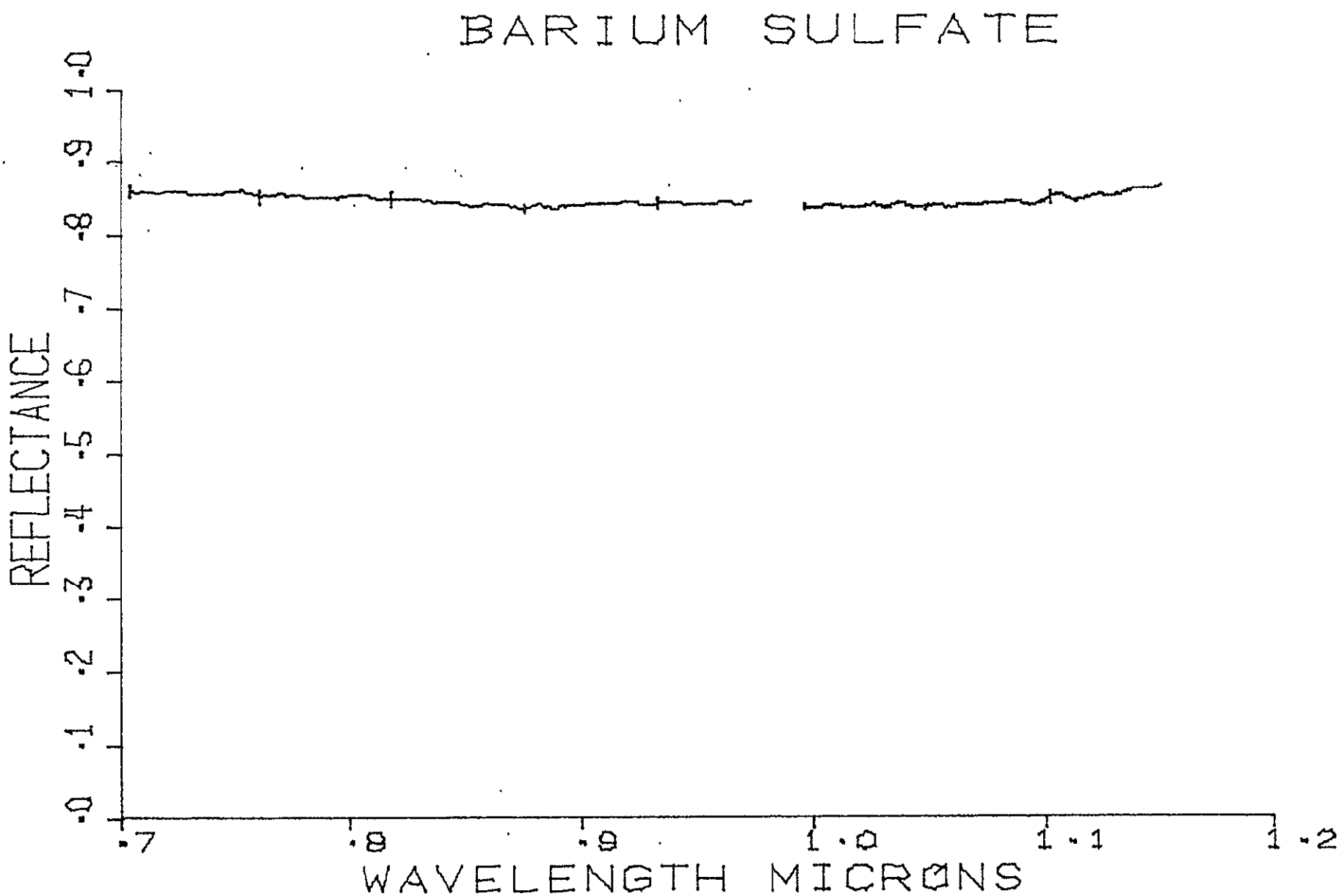
BARIUM SULFATE
REFLECTANCE
.0
.1
.2
.3
.4
.5
.6
.7
.8
.9
1.0
.7
.8
.9
1.0
1.1
1.2
WAVELENGTH MICRONS

FIG 5b

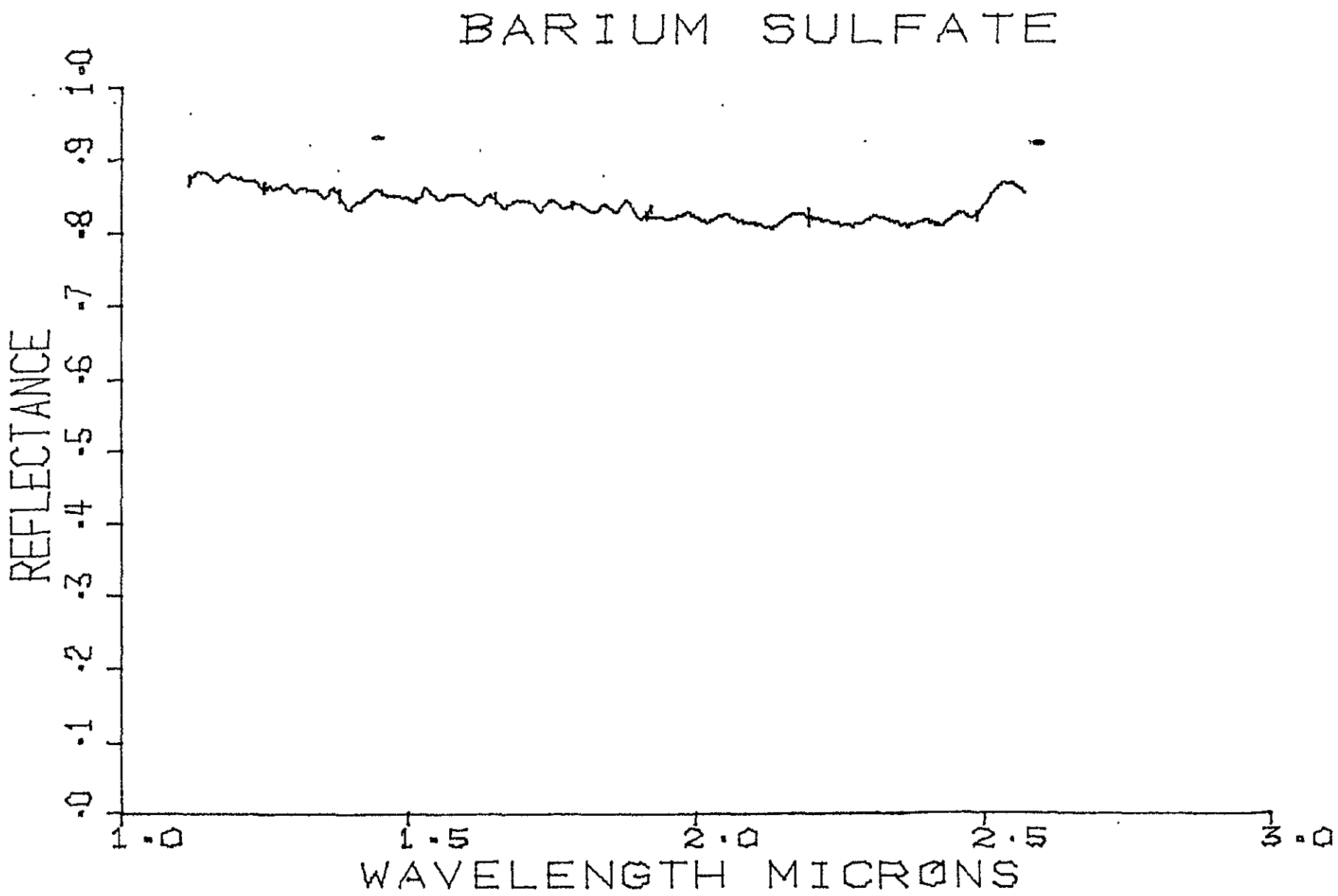
BARIUM SULFATE
REFLECTANCE
.0
.1
.2
.3
.4
.5
.6
.7
.8
.9
1.0
1.0
1.5
2.0
2.5
3.0
WAVELENGTH MICRONS

FIG 5c

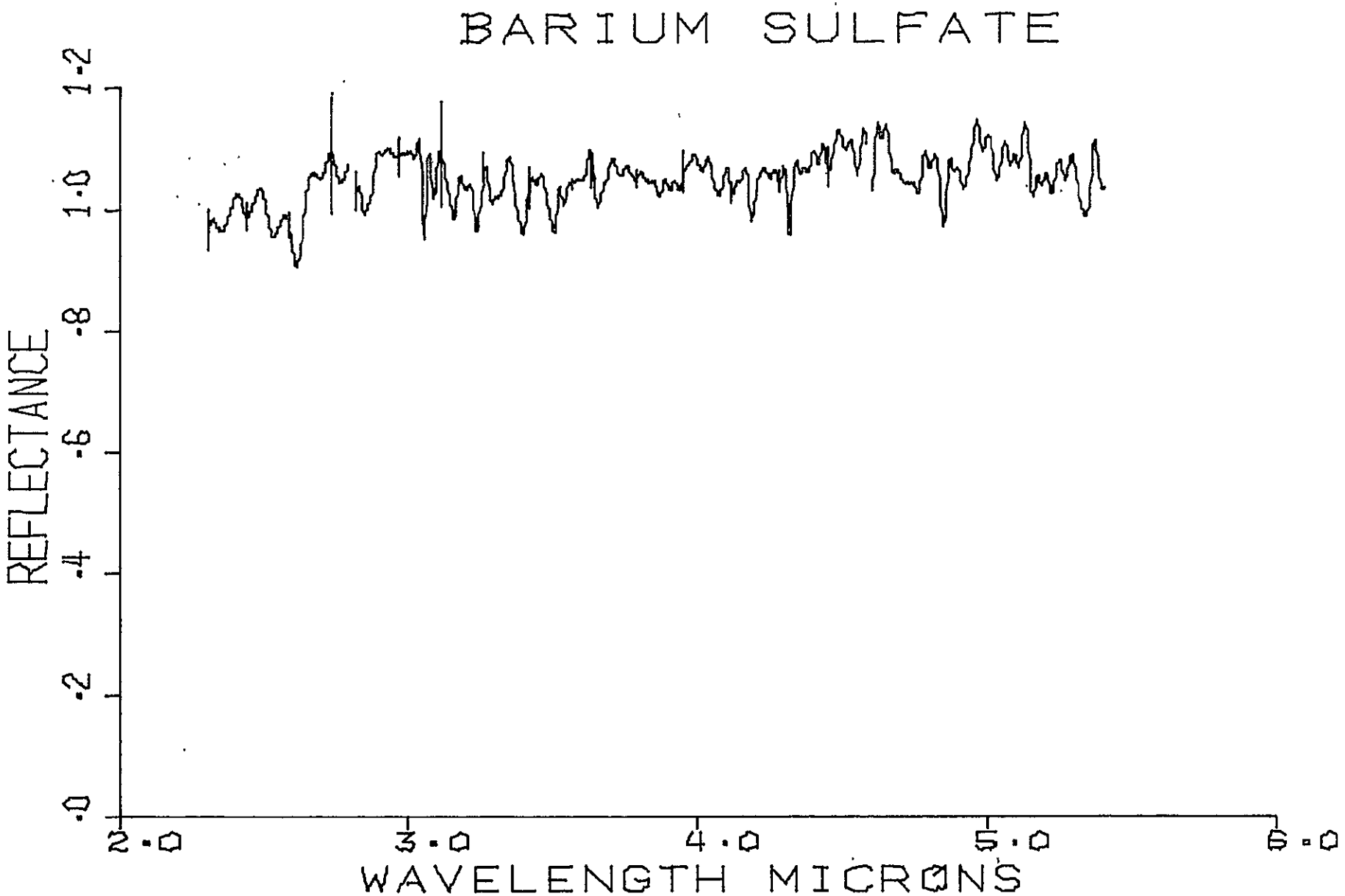
BARIUM SULFATE
REFLECTANCE
.0
.2
.4
.6
.8
1.0
1.2
2.0
3.0
4.0
5.0
6.0
WAVELENGTH MICRONS

FIG 5d

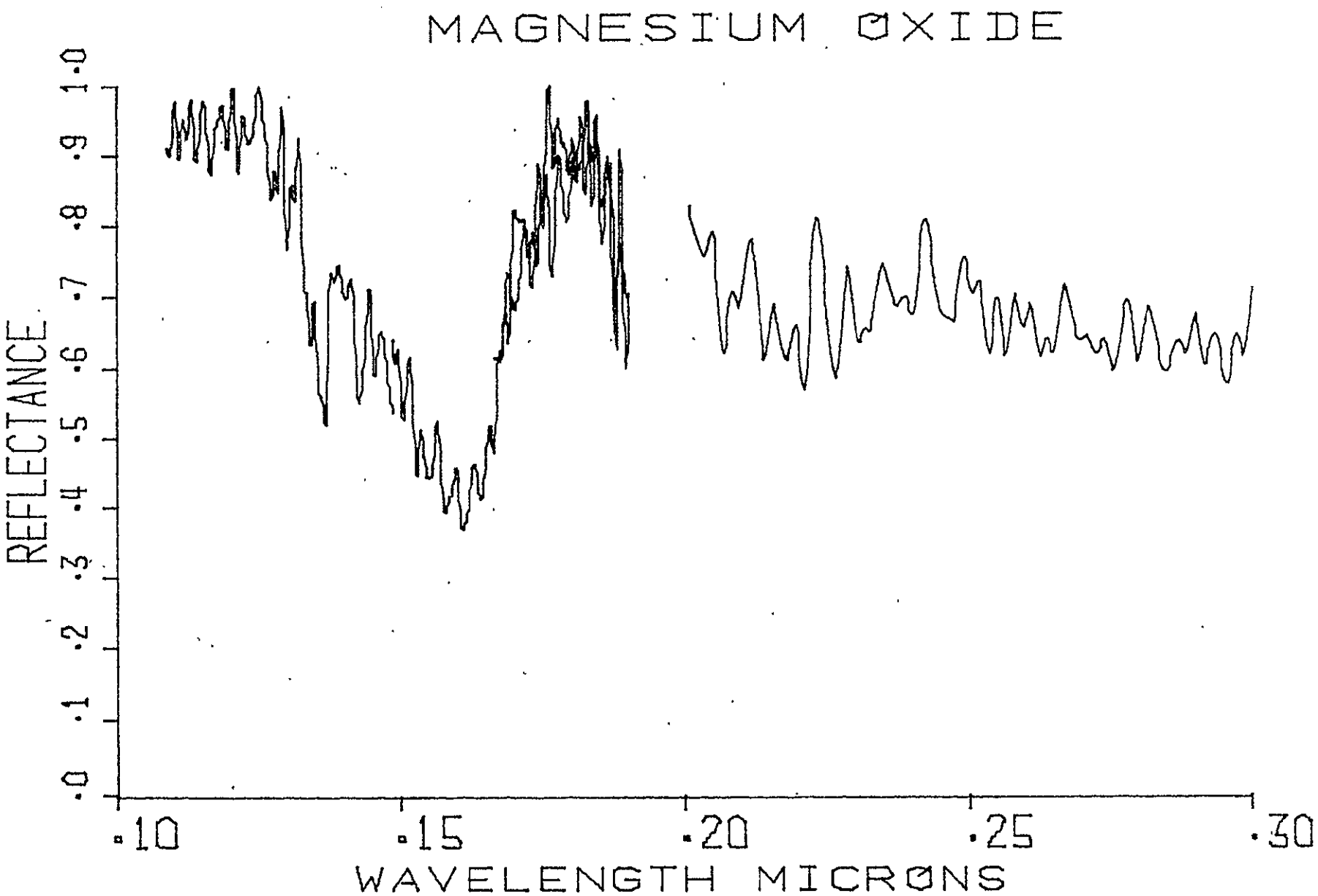
MAGNESIUM OXIDE
REFLECTANCE
.0
.1
.2
.3
.4
.5
.6
.7
.8
.9
1.0
.10
.15
.20
.25
.30
WAVELENGTH MICRONS

FIG 6a

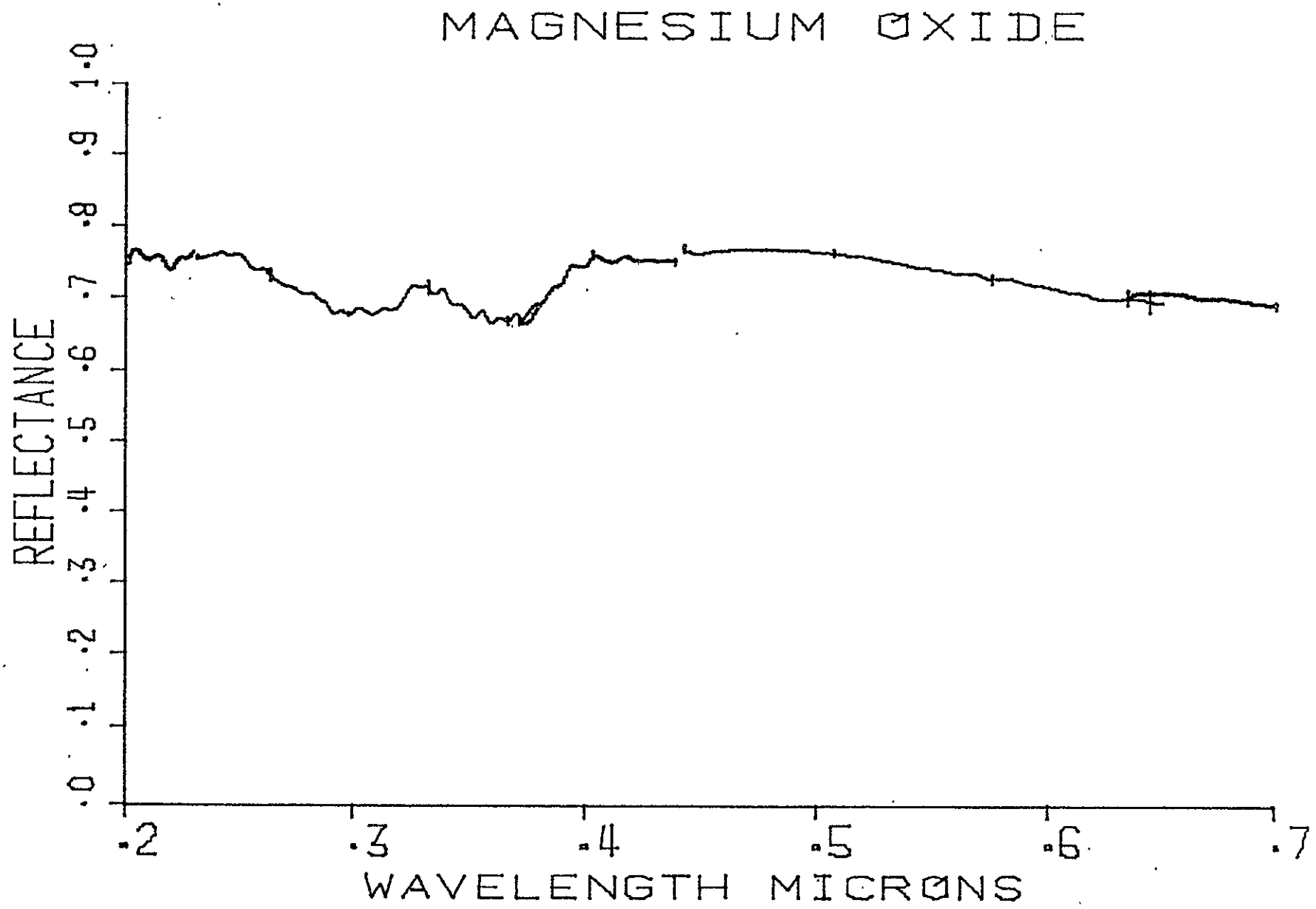
MAGNESIUM OXIDE
REFLECTANCE
.0
.1
.2
.3
.4
.5
.6
.7
.8
.9
1.0
.2
.3
.4
.5
.6
.7
WAVELENGTH MICRONS

FIG 6b

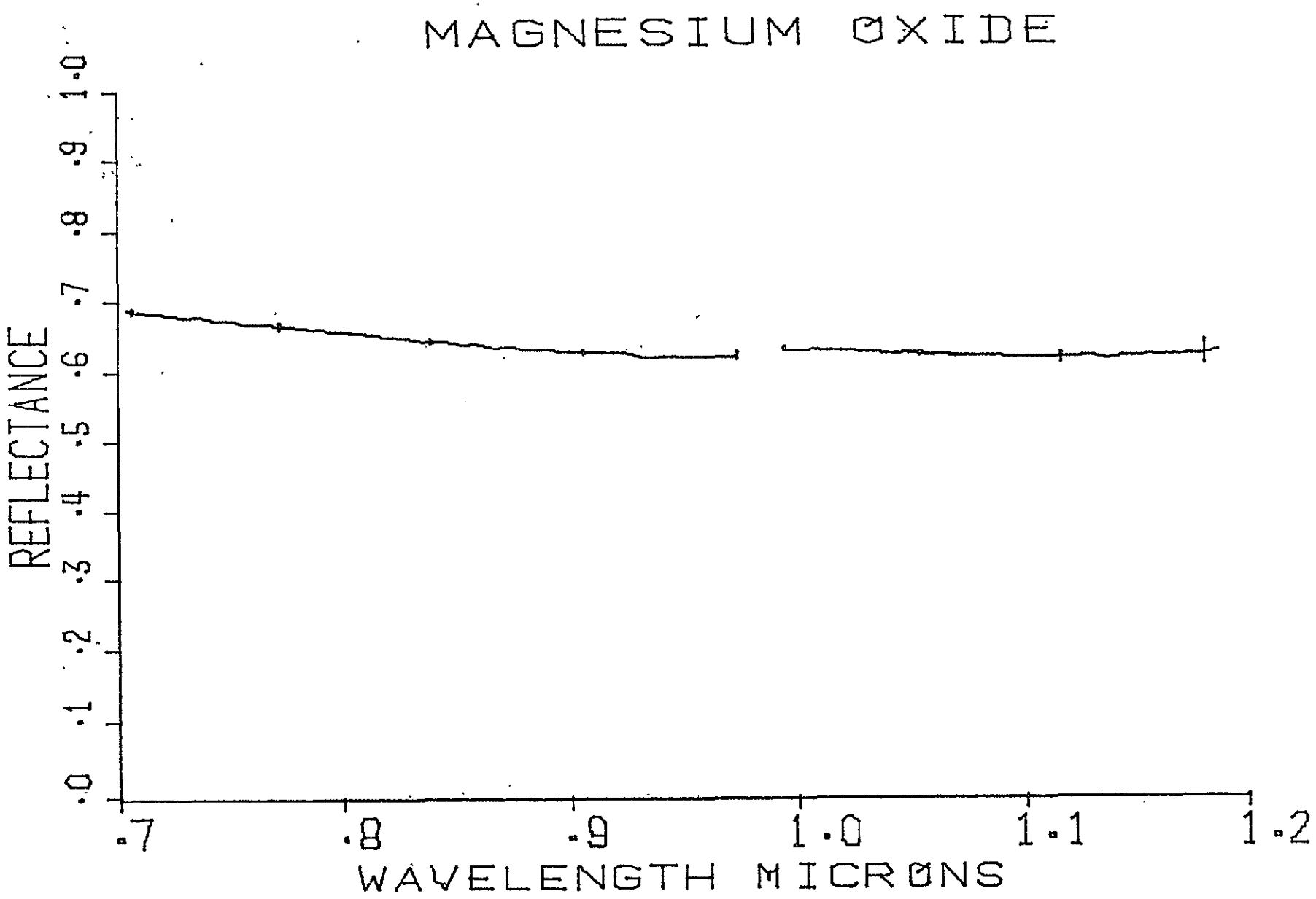
MAGNESIUM OXIDE
REFLECTANCE
.0
.1
.2
.3
.4
.5
.6
.7
.8
.9
1.0
.7
.8
.9
1.0
1.1
1.2
WAVELENGTH MICRONS

FIG 6c

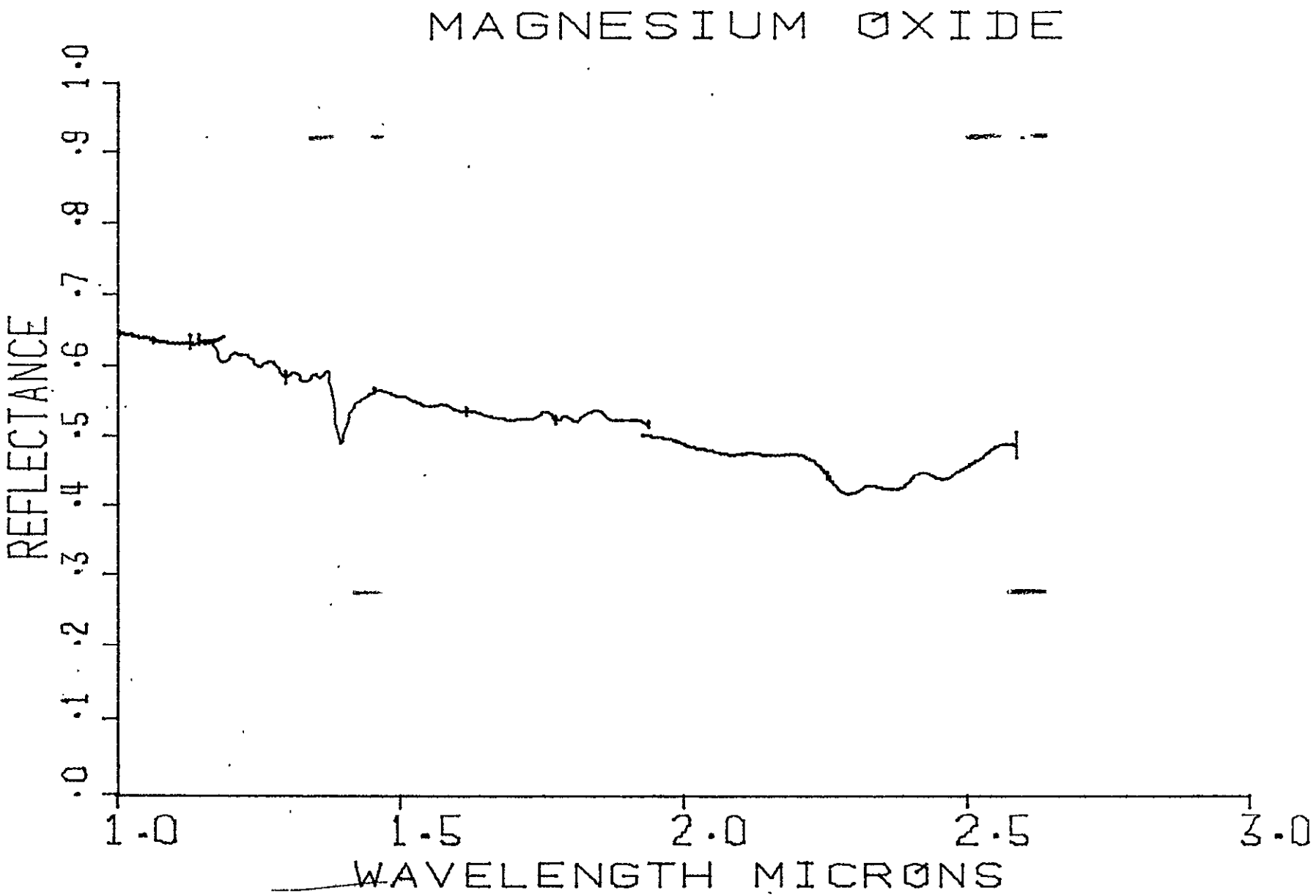
MAGNESIUM OXIDE
REFLECTANCE
.0
.1
.2
.3
.4
.5
.6
.7
.8
.9
1.0
1.0
1.5
2.0
2.5
3.0
WAVELENGTH MICRONS

FIG 6d

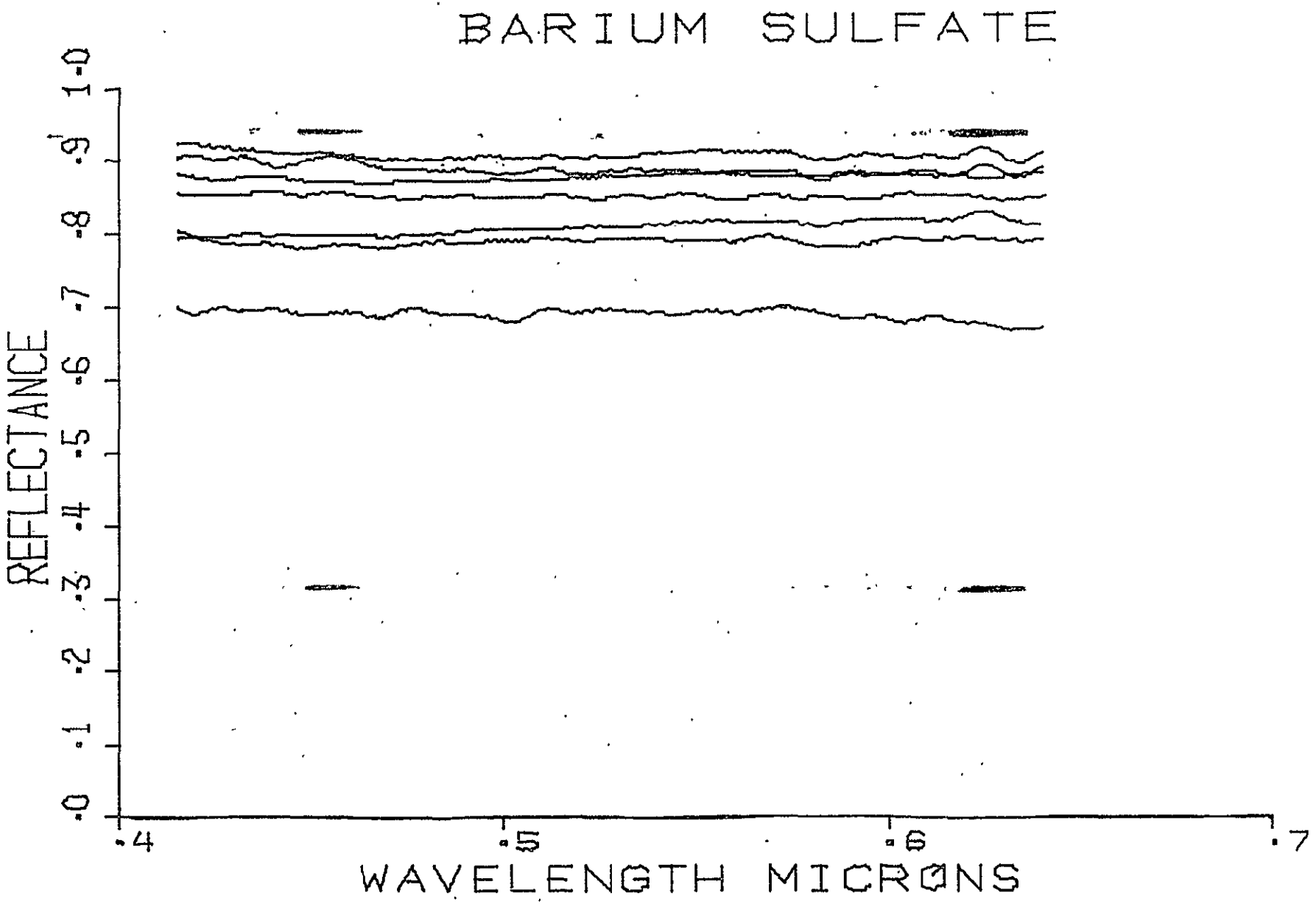
BARIUM SULFATE
REFLECTANCE
.0
.1
.2
.3
.4
.5
.6
.7
.8
.9
1.0
.4
.5
.6
.7
WAVELENGTH MICRONS

FIG 7a

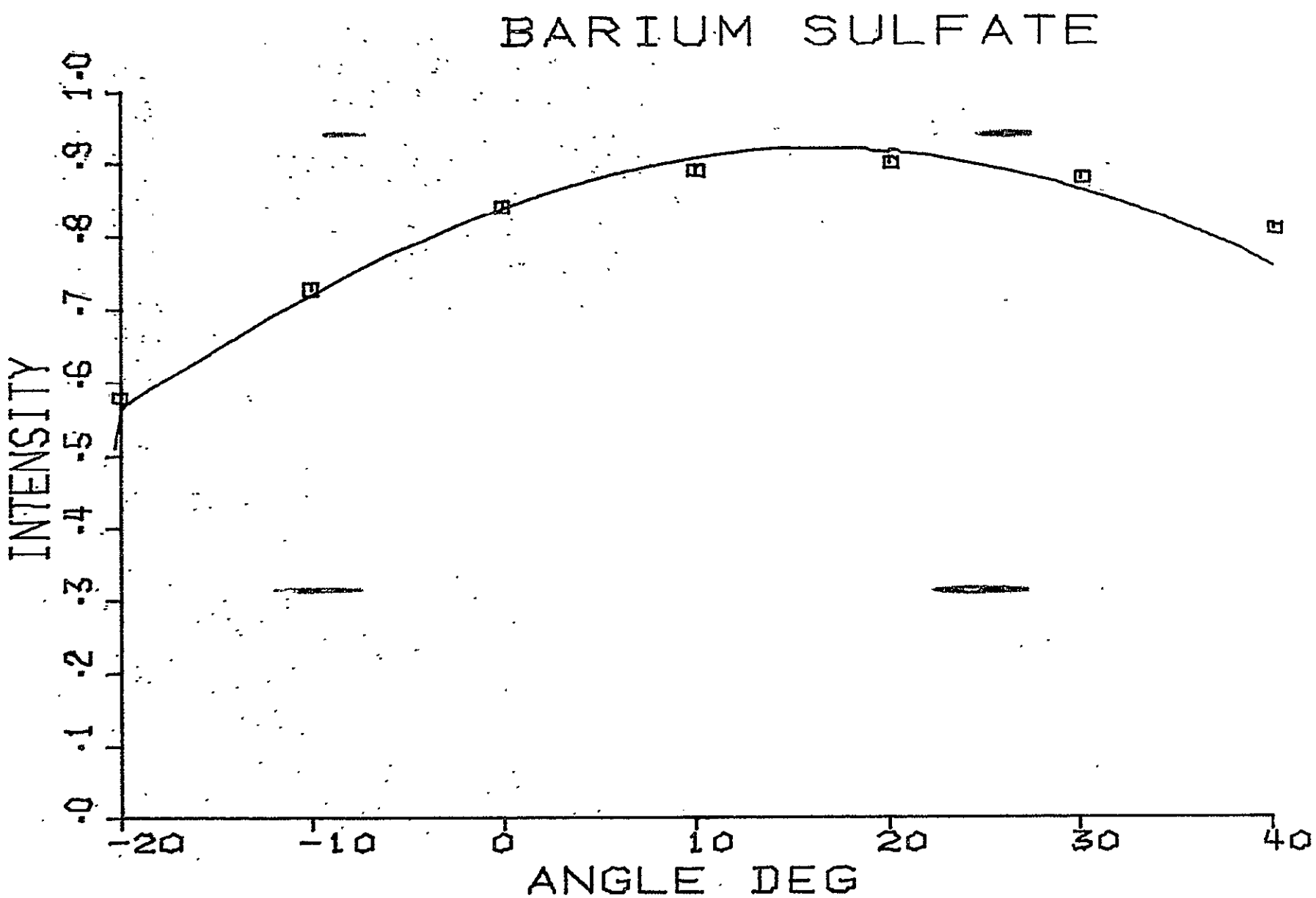
BARIUM SULFATE
INTENSITY
.0
.1
.2
.3
.4
.5
.6
.7
.8
.9
1.0
-20
-10
0
10
20
30
40
ANGLE DEG

FIG 7b

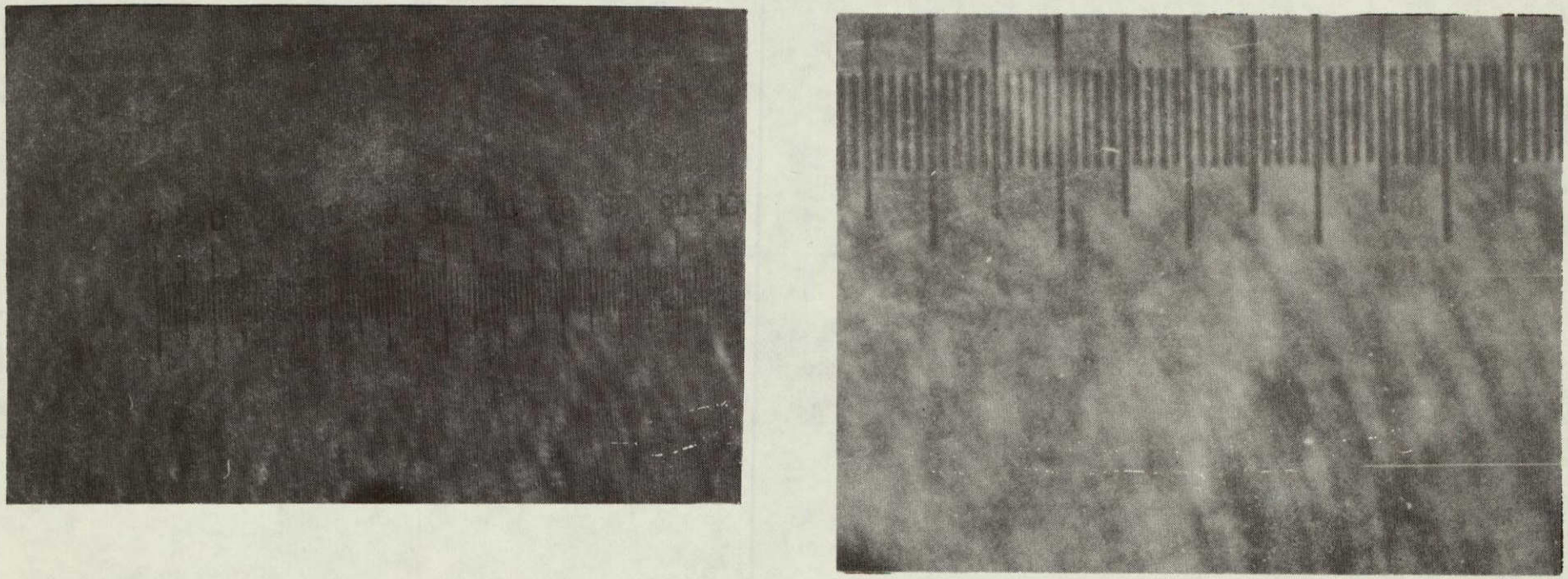

SAMPLE A

FIG 8

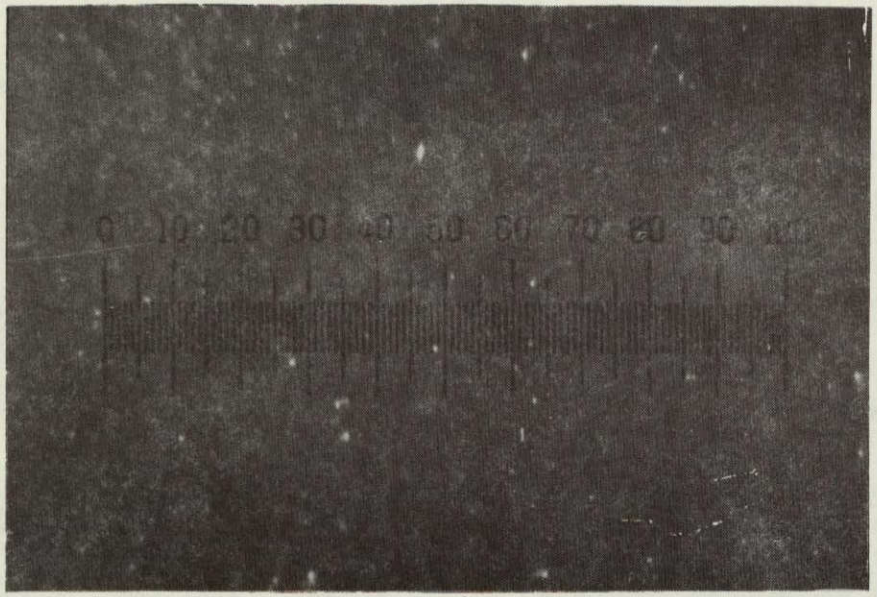

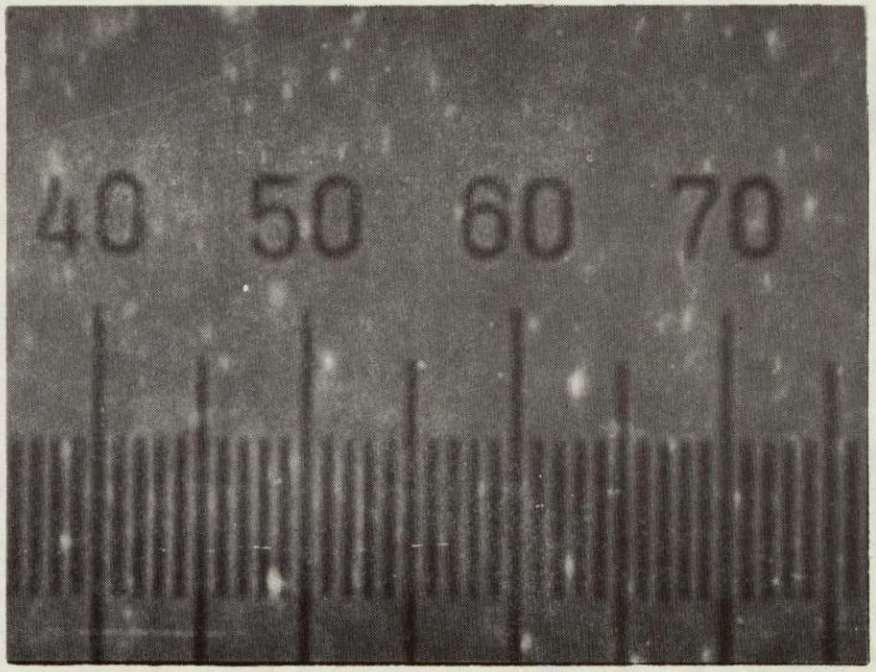

SAMPLE B

FIG 9

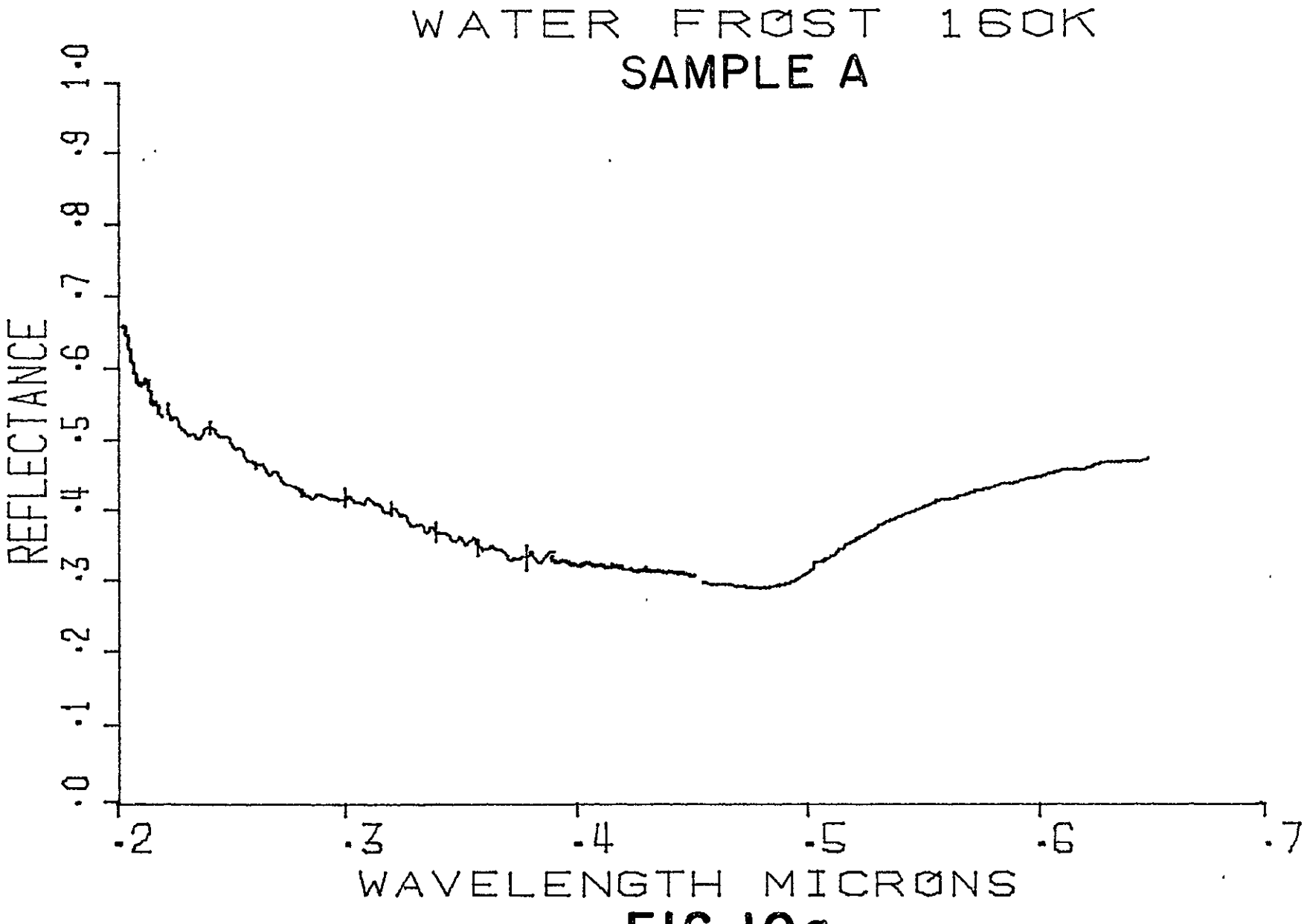
WATER FROST 160K
SAMPLE A
REFLECTANCE
.0
.1
.2
.3
.4
.5
.6
.7
.8
.9
1.0
.2
.3
.4
.5
.6
.7
WAVELENGTH MICRONS

FIG 10a

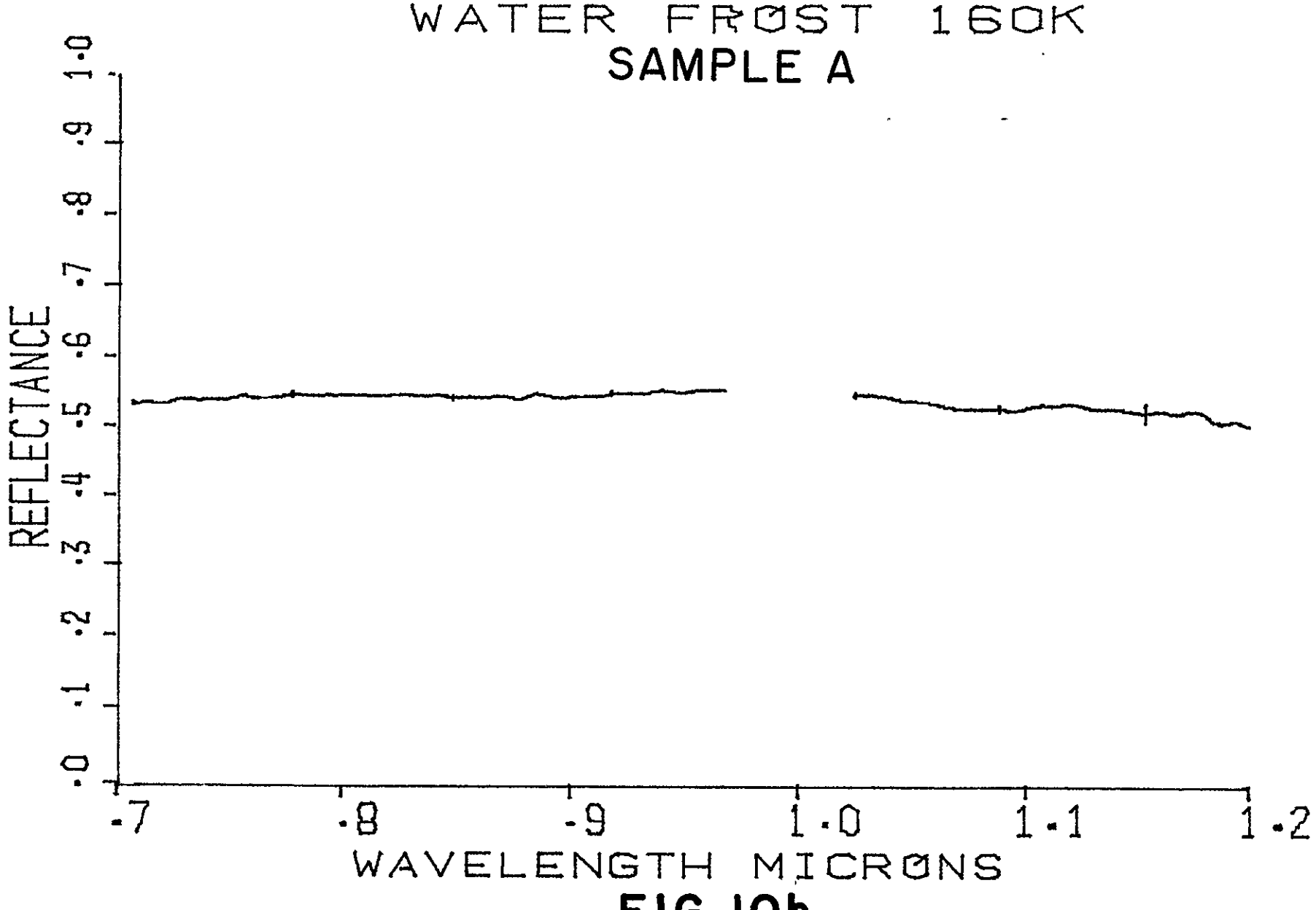
WATER FROST 160K
SAMPLE A
REFLECTANCE
.0
.1
.2
.3
.4
.5
.6
.7
.8
.9
1.0
.7
.8
.9
1.0
1.1
1.2
WAVELENGTH MICRONS

FIG 10b

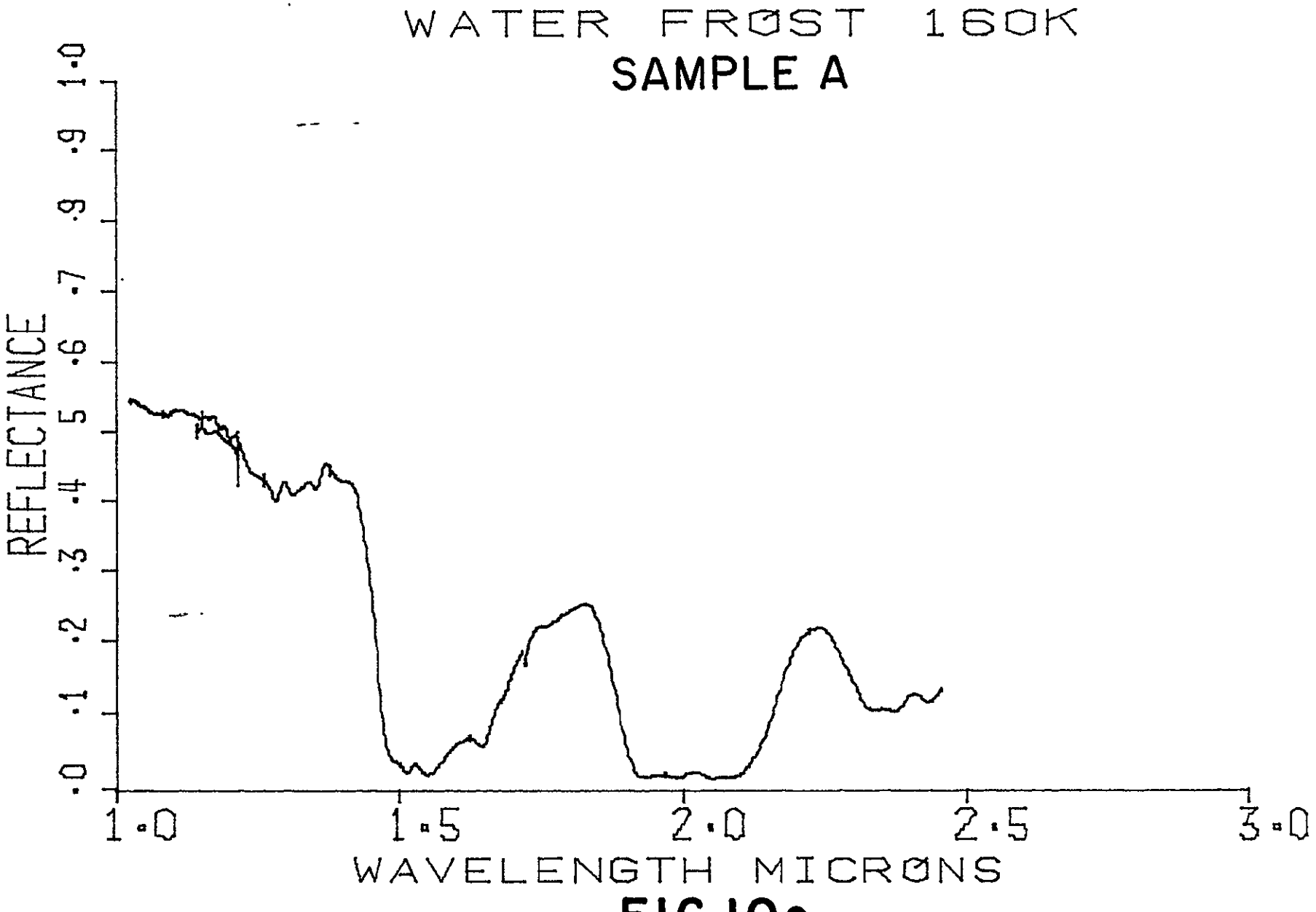
WATER FROST 160K
SAMPLE A
REFLECTANCE
.0
.1
.2
.3
.4
.5
.6
.7
.9
.9
1.0
1.0
1.5
2.0
2.5
3.0
WAVELENGTH MICRONS

FIG 10c

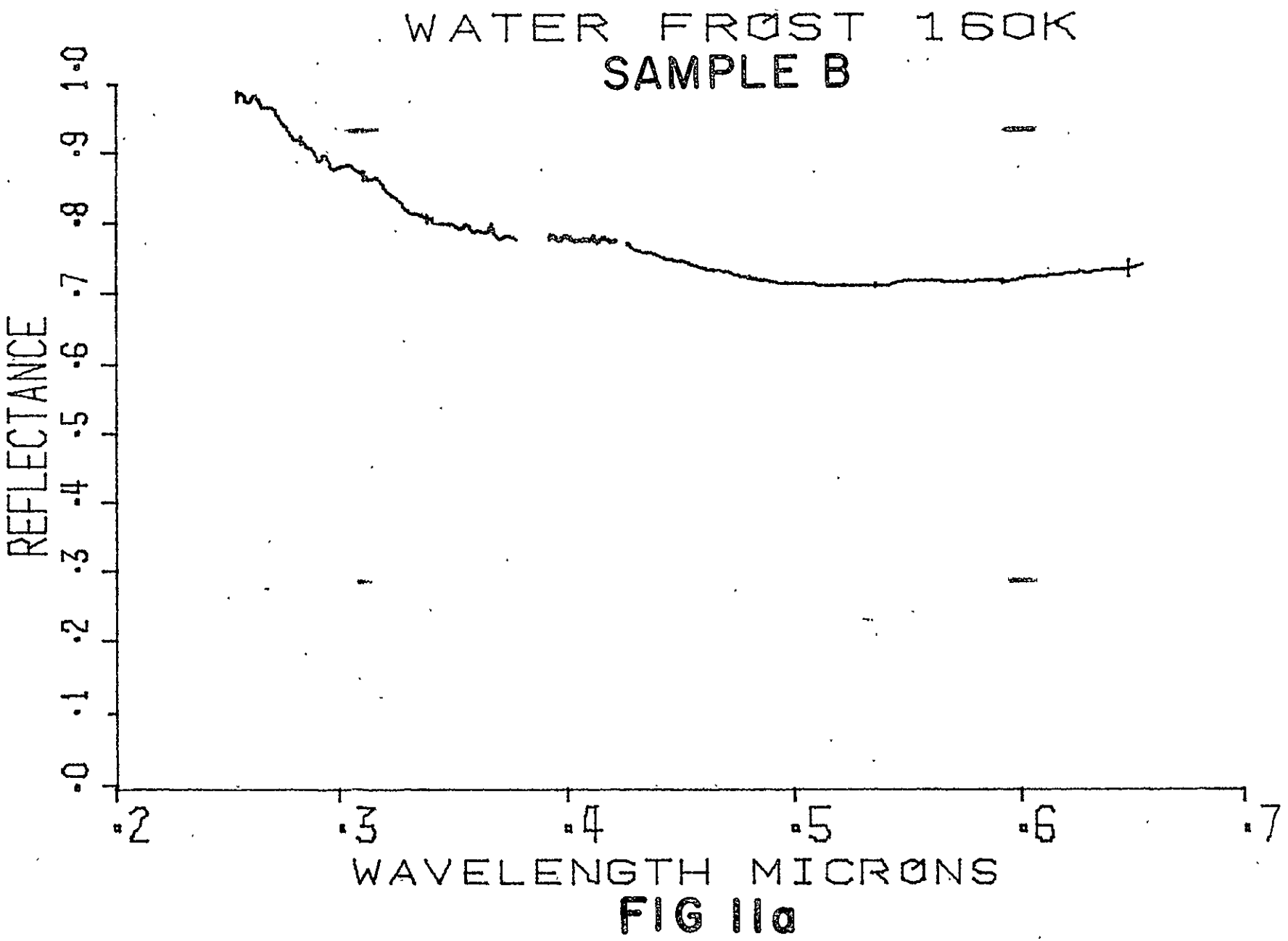
WATER FROST 160K
SAMPLE B
REFLECTANCE
.0
.1
.2
.3
.4
.5
.6
.7
.8
.9
1.0
.2
.3
.4
.5
.6
.7
WAVELENGTH MICRONS

FIG IIa

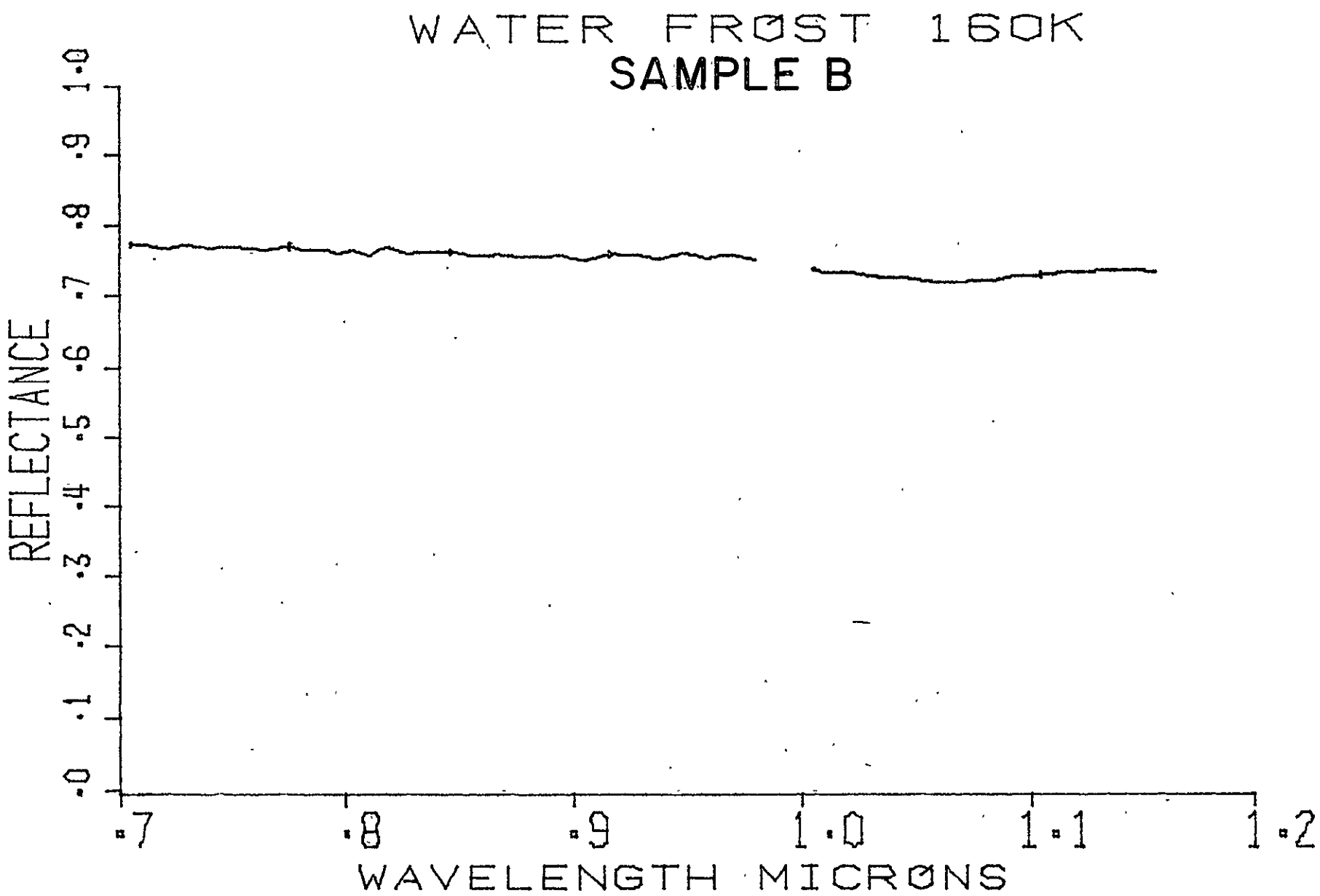
WATER FROST 160K
SAMPLE B
REFLECTANCE
.0
.1
.2
.3
.4
.5
.6
.7
.8
.9
1.0
.7
.8
.9
1.0
1.1
1.2
WAVELENGTH MICRONS

FIG IIb

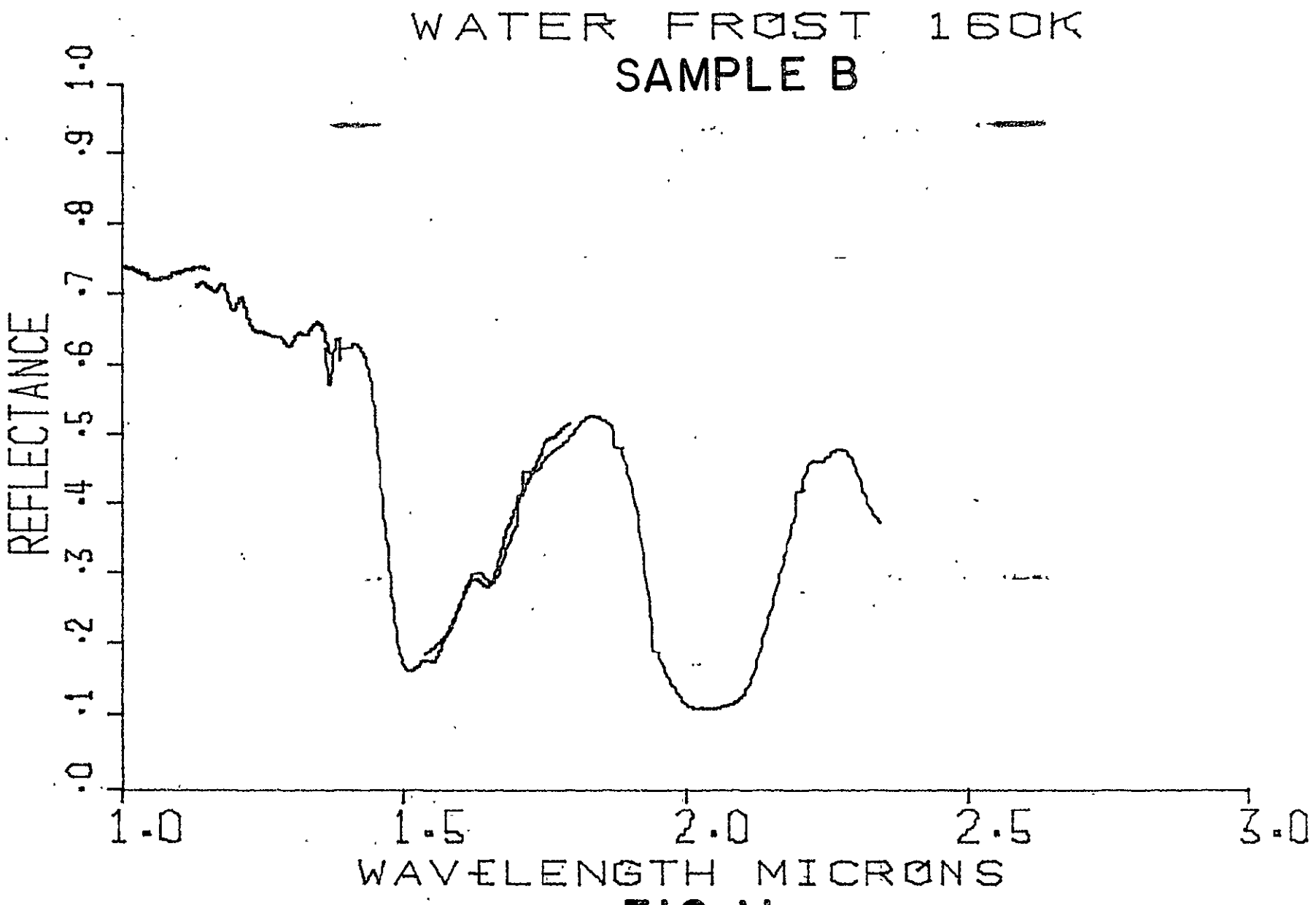
WATER FROST 160K
SAMPLE B
REFLECTANCE
.0
.1
.2
.3
.4
.5
.6
.7
.8
.9
1.0
1.0
1.5
2.0
2.5
3.0
WAVELENGTH MICRONS

FIG IIc

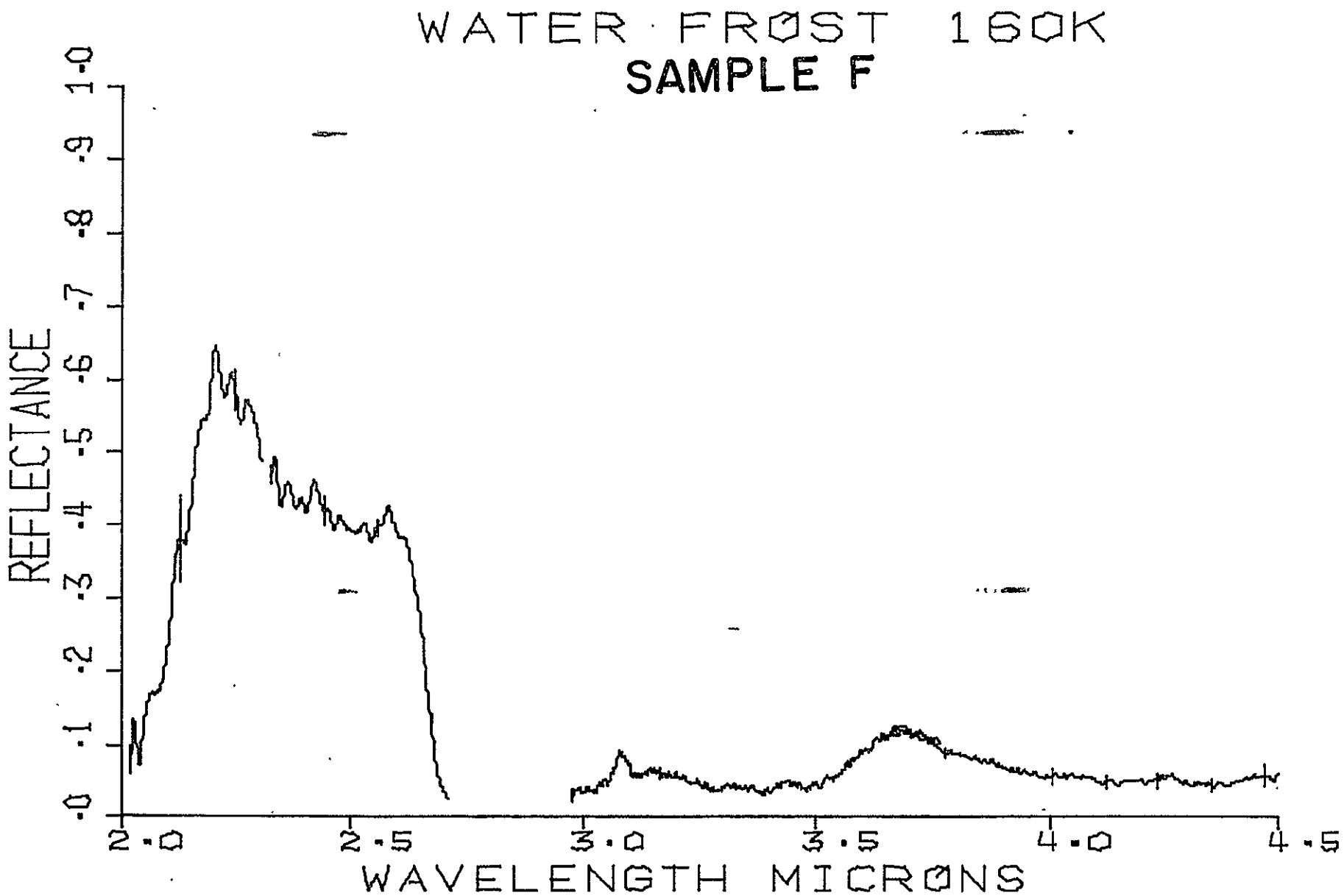
WATER FROST 160K
SAMPLE F
REFLECTANCE
0 .1 .2 .3 .4 .5 .6 .7 .8 .9 1.0
2.0 2.5 3.0 3.5 4.0 4.5
WAVELENGTH MICRONS

FIG IId

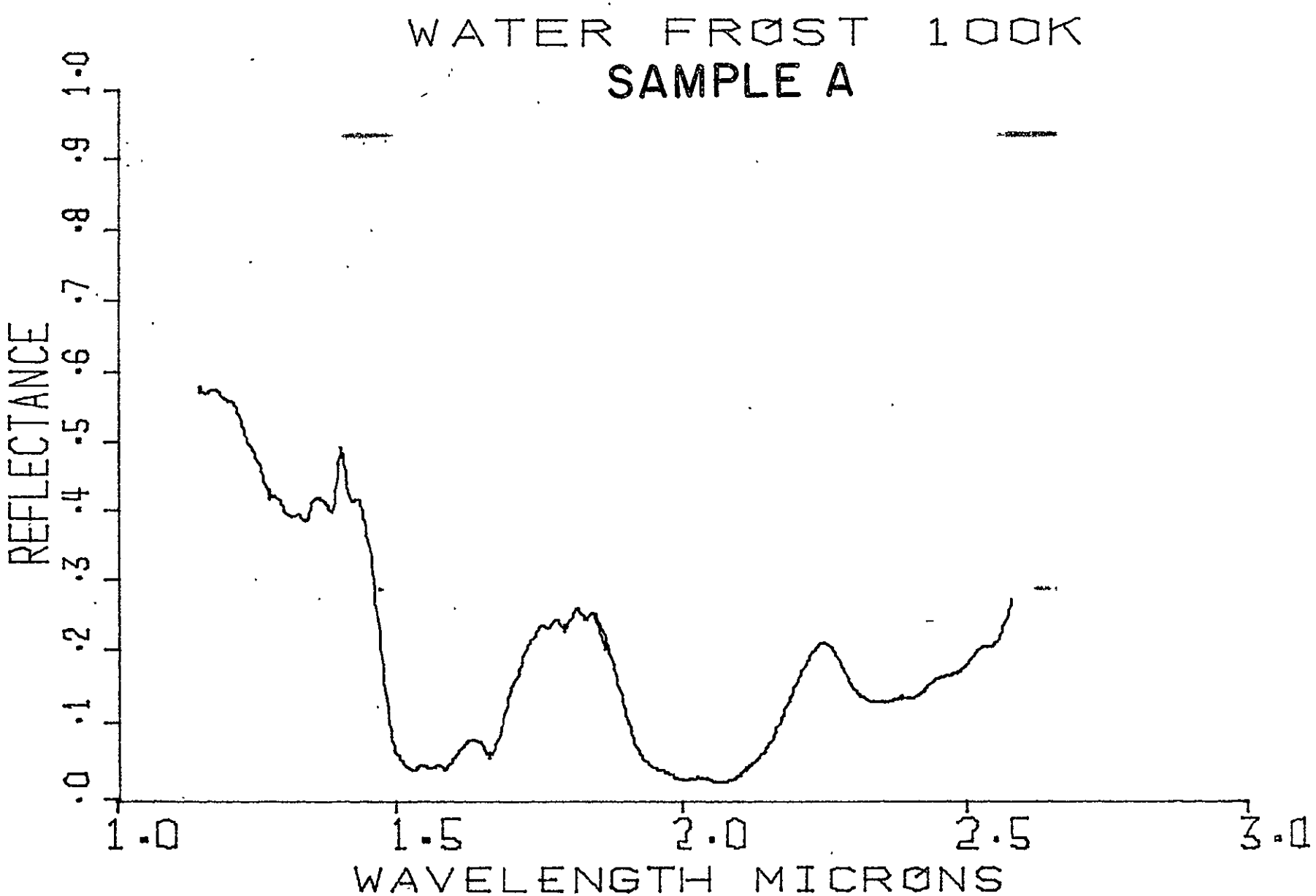
WATER FROST 100K
SAMPLE A
REFLECTANCE
.0
.1
.2
.3
.4
.5
.6
.7
.8
.9
1.0
1.0
1.5
2.0
2.5
3.0
WAVELENGTH MICRONS

FIG 12

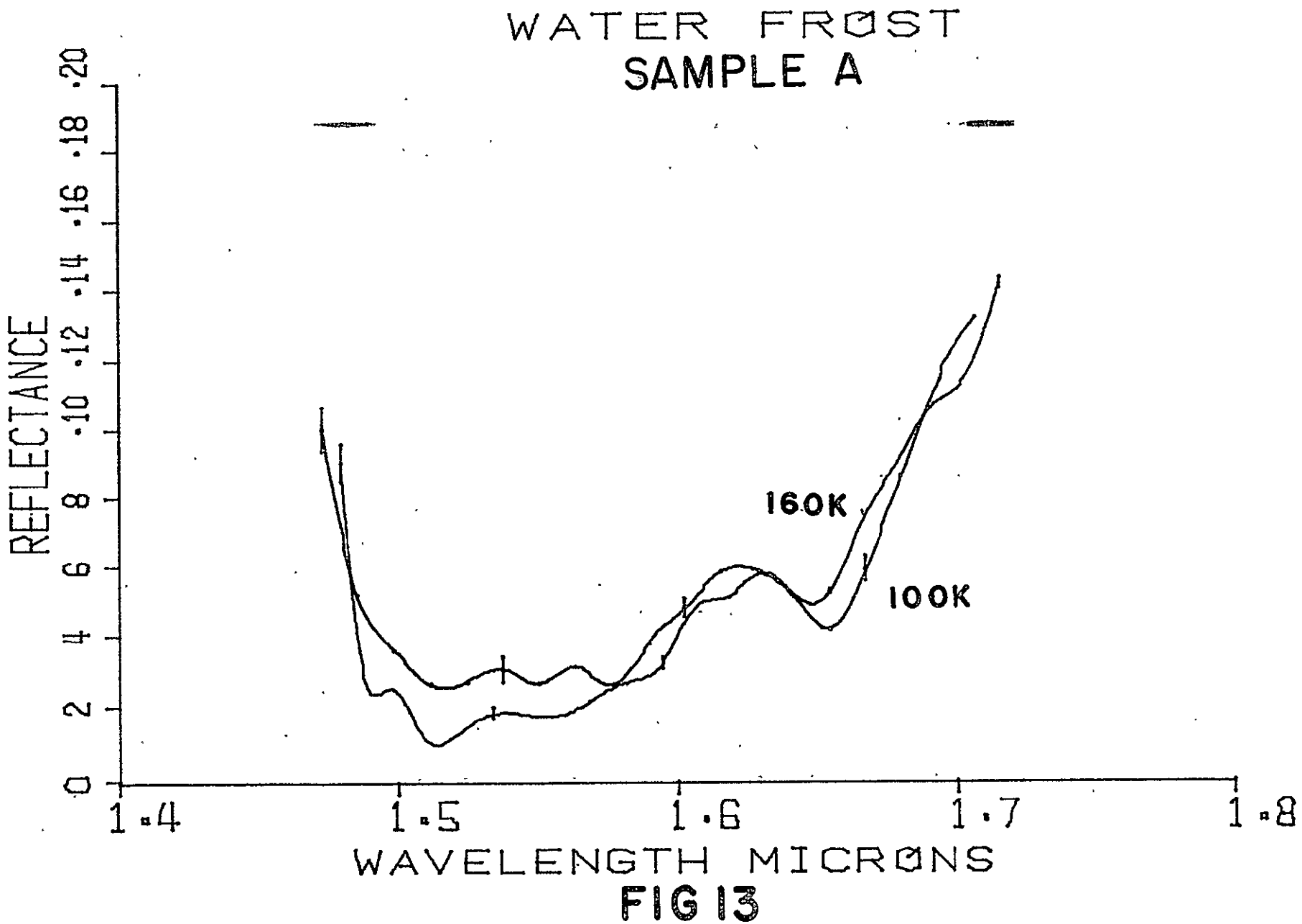
WATER FROST
SAMPLE A
REFLECTANCE
0
2
4
6
8
·10
·12
·14
·16
·18
·20
160K
100K
1·4
1·5
1·6
1·7
1·8
WAVELENGTH MICRONS

FIG 13

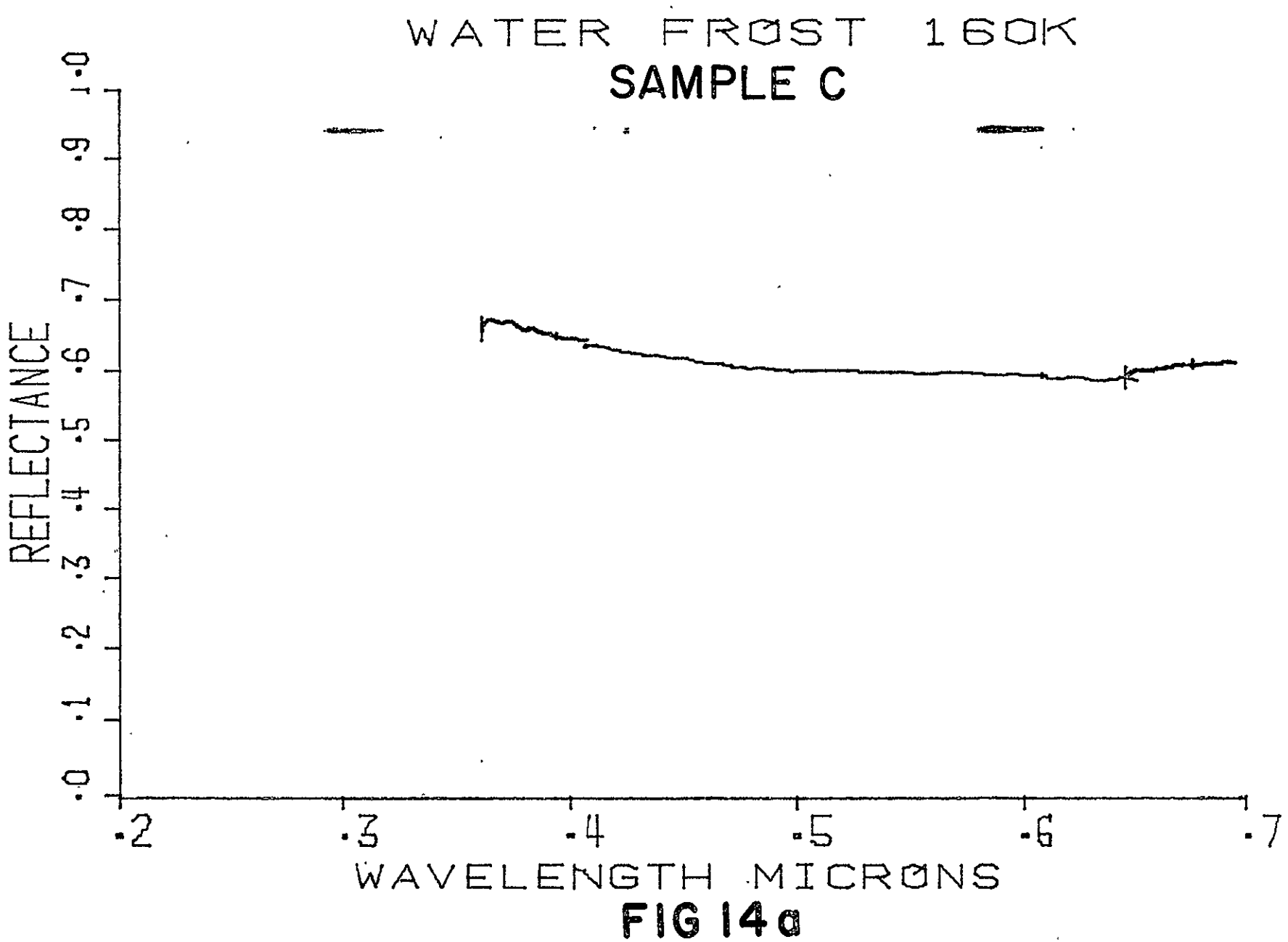
WATER FROST 160K
SAMPLE C
REFLECTANCE
.0
.1
.2
.3
.4
.5
.6
.7
.8
.9
1.0
.2
.3
.4
.5
.6
.7
WAVELENGTH MICRONS

FIG 14a

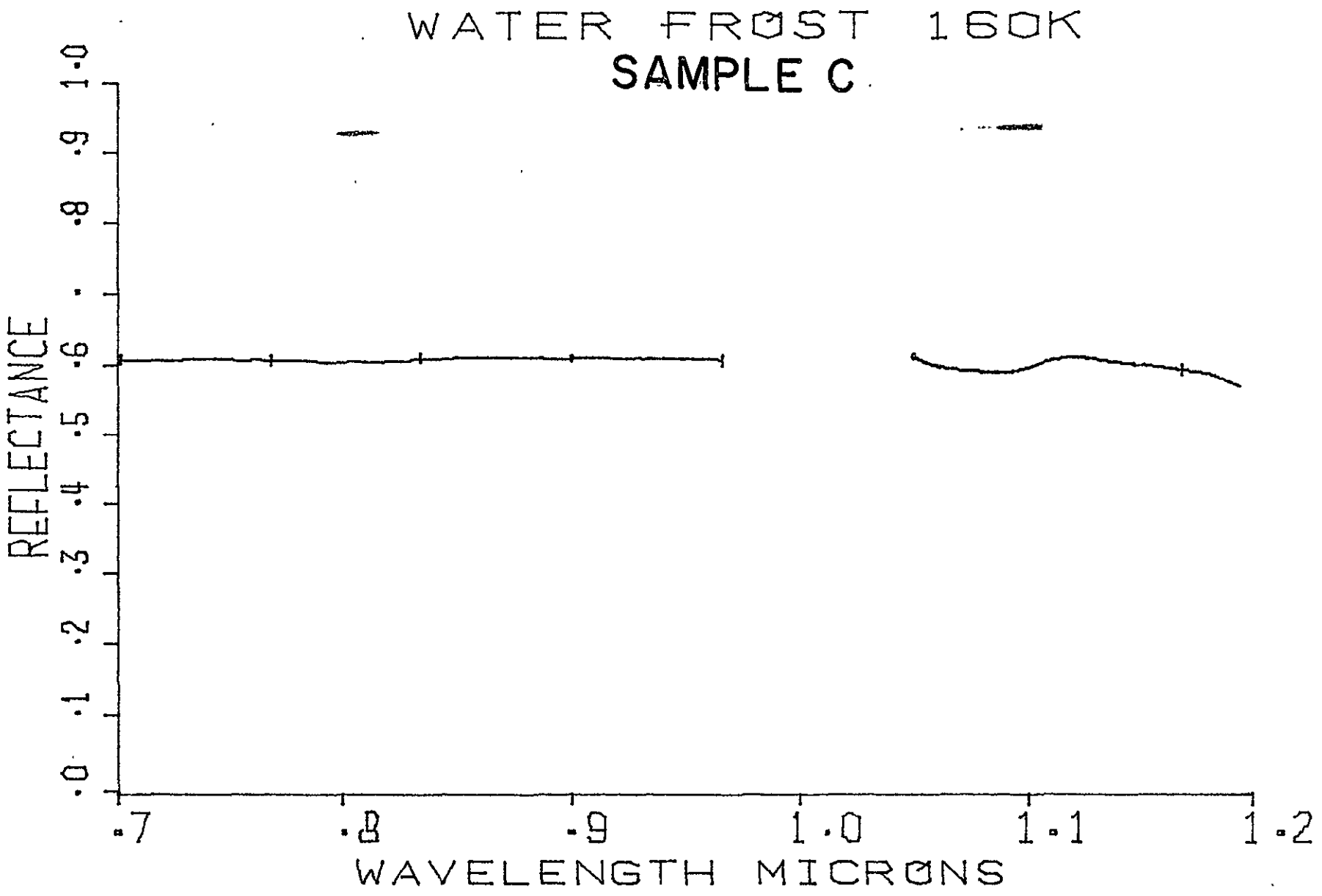
WATER FROST 160K
SAMPLE C
REFLECTANCE
.0
.1
.2
.3
.4
.5
.6
.7
.8
.9
1.0
.7
.8
.9
1.0
1.1
1.2
WAVELENGTH MICRONS

FIG 14b

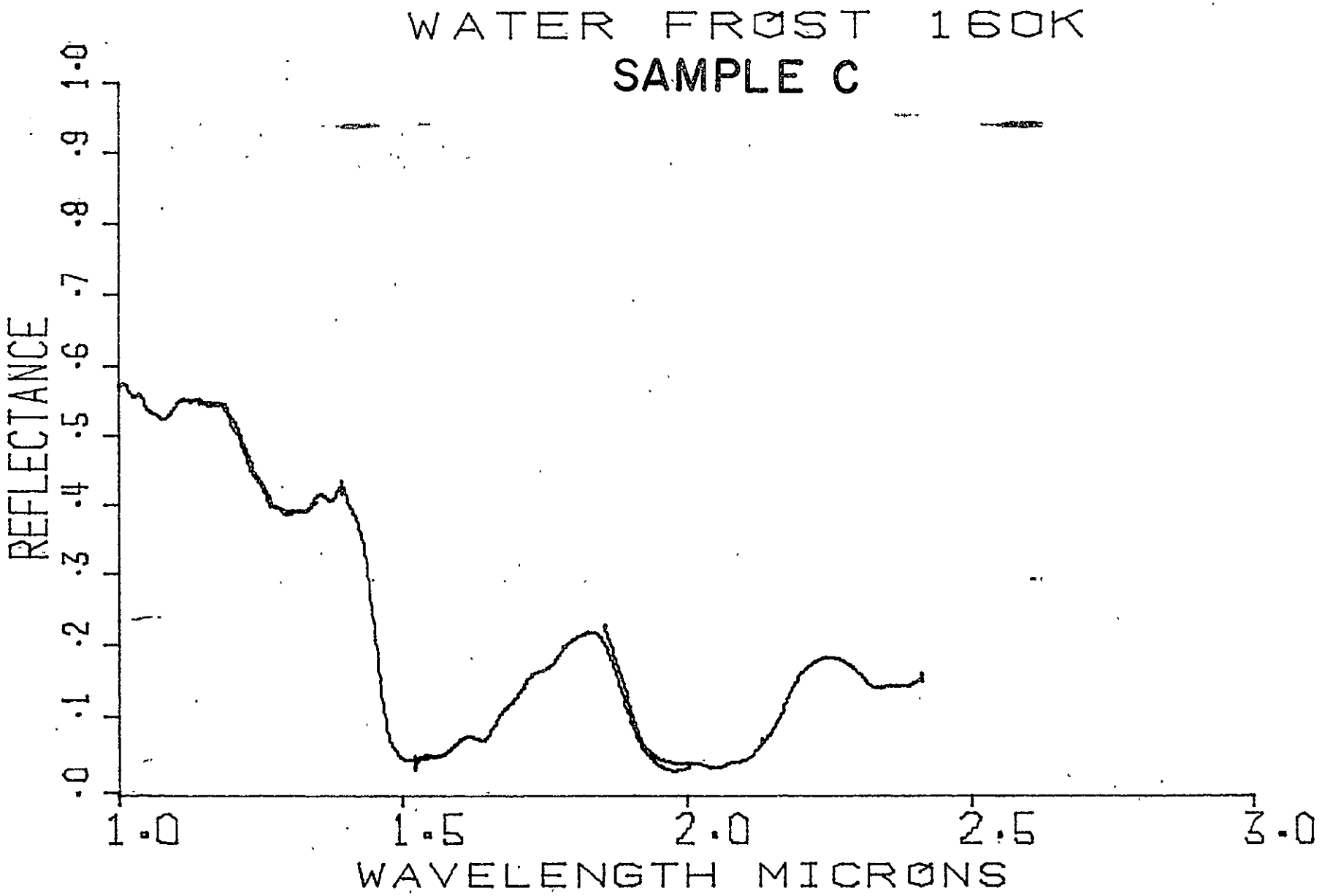
WATER FROST 160K
SAMPLE C
REFLECTANCE
.0
.1
.2
.3
.4
.5
.6
.7
.8
.9
1.0
1.0
1.5
2.0
2.5
3.0
WAVELENGTH MICRONS

FIG 14c

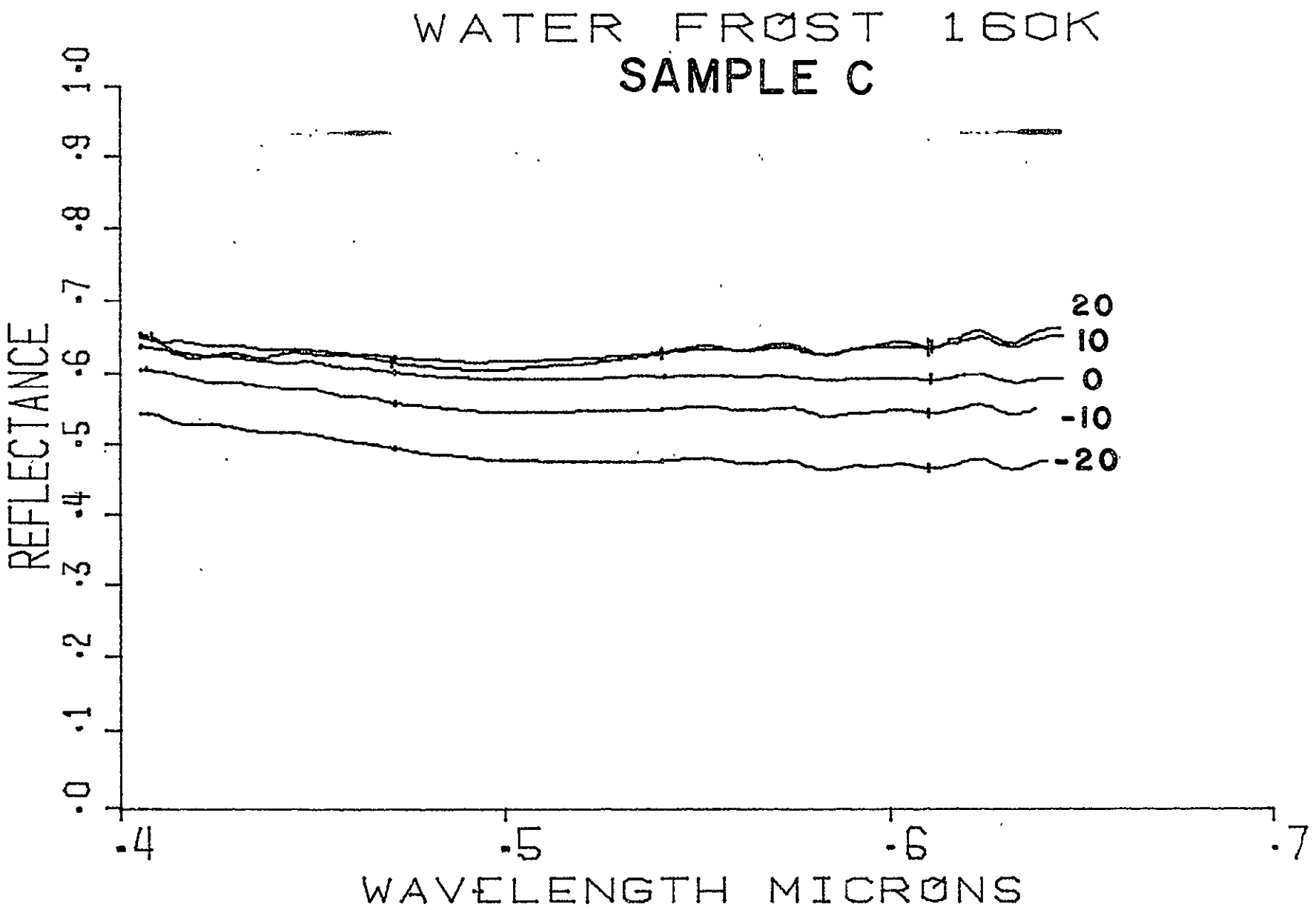
WATER FROST 160K
SAMPLE C
REFLECTANCE
.0
.1
.2
.3
.4
.5
.6
.7
.8
.9
1.0
20
10
0
-10
-20
.4
.5
.6
.7
WAVELENGTH MICRONS

FIG 15

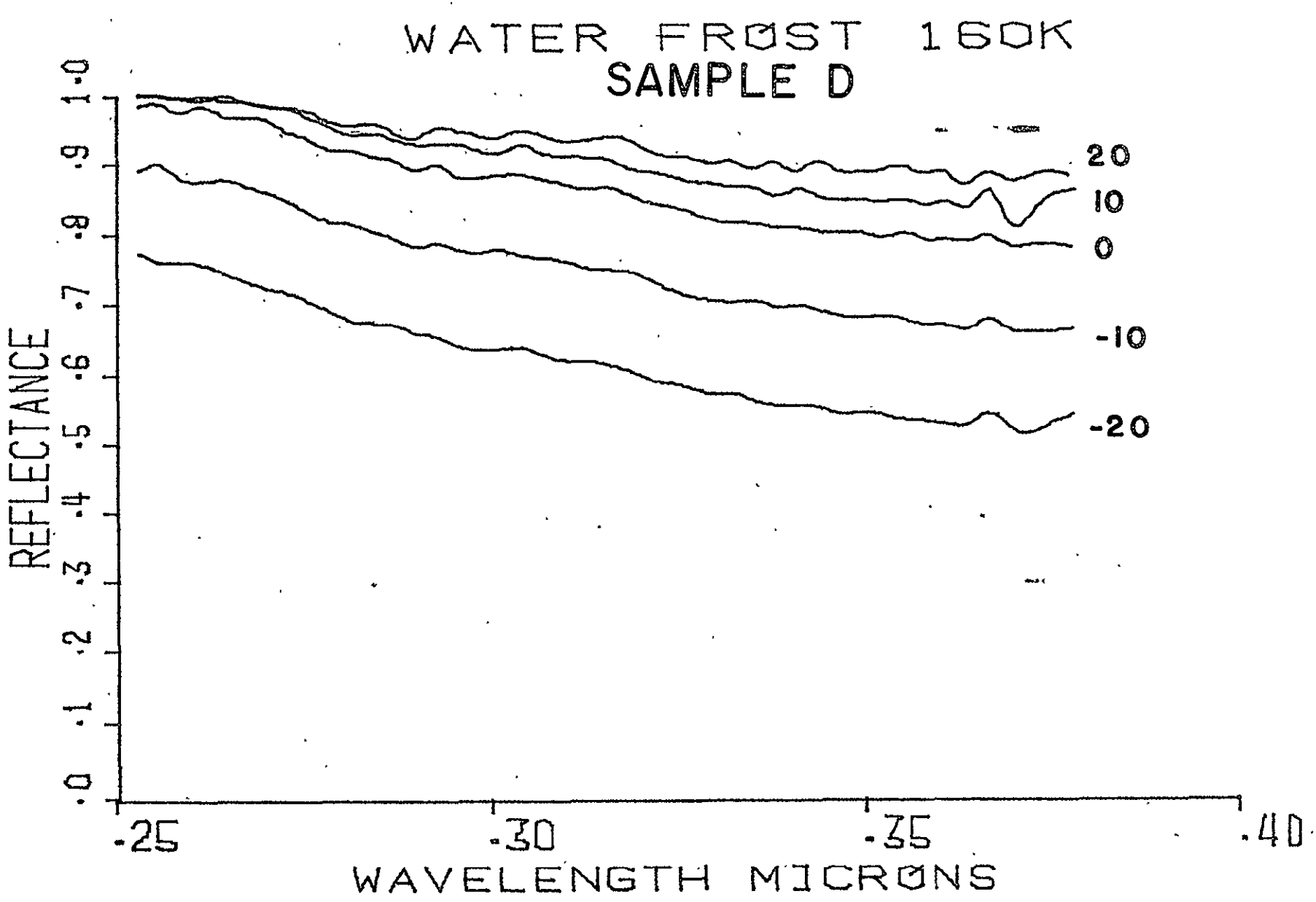
WATER FROST 160K
SAMPLE D
REFLECTANCE
.0
.1
.2
.3
.4
.5
.6
.7
.8
.9
1.0
20
10
0
-10
-20
.25
.30
.35
.40
WAVELENGTH MICRONS

FIG 16a

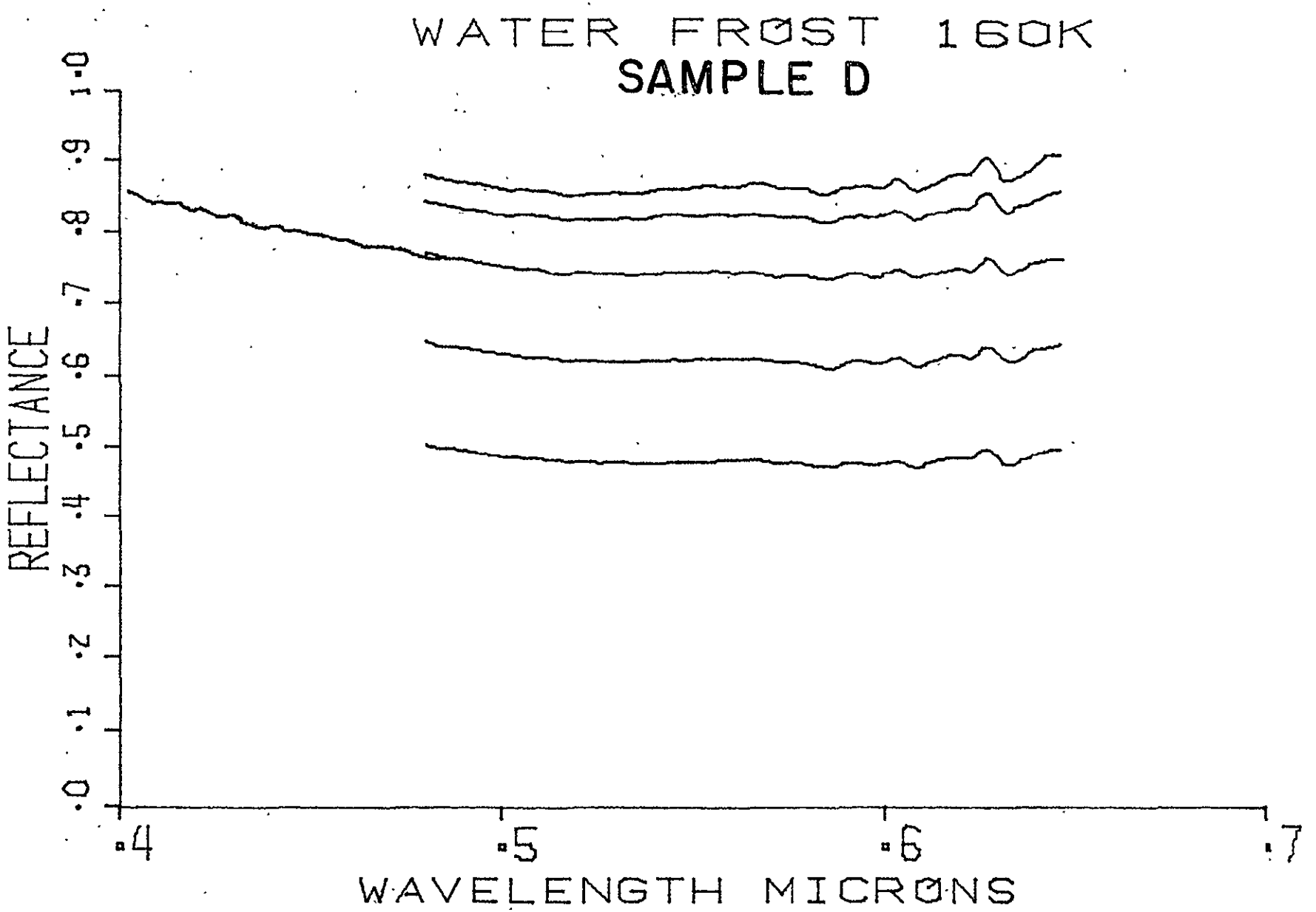
WATER FROST 160K
SAMPLE D
REFLECTANCE
.0
.1
.2
.3
.4
.5
.6
.7
.8
.9
1.0
.4
.5
.6
.7
WAVELENGTH MICRONS

FIG 16b

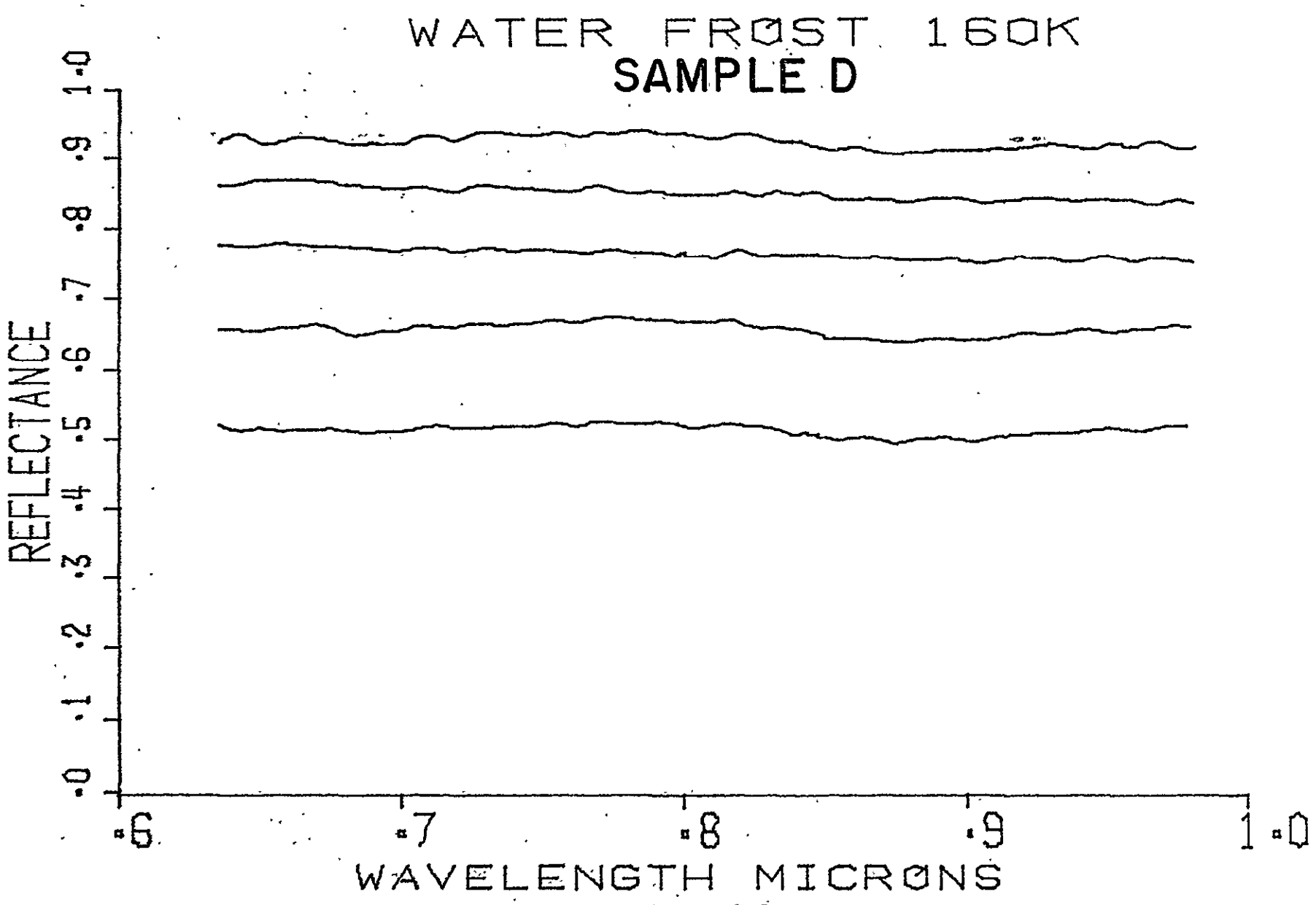
WATER FROST 160K
SAMPLE D
REFLECTANCE
.0
.1
.2
.3
.4
.5
.6
.7
.8
.9
1.0
.6
.7
.8
.9
1.0
WAVELENGTH MICRONS

FIG 16c

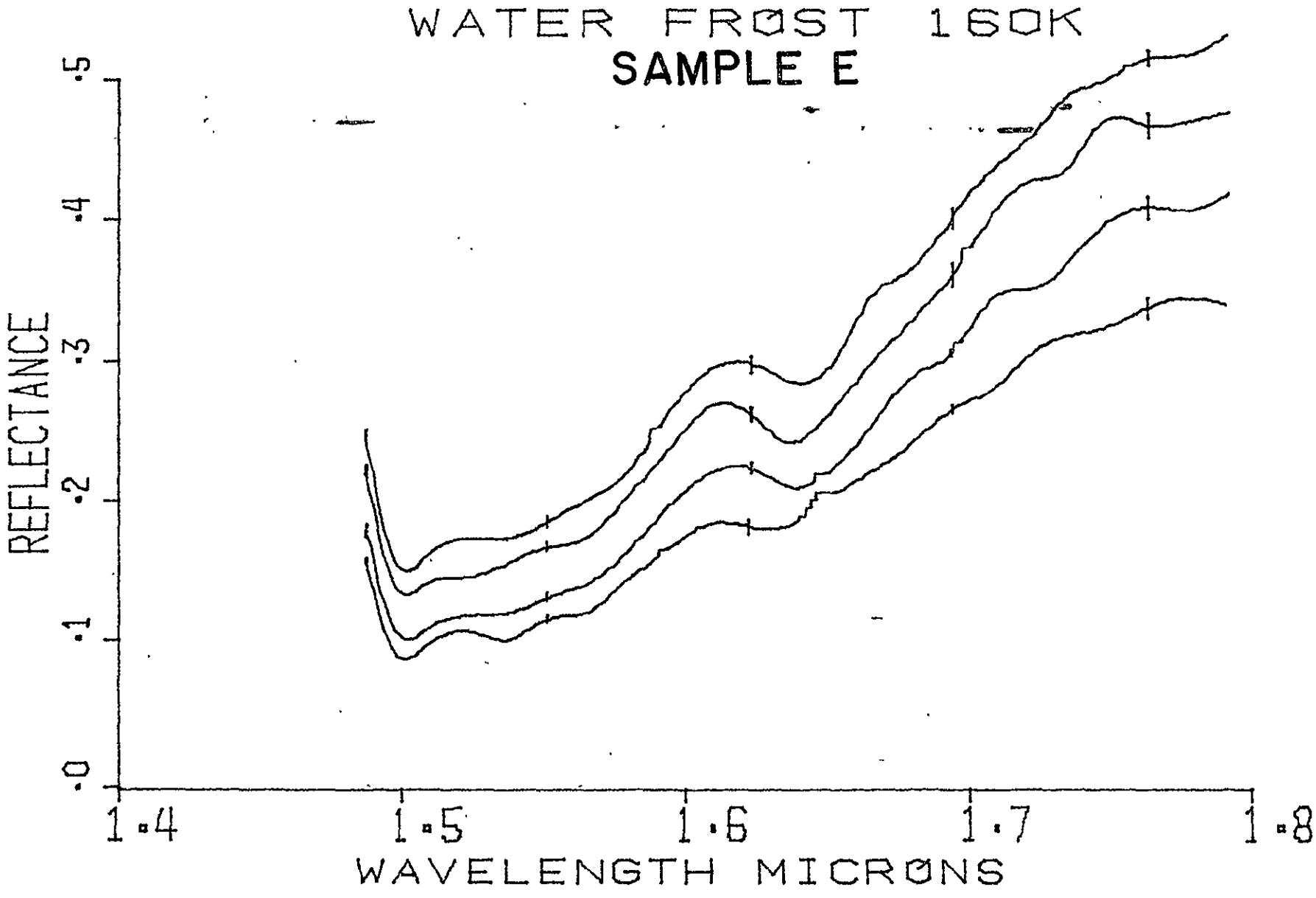
WATER FROST 160K
SAMPLE E
REFLECTANCE
.0
.1
.2
.3
.4
.5
1.4
1.5
1.6
1.7
1.8
WAVELENGTH MICRONS

FIG 16d

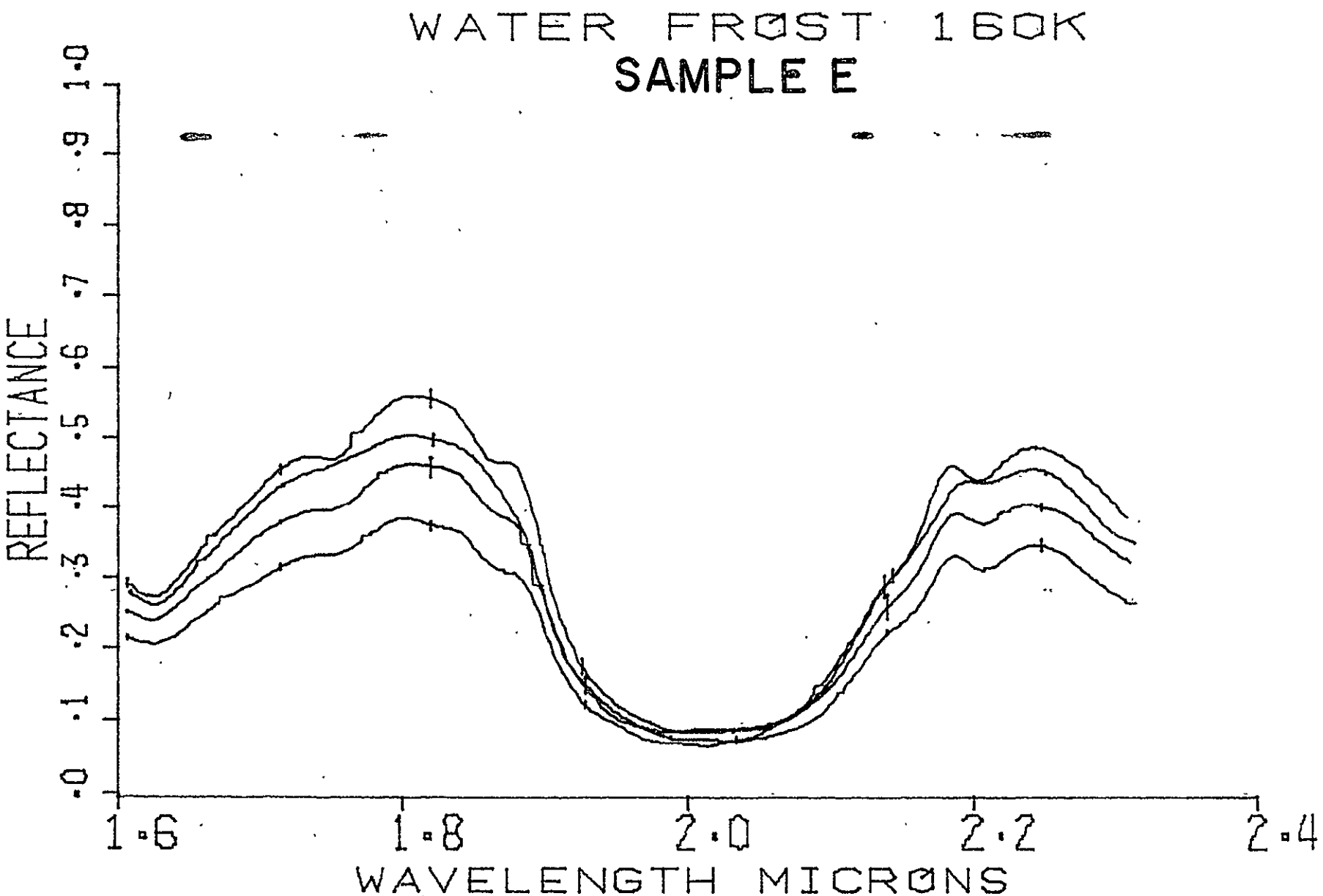
WATER FROST 160K
SAMPLE E
REFLECTANCE
.0
.1
.2
.3
.4
.5
.6
.7
.8
.9
1.0
1.6
1.8
2.0
2.2
2.4
WAVELENGTH MICRONS

FIG 16e

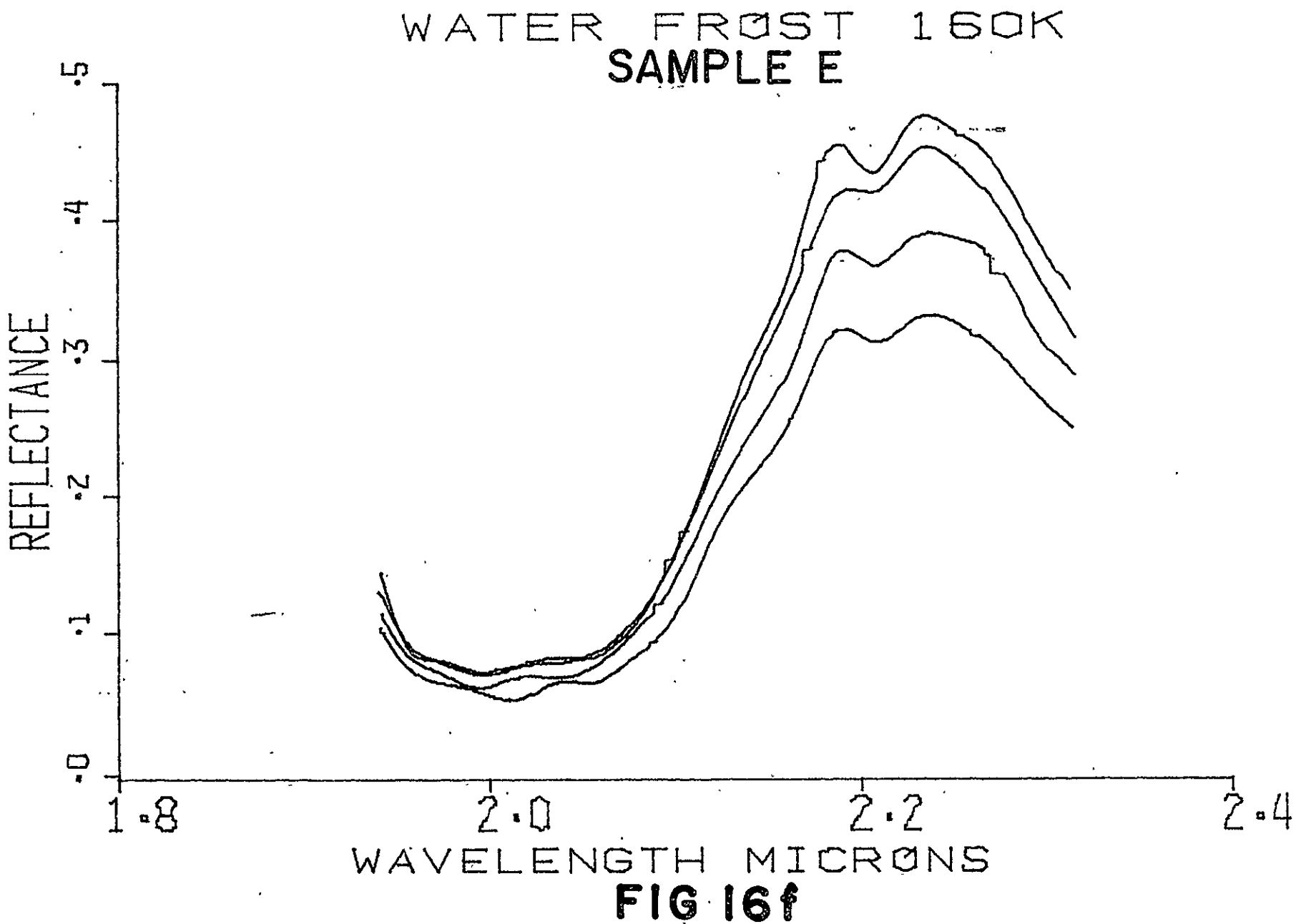
WATER FROST 160K
SAMPLE E
REFLECTANCE
.0
.1
.2
.3
.4
.5
1.8
2.0
2.2
2.4
WAVELENGTH MICRONS

FIG 16f

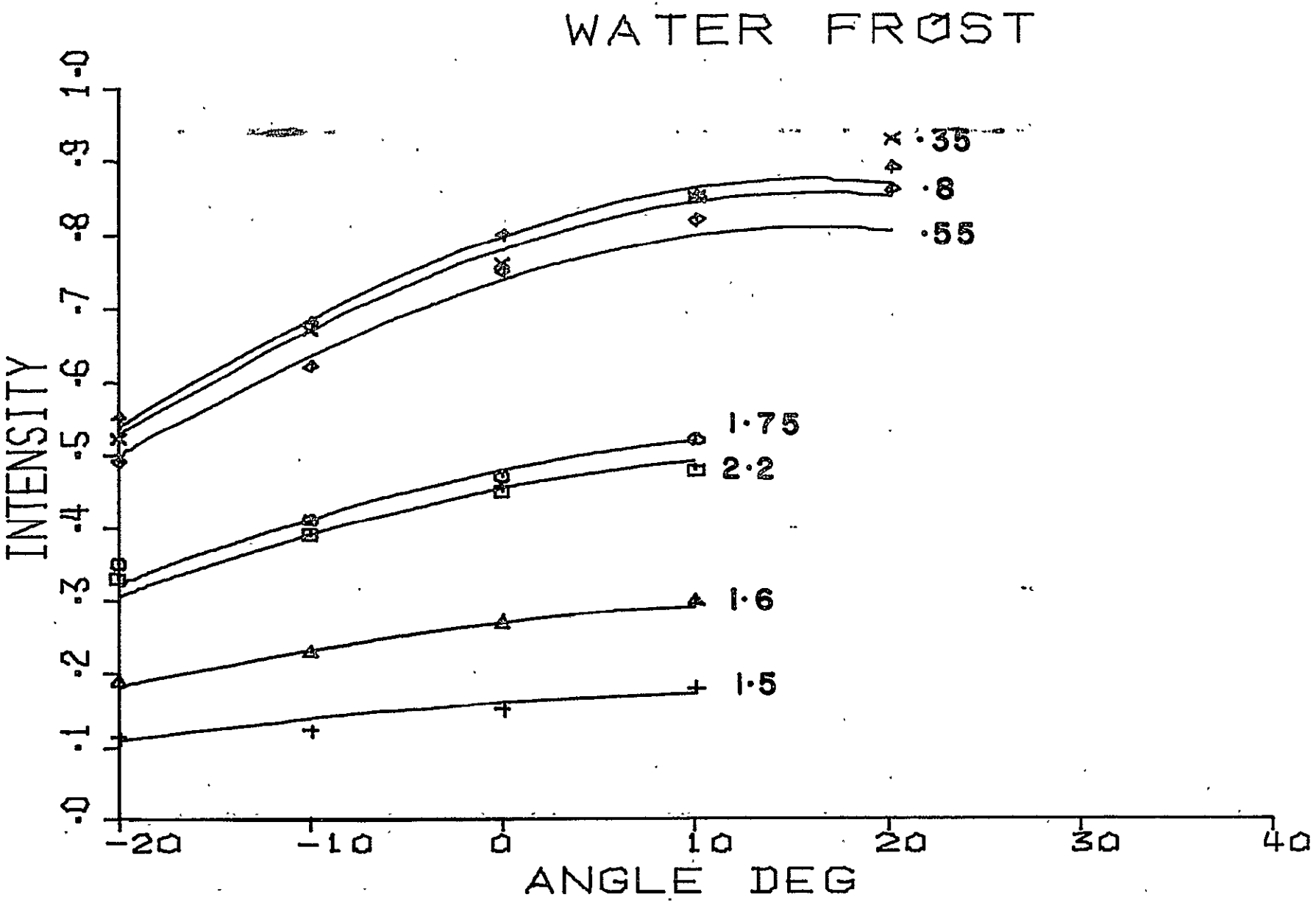
WATER FROST
INTENSITY
.0
.1
.2
.3
.4
.5
.6
.7
.8
.9
1.0
-20
-10
0
10
20
30
40
ANGLE DEG
x .35
.8
.55
1.75
2.2
1.6
1.5

FIG 17

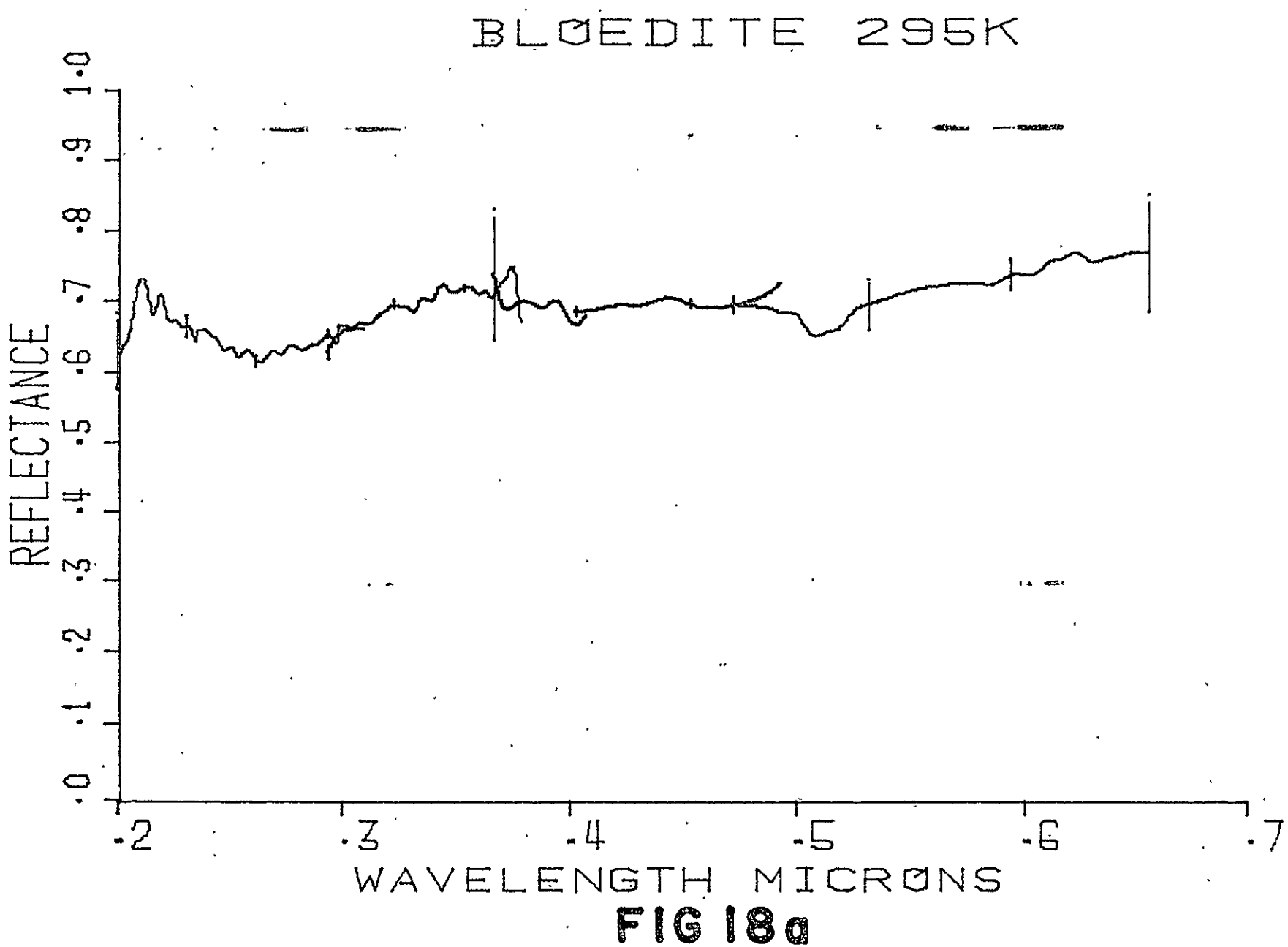
BLØEDITE 295K
REFLECTANCE
.0
.1
.2
.3
.4
.5
.6
.7
.8
.9
1.0
.2
.3
.4
.5
.6
.7
WAVELENGTH MICRØNS

FIG 18a

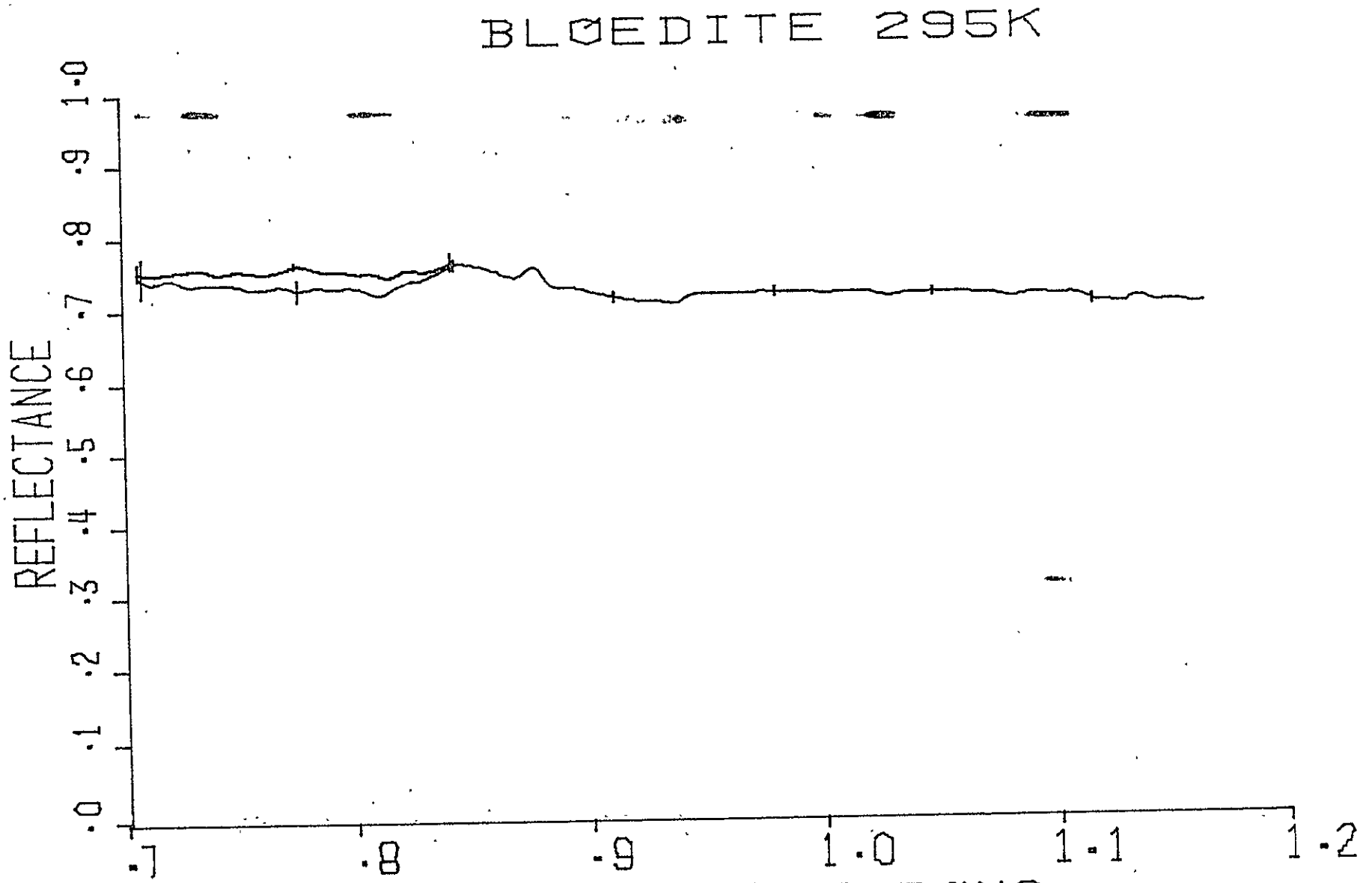
BLØEDITE 295K
REFLECTANCE
.0
.1
.2
.3
.4
.5
.6
.7
.8
.9
1.0
.7
.8
.9
1.0
1.1
1.2
WAVELENGTH MICRØNS

FIG 18b

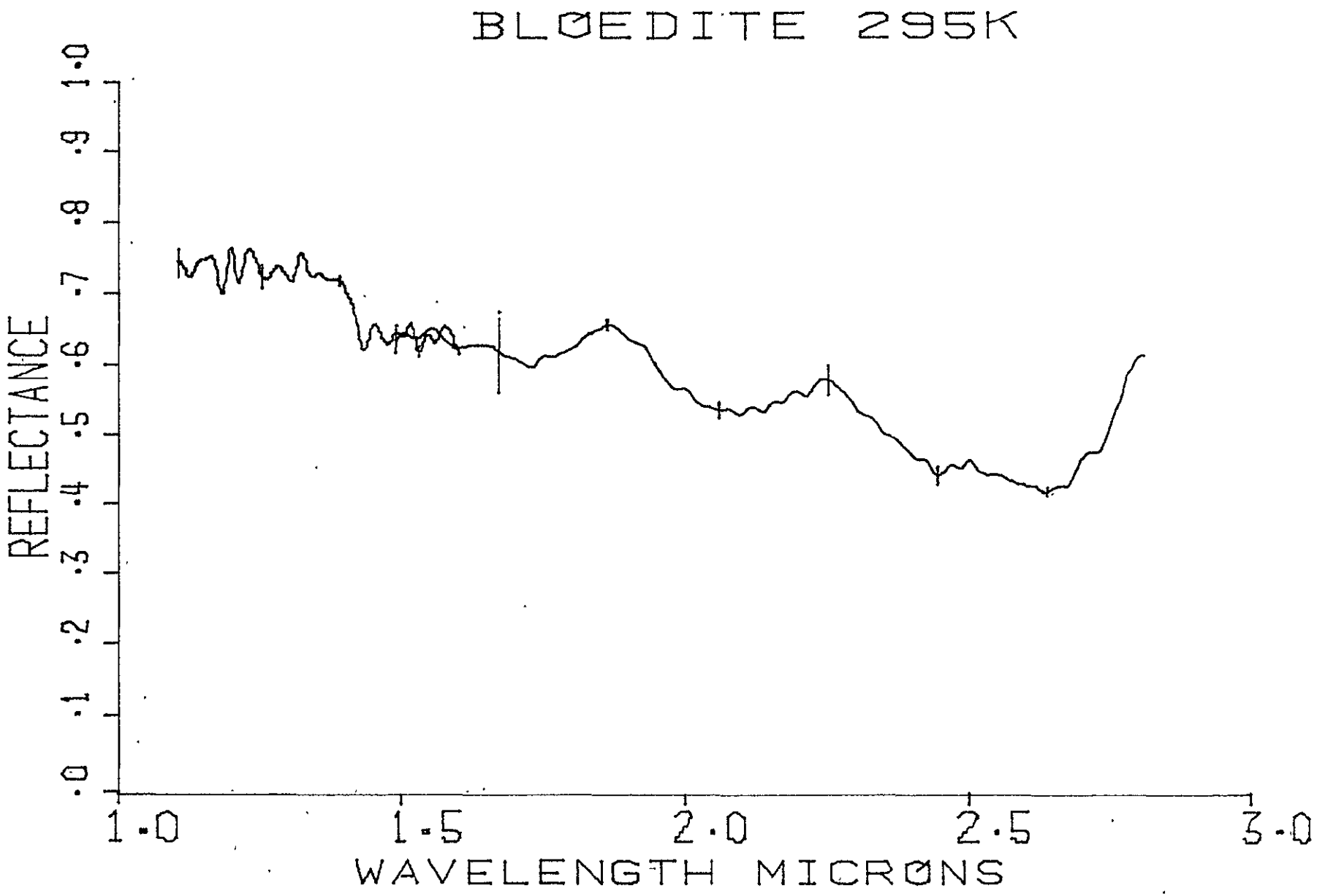
BLØEDITE 295K
REFLECTANCE
.0
.1
.2
.3
.4
.5
.6
.7
.8
.9
1.0
1.0
1.5
2.0
2.5
3.0
WAVELENGTH MICRØNS

FIG 18c

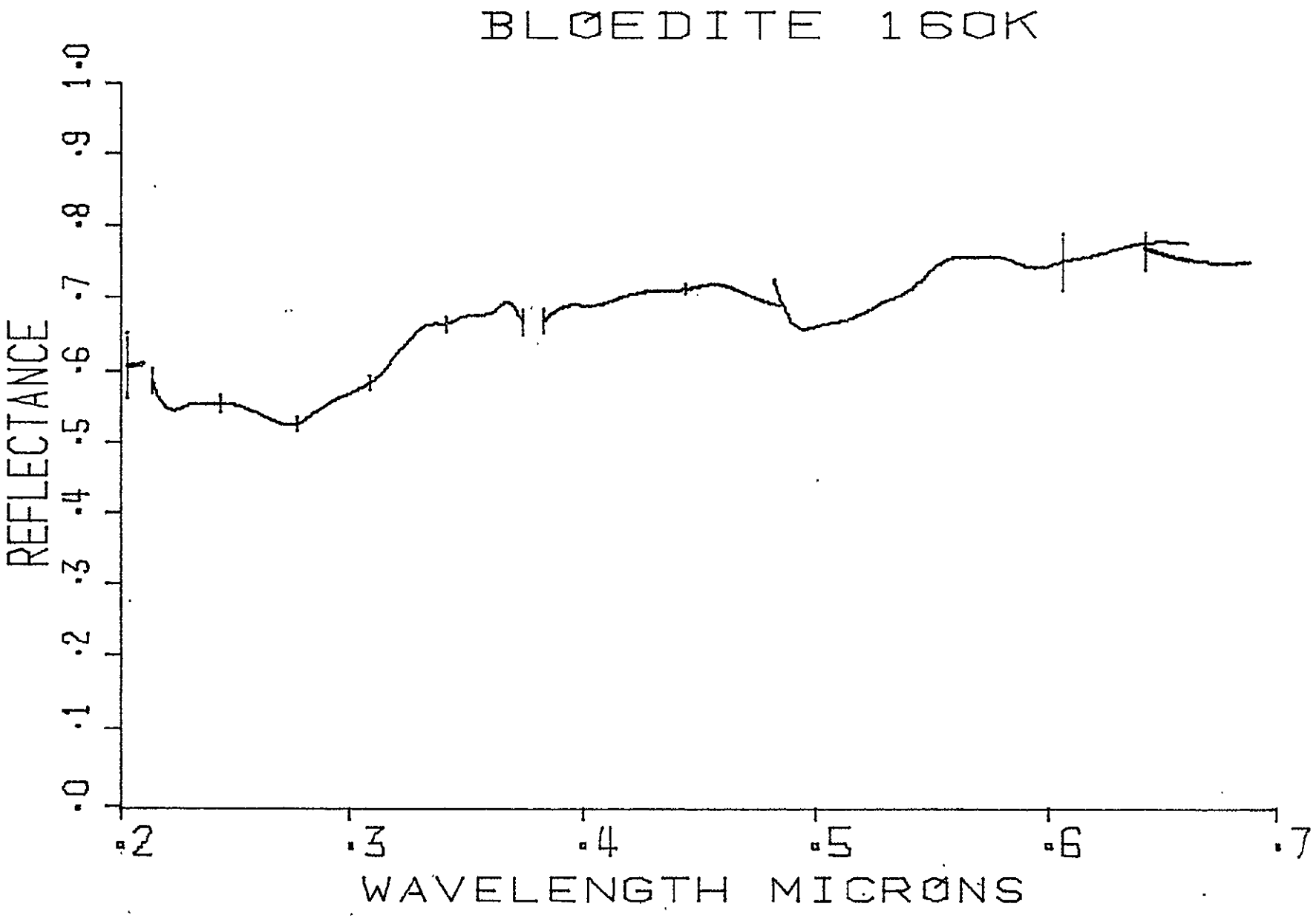
BLØEDITE 160K
REFLECTANCE
.0
.1
.2
.3
.4
.5
.6
.7
.8
.9
1.0
.2
.3
.4
.5
.6
.7
WAVELENGTH MICRØNS

FIG 19a

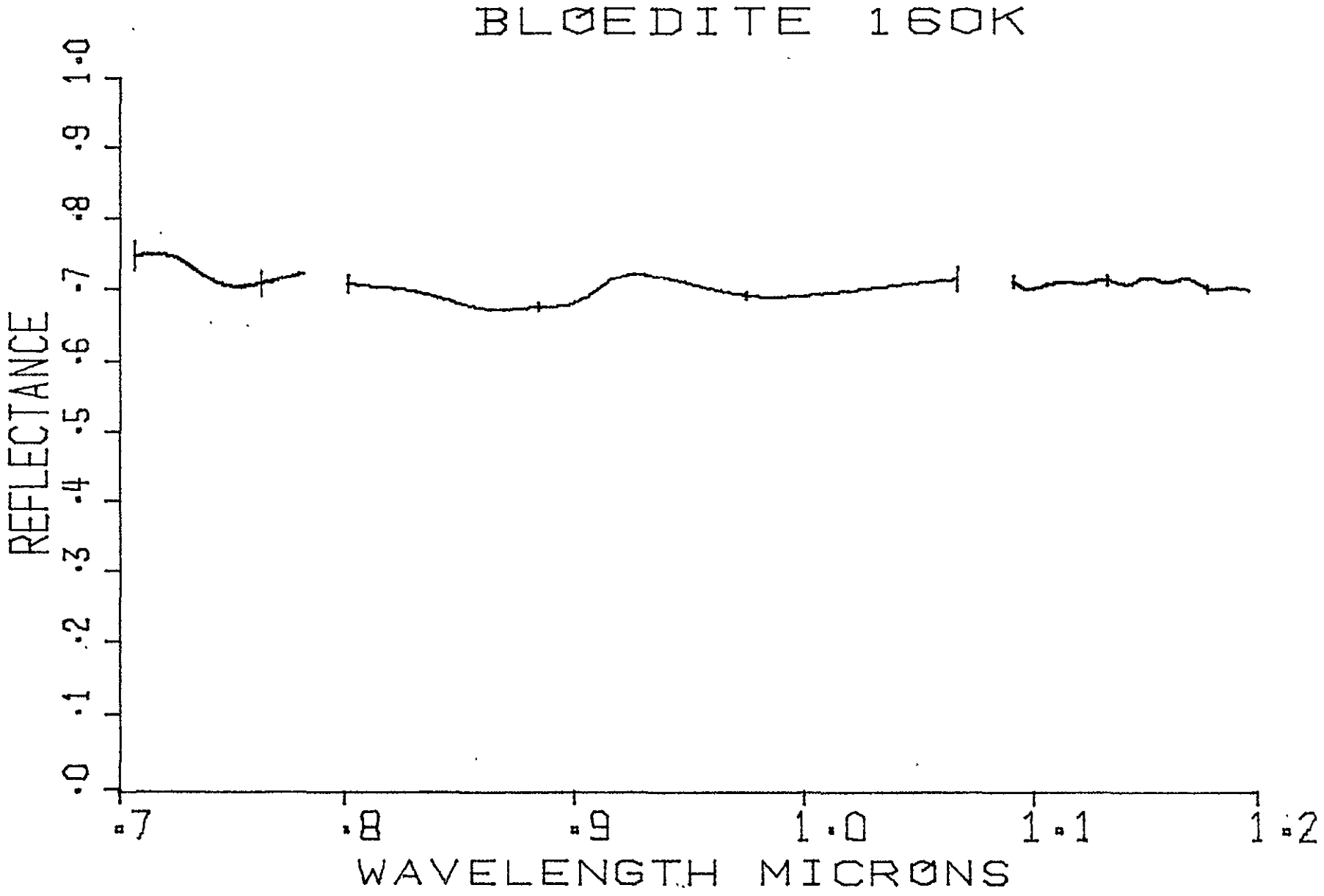
BLØEDITE 160K
REFLECTANCE
.0
.1
.2
.3
.4
.5
.6
.7
.8
.9
1.0
.7
.8
.9
1.0
1.1
1.2
WAVELENGTH MICRØNS

FIG 19b

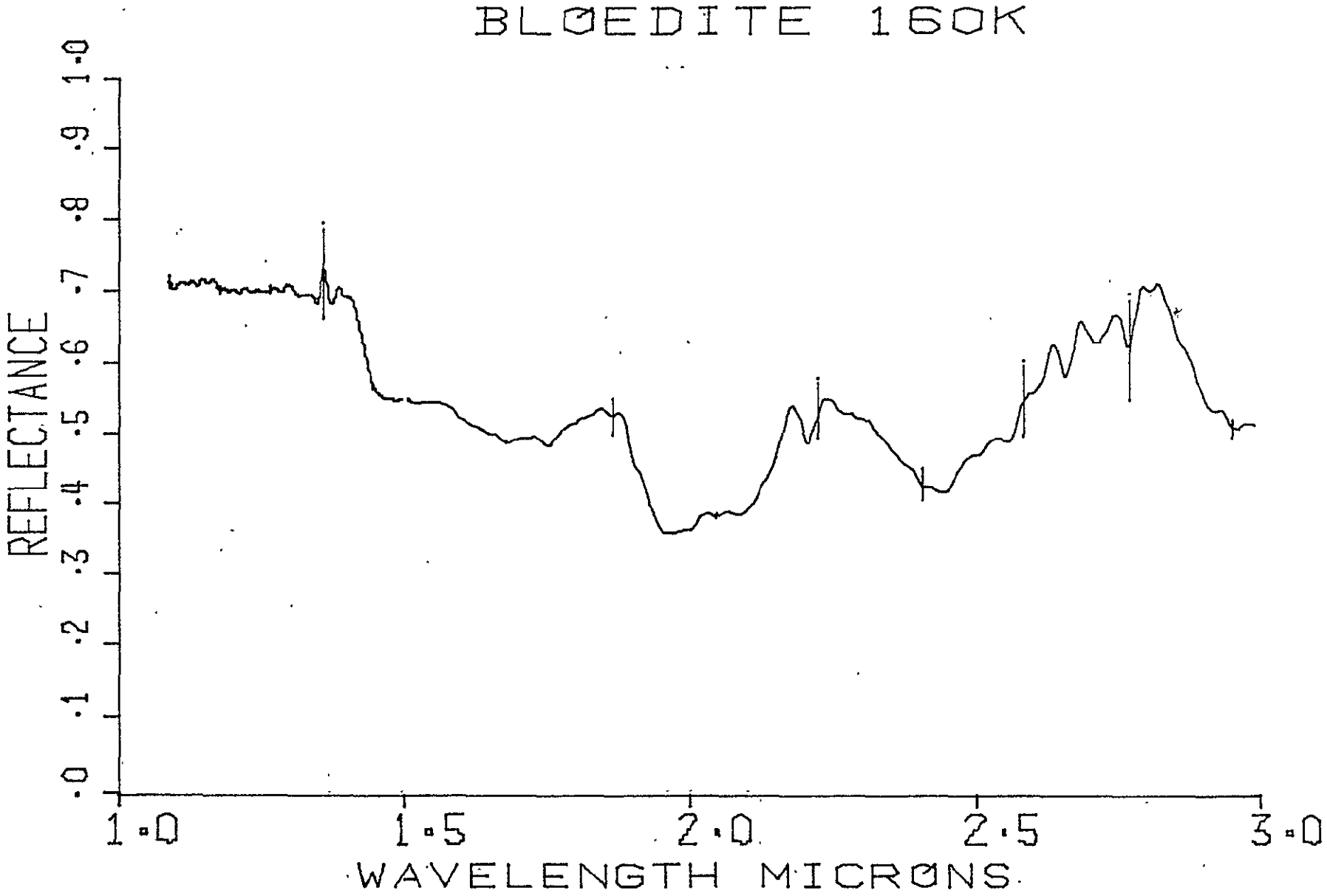
BLØEDITE 160K
REFLECTANCE
.0
.1
.2
.3
.4
.5
.6
.7
.8
.9
1.0
1.0
1.5
2.0
2.5
3.0
WAVELENGTH MICRØNS

FIG 19c

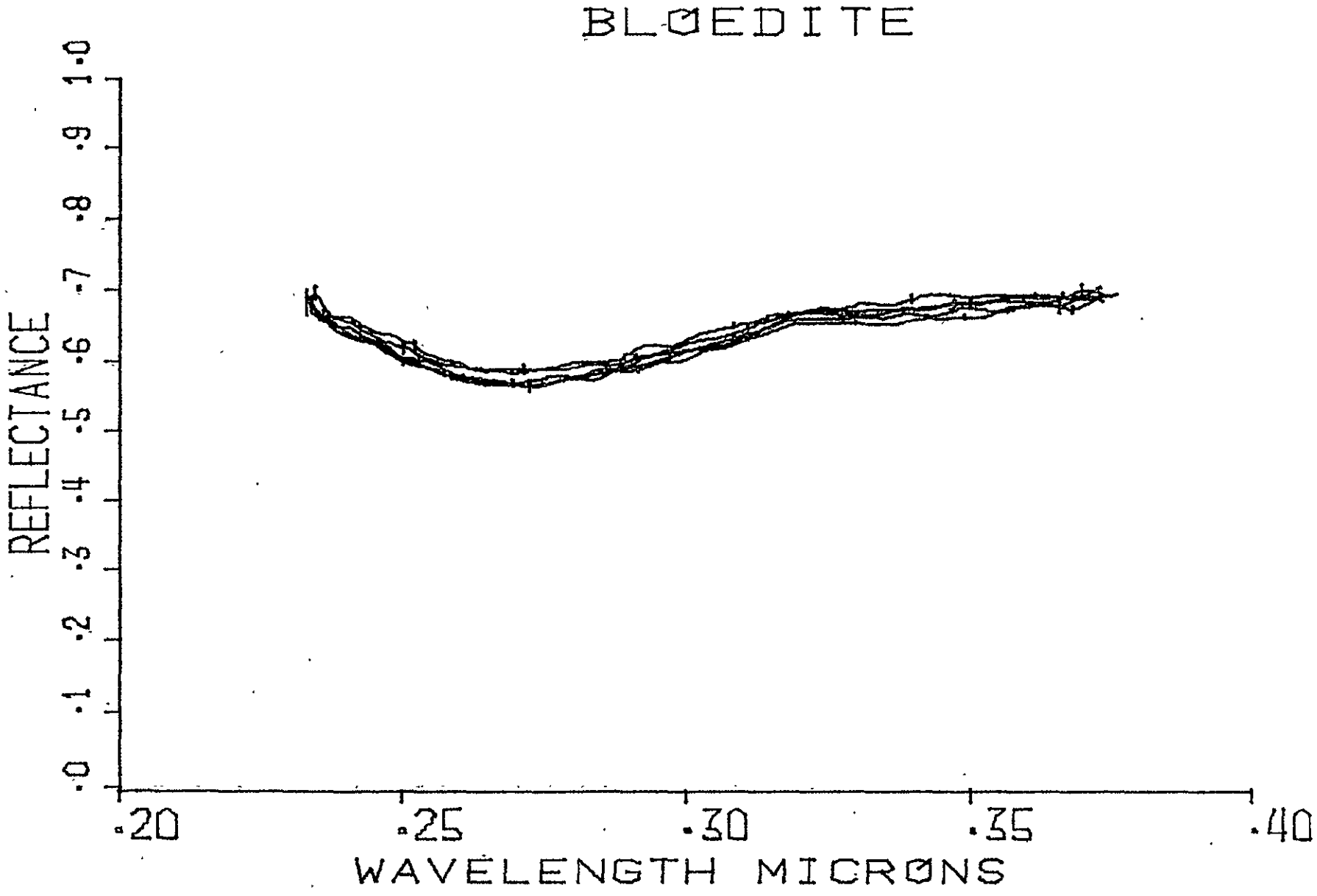
BLØEDITE
REFLECTANCE
.0
.1
.2
.3
.4
.5
.6
.7
.8
.9
1.0
.20
.25
.30
.35
.40
WAVELENGTH MICRØNS

FIG 20

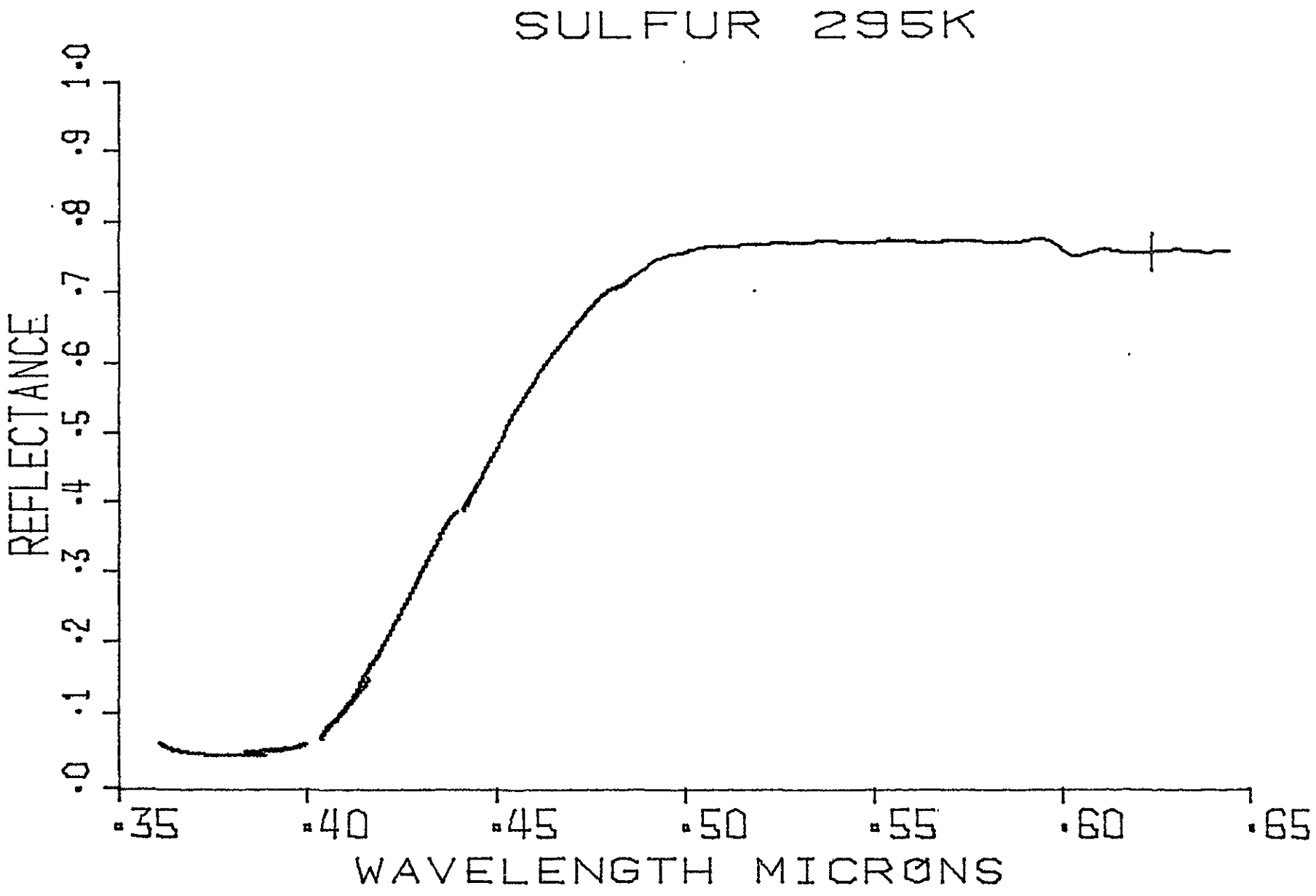
SULFUR 295K
REFLECTANCE
.0
.1
.2
.3
.4
.5
.6
.7
.8
.9
1.0
.35
.40
.45
.50
.55
.60
.65
WAVELENGTH MICRONS

FIG 21a

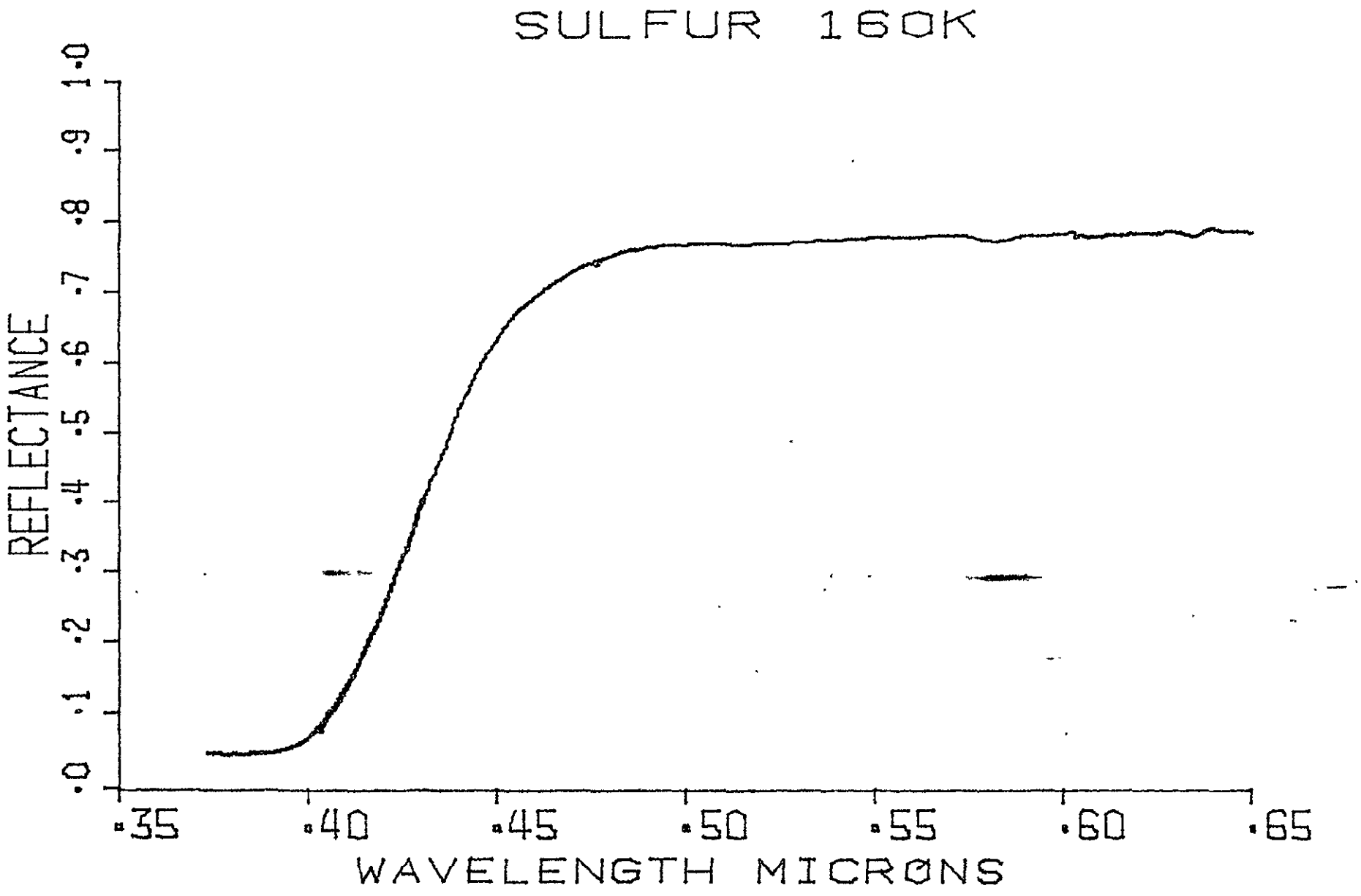
SULFUR 160K
REFLECTANCE
.0
.1
.2
.3
.4
.5
.6
.7
.8
.9
1.0
.35
.40
.45
.50
.55
.60
.65
WAVELENGTH MICRONS

FIG 21b

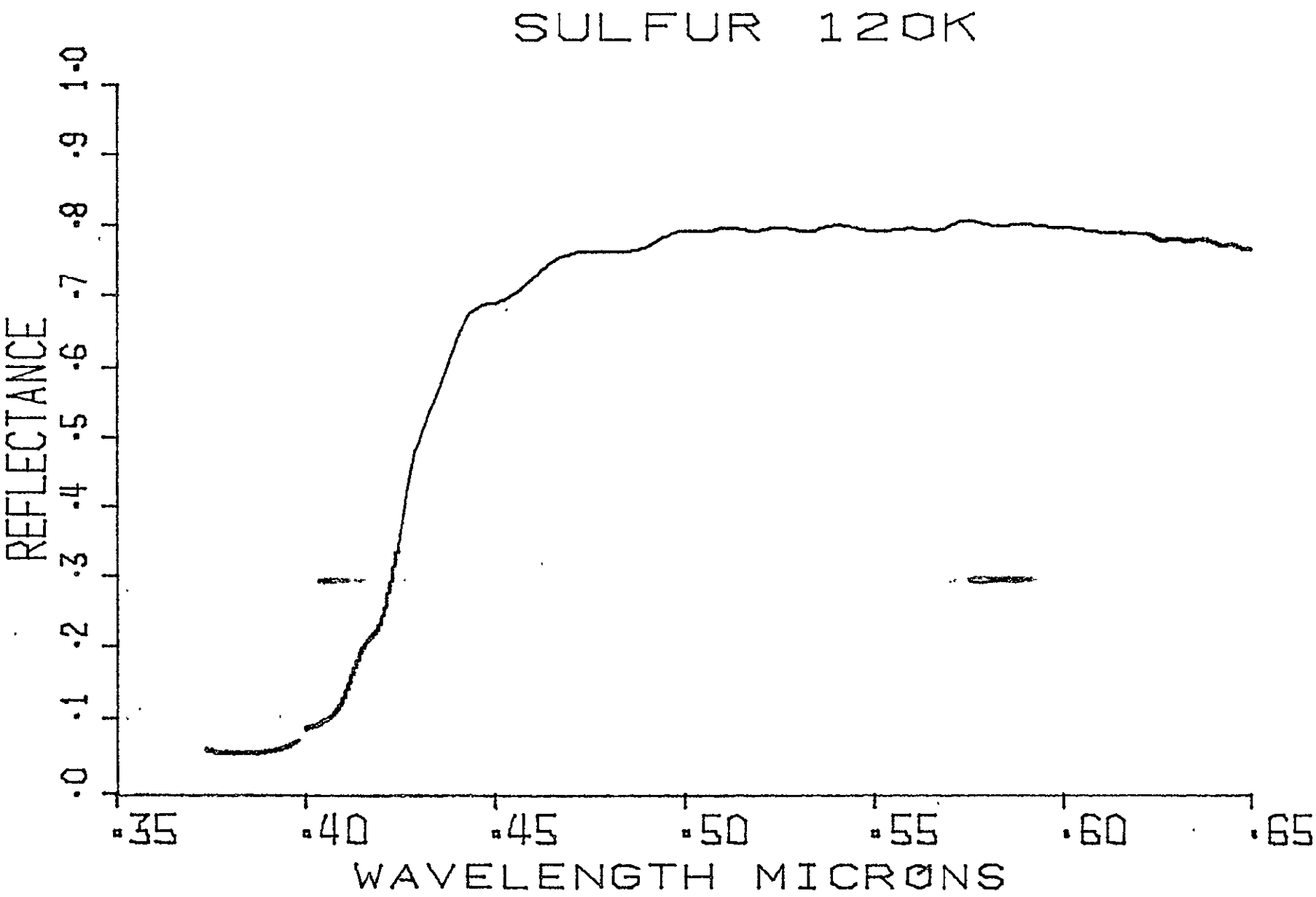
SULFUR 120K
REFLECTANCE
.0
.1
.2
.3
.4
.5
.6
.7
.8
.9
1.0
.35
.40
.45
.50
.55
.60
.65
WAVELENGTH MICRONS

FIG 21c

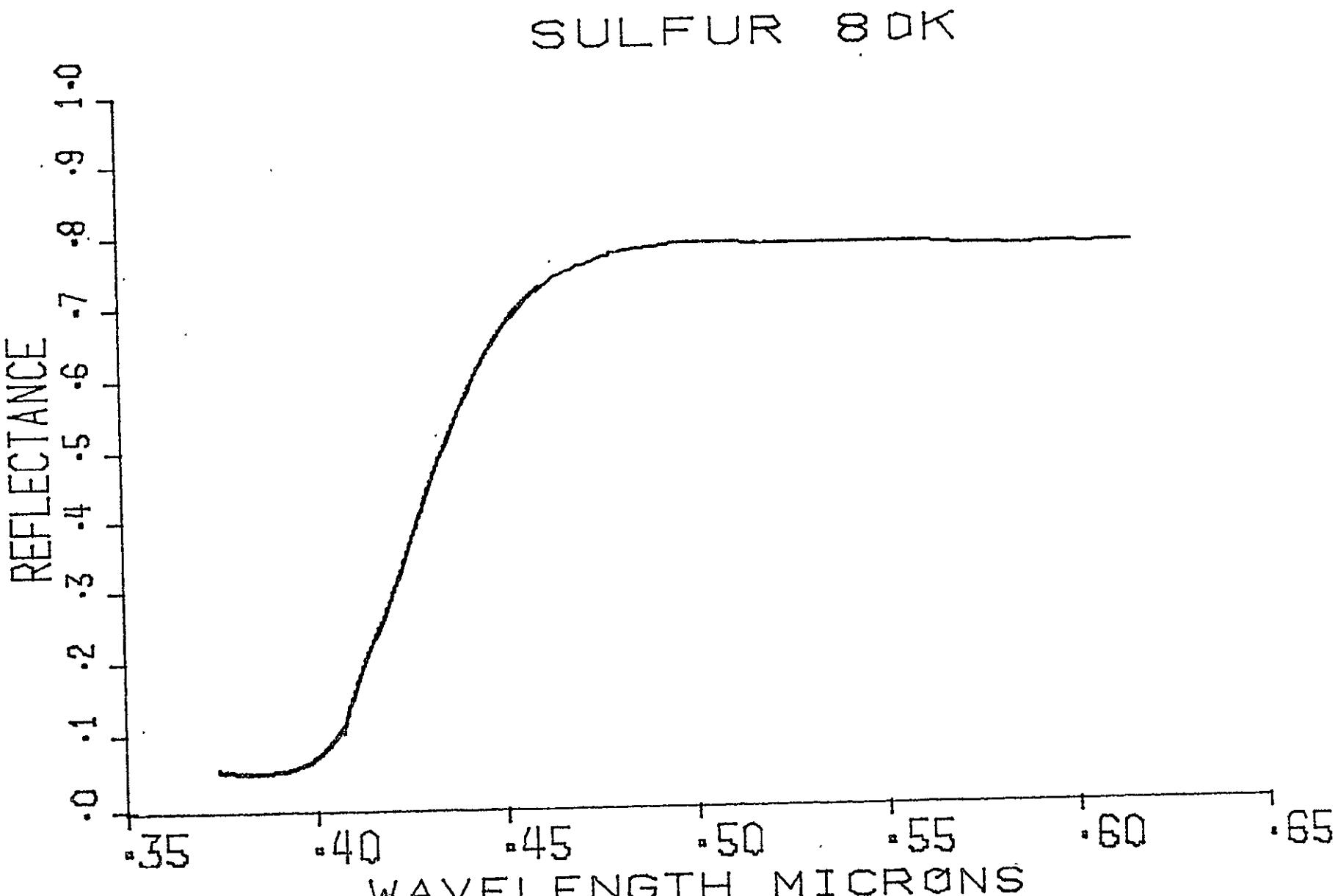
SULFUR 80K
REFLECTANCE
.0
.1
.2
.3
.4
.5
.6
.7
.8
.9
1.0
.35
.40
.45
.50
.55
.60
.65
WAVELENGTH MICRONS

FIG 21d